# A STUDY OF MULTIPHASE FLOW METERING AT PREVAILING CONDITIONS OF PRESSURE AND TEMPERATURE

By

CHARLES ADAM ULEH

A thesis submitted in partial fulfilment of the requirements of Teesside University for the award of Doctor of Philosophy

July 2012

# ABSTRACT

In multiphase flow, the velocity differences between phases means unless the velocities of individual phases and concentrations are known, the true flow rate is practically impossible to obtain. At present, there is no single multiphase flow meter design capable of providing the required accurate measurements of oil, water, and gas fractions, as well as the phase velocities of wet gas.
This research thesis introduces a prototype multi-phase flow metering system, named "*Uletech*", for wet gas measurement. The main objectives of this research is to provide individual phase velocities of wet gas, and to combine with phase volume fraction measurements to obtain individual phase volume flow rates for gas and liquid Hydrocarbon (HC).

The system comprised of a camera, laser source, synchronizer, computer data acquisition system and MATLAB based software, gas liquid chromatograph, seeds and tracer injecting devices.

The gas-phase velocity is determined based on Particle Imaging Velocimetry (PIV). An algorithm that correlates the camera's view to the volume within the pipe has been developed through this research. The computer acquires two sequential image signals from the camera, and carries out the calculation of cross correlation between the images so that the average particle displacement within each interrogation area can be found. The average gas-phase velocity is subsequently obtained by integrating pixel velocity along the distance between two image frames obtained by a Charged Couple Device (CCD) camera. The product of phase velocity and phase concentration gives the flow rate of gas phase. The HC condensate flow is measured by injecting the fluorescent tracer - Silicone Carbide (SiC) at a known flow rate, which mixes only with the condensate. By sampling and analyzing samples further downstream, the ratio of the fluorescence of the injected and sampled condensates are subsequently determined. And the HC condensate flow rate can then be derived.

The proposed method has been tested using a rig at Shell laboratory for the samples with a range of phase fractions and at several different velocities and flow rates. Due to the limitation of the rig, simultaneous measurement of the gaseous and condensate flow rate could not be done. But the experiments for liquid HC and gaseous phase measurements were carried out separately. However, this did not devalue the validation.

The test results have been analysed and provided in the thesis, which confirmed the concept of proposed method.

# ACKNOWLEDGMENTS

I would like to extend my sincere gratitude and unreserved thanks to my supervisor,

Dr. Jianyong Zhang, for his guidance and continued support throughout the various stages of this research work, especially the understanding and patience he has extended to me during the prolonged writing stage. On many occasions I contemplated the thought of abandoning the programme but after talking with him on the phone he encouraged me to continue; he was more than a supervisor.

Many thanks are due to Dr. Xu and Dr. Ian French (the supervision team) for their various contributions towards the success of the research.

I would like to acknowledge the kind support of Dr. Hans van Mannen and Mr. Hans Cussell of Shell Expro, The Netherlands, for their guidance and willingness to read my work; they were never shy of offering divergent views which helped in shaping my work.

I also owe thanks to my colleagues; Tobenna Aneto Emecheta, Abubakar Hussani, Amos Ologunleko, Ogbonnia Nwafor, Chukwu I. Lawrence, Femi Lawal, Mina Johnson-Hart and Jeff Syn Ku, for reading through my work during their spare time and offering valuable suggestions.

To my awesome God who is indeed wonderful and always doing things exceedingly, abundantly above all we may ever think or imagine. He made all this possible and I am eternally grateful.

# DEDICATION

This work is dedicated to my wife, Eneh Anita Ulehand my sons;

Owoicho-Oche Charles, Ewache Jedidiah & Echo Zephaniah.

I was not always there and they understood.

# PUBLICATIONS ARISING FROM THIS WORK

Charles A. Uleh, Jianyong Zhang, Donglai Xu and Ian French (2011) Novel Approach to Multiphase Flow Metering Using PIV and Tracer Dilution Technique. *Proceeding of the 9th International Conference on Measurement and Control of Granular materials, Shanghai China*, pp.81-84.

Charles A. Uleh and Jianyong Zhang (2011) Wet Gas Metering Using PIV and Tracer Dilution. *Proceeding of the 3rd IEEE international Conference on Adaptive Science & Technology (ICAST), Abuja, Nigeria*, pp.222-225.

# TABLE OF CONTENTS

# LIST OF FIGURES

# LIST OF TABLE

# NOTATIONS

| Symbol | Quantity | Value / SI Units |
|---|---|---|
| C | Capacitance | F |
| $\varepsilon_o$ | Permittivity of free space | $8.854 \cdot 10^{-12}$ F/m |
| $v_{,gas}$ | Superficial gas velocity | m/s |
| $v_{,liquid}$ | Superficial liquid velocity | m/s |
| $v_m$ | Multiphase mixture velocity ($v_m = v_{gas} + v_{liquid}$) | m/s |
| $q_{gas}$ | Gas volume flow rate | $m^3/s$ |
| A | Area (e.g. cross-sectional area of pipe) | $m^2$ |
| $\lambda_{liquid}$ | Liquid hold-up | |
| $\lambda_{gas}$ | Gas void fraction | |
| $\alpha_{liquid}$ | Liquid volume fraction | |
| $\alpha_{gas}$ | Gas volume fraction | |
| $t$ | Time | s |
| $\mu$ | Linear attenuation coefficient | 1/m |
| $I$ | Count rate | |
| $X$ | Lockhart-Martinelli parameter | |
| $\rho_g$ | Gas density | $kg/m^3$ |
| $\rho_l$ | Liquid density | $kg/m^3$ |
| $D$ | Internal pipe diameter | m |
| $g$ | Gravitational constant | ~9.81 $m/s^2$ |
| $F_r$ | Froude number | |
| $\eta$ | Quantum Efficiency | |

# DEFINITION OF TERMS

| | |
|---|---|
| Gas Volume Fraction (GVF) | The ratio of the gas volumetric flow rate to the total volumetric flow rate. |
| Intermittent flow | Intermittent flow is characterised by being non-continuous in the axial direction, and therefore exhibits locally unsteady behaviour. Examples of such flows are elongated bubble, churn and slug flow. The flow regimes are all hydrodynamic two-phase gas-liquid flow regimes. |
| Liquid-Gas-Ratio (LGR) | The ratio of liquid volume flow rate and the total gas volume flow rate. Both rates should be converted to the same pressure and temperature (generally for standard conditions). It is expressed as volume per volume, e.g. $m^3/m^3$. |
| Liquid Hold-up | The ratio of the cross-sectional area in a conduit occupied by the liquid phase and the cross-sectional area of the conduit. It is expressed as a percentage. |
| Liquid Load | The ratio of the liquid mass flow rate to the gas mass flow rate, normally expressed as a percentage. |
| Liquid Volume Fraction (LVF) | The ratio of liquid volume flow rate and the total fluid (oil, water and gas) flow rate. Both volume flow rates should be converted to the same pressure and temperature. It is expressed as a fraction or percentage. |
| Lockhart-Martinelli parameter | Lockhart-Martinelli parameter (LM or X) is defined as the ratio of the liquid Froude number and the gas Froude number, or in other words, the ratio of the pressure gradient for the liquid to the pressure gradient for the gas in a pipe under equilibrium flow conditions. An increasing LM parameter means an increasing liquid content or wetness of the flow. |
| Mass flow rate | The mass of fluid flowing through the cross-section of a conduit in a unit of time. |
| Measuring envelope | The areas in the two-phase flow map and the composition map in which the MPFM performs according to its specifications. |
| Microwave | Electromagnetic radiation with a wavelength of between 300 mm to 10 mm (1 GHz to 30 GHz). |
| Multiphase flow | Two or more phases flowing simultaneously in a closed conduit. This thesis deals in particular with multiphase flows of oil, water and gas in the entire region of 0-100% GVF and 0-100% Water-cut. |
| Multiphase flow meter (MPFM) | A device for measuring the individual flow rates for oil, water and gas in a multiphase flow. The total package of measurement devices for composition and velocity, including a possible conditioning unit, should be considered as an integral part of the meter. Note that under this definition a conventional two- or three-phase test separator is also a multiphase meter. |

| | |
|---|---|
| Multiphase flow velocity | The ratio of the multiphase volume flow rate and the cross sectional area of the conduit. Note that this is fictive velocity, and only in homogeneous and slips free multiphase flow does this velocity have a meaningful value. Multiphase flow velocity is the sum of gas superficial and liquid superficial velocity. |
| Multiphase volume flow rate | The total (oil, water and gas) volume flowing through the cross-sectional area of a conduit per unit time. |
| Oil | Hydrocarbons in the liquid state at the prevailing temperature and pressure conditions. |
| Oil (water or gas) volume fraction | The ratio of oil (water or gas) volume flow rate and the total fluid (oil, water and gas) flow rate. Both volume flow rates should be converted to the same pressure and temperature (generally standard) conditions. It is expressed as a fraction or percentage. |

# Chapter 1: INTRODUCTION

## 1.1 Background

Multiphase flow in the process industry is defined as the simultaneous flow of hydrocarbon gas and hydrocarbon liquid (condensate or oil) through a reservoir, transport pipelines (flow line, trunk line, and riser) and facilities (Hall et al., 2007). Often the transport of hydrocarbons is accompanied by non-hydrocarbons, including $CO_2$, $H_2S$, and water.

The multiphase flow in this study is defined using the gas volume fraction (GVF), which is referred to as a fluid whose GVF is $\leq 80\%$. Wet gas is a fluid whose GVF is $\geq 90\%$, and fluids with a GVF of between 80% and 90% are high GVF flow. These definitions are often used in Shell Explorations, and will be used throughout this thesis.

Single-phase transport in this thesis refers to either dry gas only (i.e. no condensate and no free water for all pressures and temperatures encountered along the pipeline), or oil only (i.e. no associated gas and no water for the pressures and temperatures encountered). Two-phase flow is most often the simultaneous flow of gas and condensate for a gas system, or oil and associated gas for an oil system. However, in this thesis two-phase flow also refers to the simultaneous flow of oil and gas. Three phase flow refers only to the simultaneous flow of gas, condensate, and free water in a gas system, or gas, oil, and free water in an oil system. Multiphase flows with solid particles (such as slurries with hydrate or wax particles, or transport of sand particles) are not described in this research thesis.

The measurement of wet gas becomes increasingly important. Natural gas is rapidly growing as an energy source for the world due to the fact that it is clean and low in carbon emission, and it is easy to distribute (Van Maanen, 1999).

Well measurements involving metering gas, HC liquid and water fractions and flow rates have an economic impact on the business. The implementation of these well measurements not only costs money, but also delivers data that is used in measuring the economic returns and used in decision making processes (Babelli, 2002). Figure 1.1 helps to illustrate this. Take the Ultimate Recovery (UR) for a particular field, initially only appraisal well test results, logging information, geophysical data, etc are available to determine the UR and its uncertainty. Regular well testing and the production data that become available in the lifetime of the field will be used as input to the reservoir model and consequently lower the uncertainty band of the UR. How fast this uncertainty band will decrease depends on the uncertainty of the information used (Jamieson, 1998).

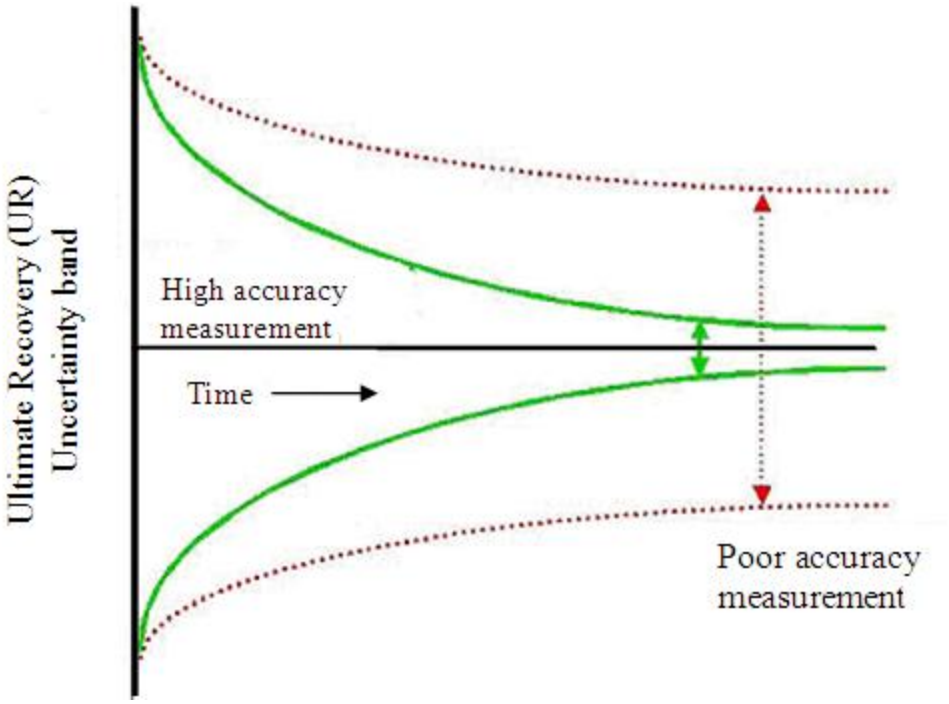


Figure 1.1 - Better quality data reduces the uncertainty in the UR faster.

From Figure 1.1 it is obvious that with highly accurate data the decrease is faster than with very poor quality data. There is a need to better quantify the measurement accuracy requirements for each individual well.

Further, optimization of oil production from a thin oil layer depends on flow rate measurement of individual phases. It increasingly becomes case in many old gas and oil fields. Scheers et al (Scheers et al., 2002) considered that an onshore field with a small thin oil bearing reservoir and horizontal wells to produce the oil. Production is expected to decline very rapidly from about 120,000 barrels per day (bpd) to some 20,000 bpd in 6

years time. This means that, if the decline is linear in time, the total oil still to be recovered is approx. 150 million bbl at US$ 80 per bbl (De Leeuw, 1997). This represents a value of approximately US$ 12 billion. With a sub-optimum production, e.g. with gas coning in the reservoir and thus excessive gas production from the above gas cap, the oil rim will move upwards. In that case the horizontal wells will show a decrease in oil production and an increase in water production. In terms of money, this loss of a few percent of the US$ 12 billion total value of the field is several tens of millions of US dollars. With this amount of money at risk it is important to see where measurement efforts need to be concentrated upon. For this particular field described, the development of gas production, or even better the gas oil ratio (GOR) is a very critical parameter in maximising the total oil recovery. Any sharp increase in GOR (which can occur in days) will indicate gas breakthrough and further depletion of the gas cap. When this happens an immediate reduction in the production rate is required to stop gas coning. GOR is not a direct measurement and its value is determined through other measurements such as liquid flow rate, water-cut, gas flow rate, etc. A sensitivity analysis for the GOR determination shows that the water-cut measurement is highly critical and any investment should be focused on this particular measurement, either through a conventional three- or two-phase test separator or via multiphase flow meters (MPFMs). In a thin oil layer development with approximately 100 wells and several tens of millions of US dollars at stake, it still felt that only MPFMs that fall in the US$ 40-60,000 range are realistic considerations for an individual well application. At prices of US$ 80,000 and above, a MPFM must be shared between a number of wells. However, even with this latter scenario, the advantage of using a MPFM over conventional test separators is the fast

response time and consequently the opportunity for more frequent testing and therefore the earlier detection of gas breakthrough.

In addition, in a gas field, many wells produce with high water-cut (for example > 90%) and at some point in the well life a decision has to be made whether the well should be abandoned or whether production is still economical. At the lower water-cut, generally the oil revenue is significantly higher than the operating costs, but with increasing water-cut the water handling and disposal costs will start to play a more dominant role. Scheers (Scheers, 2002) in Figure 1.2 demonstrated with a simple equation the breakeven point using hypothetical figures to be around a water-cut of 98%. Once this break even point is determined, the question is how accurate the water-cut measurement needs to be in order to make a good abandonment decision.

If the water-cut measurement shows a systematic error the well can be shut in too early or too late. With a systematic over reading in the water-cut measurement the well is shut in too early there is obviously loss of revenue. On the other hand if there is a systematic under-reading in the water-cut measurement the well is shut in too late and there is excessive cost for water handling and disposal. A detailed analysis of fluid property and fluid dynamics is presented in Appendix B.

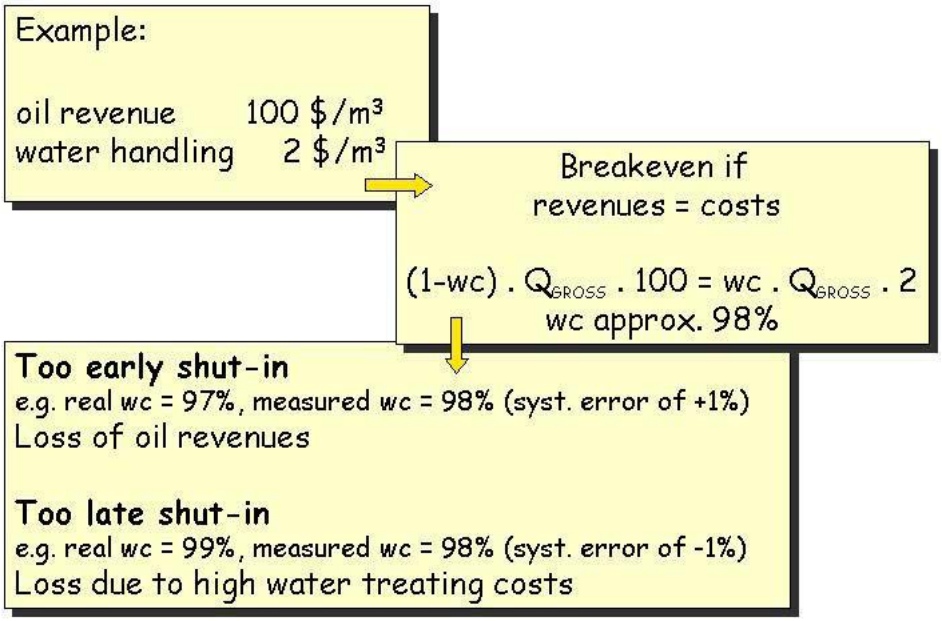


Figure 1.2 - At what water-cut level should a well be abandoned?

The vertices of the triangle (Figure 1.3) represent single-phase gas, oil and water, while the sides represent two-phase mixture and any point within the triangle represents a unique three-phase mixture (Jamieson, 1998). The transition region indicates where the liquid fraction changes from water-in-oil to oil-in-water. The ranges of common multiphase flow regimes, which are affected by temperature, pressure, viscosity and flow line orientation, are indicated at the side of the triangle.

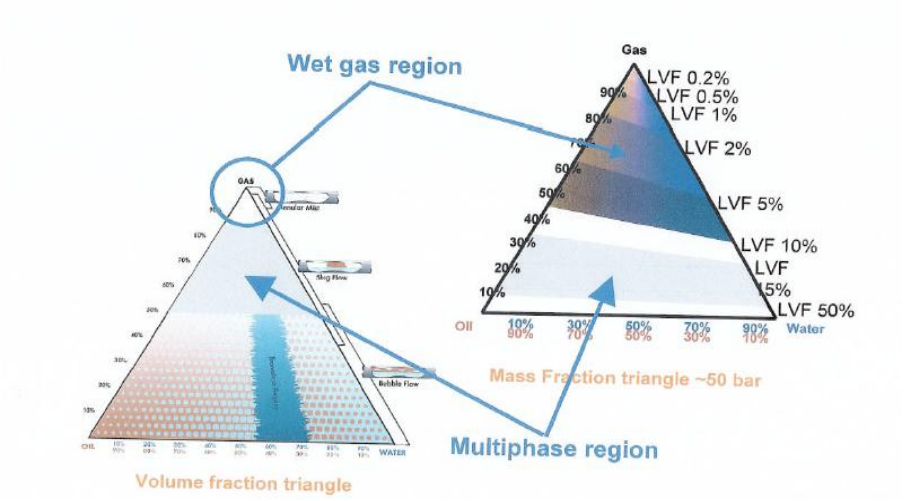


Figure 1.3 - Multiphase composition triangle

The problem is that the fluids of most gas fields contain heavier components as well as water vapour. Due to the drop in both pressure and temperature that occur when these fluids are produced to the surface, liquids (condensate and water) will form in the well fluid. In many cases water from an aquifer accompanies the gas to the surface, which is challenging for metering using single phase flow meters. Traditionally, flow metering to a high level of accuracy has meant metering a single phase flow, either as a gas or as a liquid, which often involves using test separation equipment mounted on fixed or floating platforms (Van Maanen, 1999) in oil and gas productions. This requires separation of the fluids into single-phases oil, gas and water from where the flow rates can be measured using proven meters such as turbine, positive displacement meters and orifice plates. This cumbersome and expensive approach is not acceptable for many future developments, especially on unmanned satellite platforms. Instead, novel metering techniques, employing a variety of technologies have been developed, which eliminate the need for

the deployment of three phase separators (Jamieson, 1999). These multiphase flow meters (MPFMs) offer substantial economic and operating advantages over their phase separating predecessors. However, it is widely recognised that no single measurement technique has proved to be effective over the complete range for all multiphase metering requirements (Xu et al., 2011).

## 1.2 Aims and Objective

The fundamental objective of this research is to advance the understanding of the phenomena of wet gas flow metering. The focus is on the development of a simple "low cost" and "cost effective" solution to multiphase flow metering. The method adopted is a combined PIV-tracer dilution approach, which will be used to target measurement of wet gas with HC condensate below 10%. The research work comprises theoretical study and software development, experimental data collection and data analysis. The validation has been done by comparing the controlled flow rates of the samples with several different fractions at various velocities to that of known flow rates of gas and HC liquid phases.

The main objective of the research work are summarised as follows:

- To review the literature describing components of the multiphase metering systems, and the application of image visualization techniques in multiphase flow measurements.
- To experimentally collect the response from a range of simple sensors when subjected to three-phase (oil/water/gas) flow conditions, with operating conditions covering a wide range of gas and liquid superficial velocities, in a 2 to 4 inch (50 to 102mm) horizontal pipe.

- To analyse features from the other multiphase vendor in relation to key multiphase flow parameters.
- To apply an appropriate image visualization model (PIV in conjunction with tracer dilution) for the identification of individual phase flow rates.
- To assess the performance of the system, for a range of wet gas under various phase fractions and velocities.
- Based on the outcomes of the present research, determine the plan for the next step development.

## 1.3 Thesis Layout

In the introduction, the author strives to emphasise that multiphase flow meter per well can save a large capital expenditure, space on off-shore platforms and yet give a continuous record of gas production. The advantages of the first are obvious and will improve reservoir engineering and thus save cost and increase revenues.

The rest of the report is organised as follows:

In Chapter 2, literature review has been presented describing existing systems used for wet gas measurement in natural gas fields at present.

Chapter 3 provides methodology, theoretical back ground and algorithm development based on MATLAB system.

Chapter 4 introduces the implementation of the concept in a prototype system, and provide experimental results, analysis and validation.

In Chapter 5 this research work is summarized, the conclusions have been drawn and future work has been recommended

# Chapter 2: LITERATURE REVIEW

In this section established and novel technologies suitable for measuring the flow rates of gas, oil, and water in three-phase flow are reviewed and assessed. Technologies already implemented in various commercial meters are then critically evaluated for operational and economical advantages or shortcomings.

## 2.1 Traditional Test Separators

Flow metering to a high level of accuracy has traditionally meant the metering of a single phase flow, either as a gas or as a liquid, and often involves using test separation equipment mounted on fixed or floating platforms (Van Maanen, 1999). This requires the separation of fluids into single-phase oil, gas and water so that the individual flow rates can be measured using proven meters, for example turbines, positive displacement meters and orifice plates. This cumbersome and expensive approach is not acceptable for many future developments, such as unmanned satellite platforms and seabed well completions. Instead, novel metering techniques employing a variety of technologies have been developed, thereby eliminating the need for the deployment of three phase separators (Jamieson, 1999). These multiphase flow meters (MPFMs) offer substantial economic and operating advantages over their phase separating predecessors. However, it is widely recognised that no single measurement technique has been proved to be effective over the complete range for all multiphase metering requirements (Xu et al., 2011).

In fact, multiphase measurements are routinely used at most production facilities as a test separator combined with its associated instrumentations forms a multiphase flow meter (Scheers, 2002).

Figure 2.1 shows a schematic of a traditional three phase separator with its associated instrumentation. The test separator consists of the following major parts:

1. Inlet emergency shutdown (ESD) valve
2. Three ESD valves - one each at the outlet for water, gas and oil
3. The vessel
4. Level control valves for oil and water (LCV)
5. Pressure control valves

The inlet to the separator is a mixture of gas, oil and water. As the oil is less dense it sits on top of the water and flows over a weir from compartment A into a separate compartment B. From here the outlet LCV is activated by a level controller (LC) and the oil level is maintained. A second LC maintains a constant water/oil interface by adjusting the water output from compartment A. The gas section is fitted with a series of baffles that encourage the separation of condensed liquid droplets from the gas, thus ensuring that the gas leaving the separator is liquid-free. The gas control valve is used to maintain the pressure of the separator.

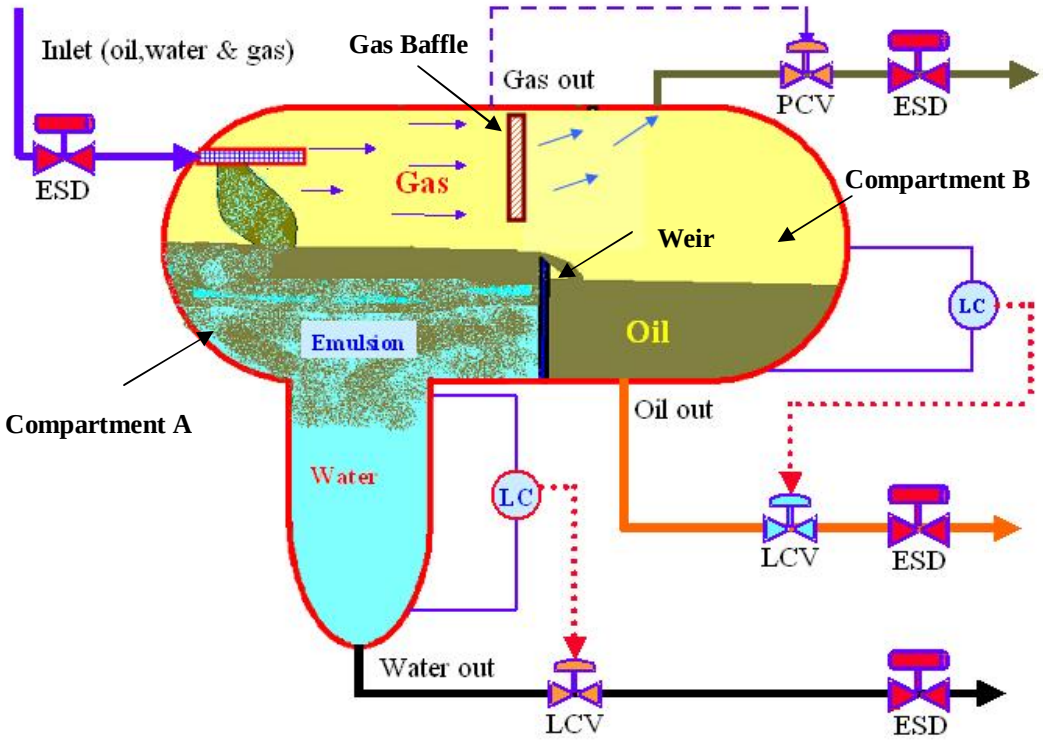


Figure 2.1- Simplified oil well separator

This test separator can be used to determine the phase flow rate following the physical separation of the liquid from the gas, with each phase then metered separately (Van Maanen, 1999).

Today, multiphase measurement technology in the form of a test separator is used primarily for production testing and consequently measurement using a three-phase separator is performed only periodically to determine individual well production performance. Test separators are used to establish the amounts of oil, water and gas per well as they may appear in the fluid under prevailing conditions of pressure and temperature. This data can then be correlated to either a dedicated flow device, e.g. a Venturi wet gas meter, or may be correlated to the valve position of the choke valve on

top of the well. In the case of wet gas metering, the relationships are well known and are theoretically underpinned, whereas for other flow regimes, e.g. slug flows, the correlations are crude and simpler. However, the ultimate aim is to replace test separators with flow meters that are capable of distinguishing between the various phases with sufficient accuracy. Therefore the prime use of multiphase measurement technology (other than a traditional test separator) is not for testing, which suggests non-continuous operation, but instead for continuous on-line real time measurement.

In facilities which service a number of wells, combined production flows into a production separator via the test header, and one well at a time is routed to the test separator. Replacing a conventional test separator with a multiphase measurement system will have a number of distinct advantages, however some of the identified disadvantages include:

1. Long stabilisation period
2. Long test lines
3. Shared test-separator
4. Limited rangeabilty of the test-separator
5. High capital expenditure
6. Test-lines require additional investments
7. Change in steady state behaviour

### 2.1.1 Long Stabilisation Period

In order to obtain reproducible values, the flow through the system (tubing, test-line and separator) has to be steady. With regards to the large volume involved, usually a 24 hour

time period is required, however this is not always sufficient, especially at lower flow rates. As several different flow rates need to be measured in order to describe the well behaviour, a well test takes several days. After testing the test-separator is used for the testing of another well and it is assumed that the first well will behave according to the behaviour measured during the well test; this will not always be the case e.g. when water breakthrough occurs (Ling and Shen, 2012).

### 2.1.2 Long Test Lines

Depending on the way a field has been developed, the distance between the well and the test-separator can be quite large, and as a result, the volume of the line is significant, e.g. an 8" line has a volume of 31.5$m^3$/km (Falcone et al., 2002). It can take quite some time before such a flow line has established equilibrium in its hold-up, which is required for obtaining correct readings for the liquid flow rates and this can pose a serious problem especially at lower flow rates (Atmaca et al., 2008).

### 2.1.3 Shared Test-Separator

As a test-separator is large, cumbersome and costly, it is impossible to install one at each well. Consequently, each well can only be connected to a test-separator for a limited amount of time (the well-test time period) and it has to be assumed that the well will exhibit the same behaviour demonstrated during the well-test period until the next well-test can be performed (Dykesteen, 2005). In general, this is not a true reflection of a well, as production can change in between two tests, and the characteristics of a well are determined only at steady conditions with phenomena such as water-breakthrough not being detected (Costa et al., 2008). Another complication may be changes in the

condensate banking in gas-condensate reservoirs, which influences (degrades) the permeability of the reservoir rock around a bore hole (Huerta, 2012).

### 2.1.4 Limited Rangeabilty of the Test-Separator

Van Maanen (Van Maanen, 1999) stated that the rangeabilty of test-separators is more limited than is generally thought. At low flow rates it is limited by the accuracy of the single-phase flow metering installed and the requirement for a steady state, whilst at high flow rates it is limited by the requirement for separation. Liquid carryover in the gas leg (due to droplets dispersed in the gas) is a frequent occurrence which often goes unnoticed because the flow meter will still provide figures, but there is no way to detect liquid in the gas leg. Sivaiah et al. (Sivaiah et al., 2012) also reported liquid carry-over in the gas leg of a separator used for liquid, gas and solid flow. Gas carry-under in the liquid leg is the opposite phenomena, but again no detection of gas in the liquid leg is available unless for example a Coriolis meter starts to generate figures which are obviously in error. In combination with the different requirements for the different wells, the accuracy of the results is less than one would expect and often no indication of erroneous results is available.

### 2.1.5 High Capital Expenditure

The capital expenditure for a test-separator is high, simply because it consists of a large amount of steel, which is rated at high pressures and which often has to withstand corrosion. For off-shore operations its size and weight contribute significantly to the costs of platforms.

### 2.1.6 Test-Lines Require Additional Investments

When test-lines for connection and disconnection (line-up) of wells are applied this require a significant additional investment, especially for off-shore installations, although even on-shore this can exceed the cost of the test-separator itself.

### 2.1.7 Change in Steady State Behaviour

A change in production from a well means that the equilibrium it had previously reached is lost. It usually takes 24 hours to attain equilibrium and during this time a well can produce a different amount of liquid than has previously been determined during a well-test at this flow rate. Depending on the variability in production, this can lead to significant differences between the actual and predicted liquid productions (Anisimov, 2012).

The ideal situation would be to have a multiphase flow meter available which could then be utilised to measure the flow rates of the different phases on all wells on a continuous basis. This would eliminate the disadvantages of the test-separator approach described above and could significantly improve the operation of a field; production variations would be easier identified and reservoir management would be more accurate. This would reduce the costs and increase the ultimate recovery, especially of the valuable condensate. When such a meter could be applied subsea, then it would further enhance the number of advantages. However, such a meter must be relatively low in cost, yet robust, reliable and reasonably accurate.

## 2.2 Cost Benefit of MPFM

The conventional way of developing smaller fields in the vicinity of an existing production facility is through the use of a test separator at the existing facilities. This can either be an existing test separator or a new test separator that is dedicated fully to the satellite production. In this manner the satellite platform is kept as simple as possible, as only wellheads and a test and bulk header are required to direct the production streams to the test- or bulk separator on the existing platform (Figure 2.2). With such a configuration extreme care should be taken on how representative the well test is, and the further away a site is located from the existing facilities, the more carefully the test results should be interpreted (Scheers, 2007). If a new dedicated well test unit for the satellite development is considered, then the space and weight limitations on the existing facilities often result in the selection of a MPFM.

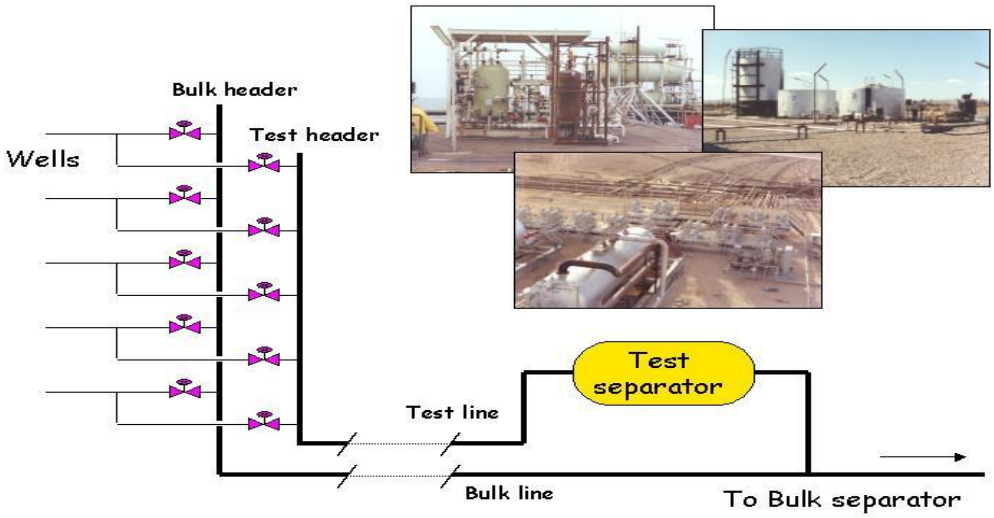


Figure 2.2 - Conventional way of linking satellite field to existing facilities

This solution only has economic benefits; it does not remove the measurement problems related to representative testing. A rough indication for test separator costs is in the order of US$ 500,000 to 1,200,000, dependent on size and pressure, and this is for onshore and for topside applications, respectively. These costs are simply the hardware costs, i.e. the test separator including its associated instrumentation (Jamieson, 1998).

The operating expenditures should also be taken into account, and it is obvious that for offshore applications the operational expenditures are much higher than for the easy access onshore locations. At present, rough cost indications are in the order of US$ 20,000 to 100,000 per year for onshore and topside locations, respectively. For the currently available commercial MPFMs, a rough price guide is between US$ 80,000 and 240,000, and there seems to be a relatively small difference between onshore and offshore applications (Scheers, 2007).

Tosic and Mehdizadeh (Tosic and Mehdizadeh, 2010) noted that MPFMs require less maintenance than traditional test separators. Therefore it is easy to conclude that a MPFM application offers significant cost savings; both in terms of capital and operational expenditures.

Further stripping of the facilities is possible by replacing the test- and bulk manifolds with a multi port selector valve. This type of valve can provide a cost effective method of connecting individual flow lines into a common bulk header and simultaneously provide the ability to direct any of the flow lines to the test facilities. Costs for multi-port selector valves depend on size, pressure rating and material, but a rough estimate is US$ 100,000. Operating costs seem to be comparable, with normal manifold valves and the required

plot space for multi-port selector valves being much less than for a test/bulk manifold. The costs for manifolds, for example for a five well manifold, are in the order of US$ 400,000 and the operating costs per year are estimated to be US$ 10,000. For subsea applications the manifolds are almost 10 to 20 times more expensive than for topside applications as subsea valves are designed such that they require minimum intervention.

From the above it can be concluded that with just one MPFM installation (instead of a test separator) there are a significant economic benefits to be made (Scheers, 2007). This is even true if a worst-case scenario is applied (i.e. low costs for separator, flow line and manifold and high costs for multiphase metering). Although the end result of a well test with a test separator and a MPFM is the same (i.e. both give cumulative oil, water and gas flow rates over the test period but the uncertainties might be different), from a data collection point of view there is a distinct advantage to installing a MPFM.

A MPFM gives continuous information on variations in the production rates, e.g. large variations in the gas flow rate compared to the liquid flow rates, which might indicate that there are problems with the gas lifting system or large variations in the liquid production flow rate which might indicate severe slugging of the well. The value of this information should also be taken into account. A further increase in the value of the production data is achieved if MPFMs are installed on a per well basis. However, with the above-mentioned capital and operating costs, it becomes clear that a multiphase meter installation on a per well basis in a development with more than 4-5 wells, may be difficult to justify with only economic considerations on the facility layout, although

other economical justifications, such as reservoir engineering reasons, might be sufficient to justify the use MPFMs on a per well basis (Scheers, 2002).

Four general approaches to multiphase metering have been identified, all of which are actively being developed and applied in the field. These are as follows:

- Compact separation systems
- Phase fraction and velocity measurement
- Tracers
- Pattern recognition

## 2.3 Compact Separation Systems

The compact separation system uses rotary separation technology. This is an efficient and compact method of gas-liquid separation that uses centrifugal force to separate gas, oil and water whilst also removing solids from the flow stream. This separation technology achieves equal or better efficiency than gravity-based systems and is significantly more compact than a traditional test separator.

Ting (Ting, 2001) and Cavalcanti (Cavalcanti, 2005) separately reported on tests of an inline rotary separator that also showed promise as a meter to measure the flow rate of the gas phase in a wet gas stream. The device under test was an IRIS™ separator manufactured by Multiphase Power and Processing Technologies, LLC. From Figure 2.3 it can be seen that dry gas exits through the top of the separator, while the separated liquid on the drum wall spins off and moves along the outer wall toward a drain. Unlike conventional static separators, the IRIS device includes a rotor assembly that collects liquids on its outer wall, and an inlet swirl generator directs the flow to the "separation

zone" at the rotor, where the rotating flow acts as a centrifuge forcing the liquid to the outer wall of the rotor. Dry gas exits through the centre of the separator, while the separated liquid on the drum wall spins off and moves along the outer wall towards a drain.

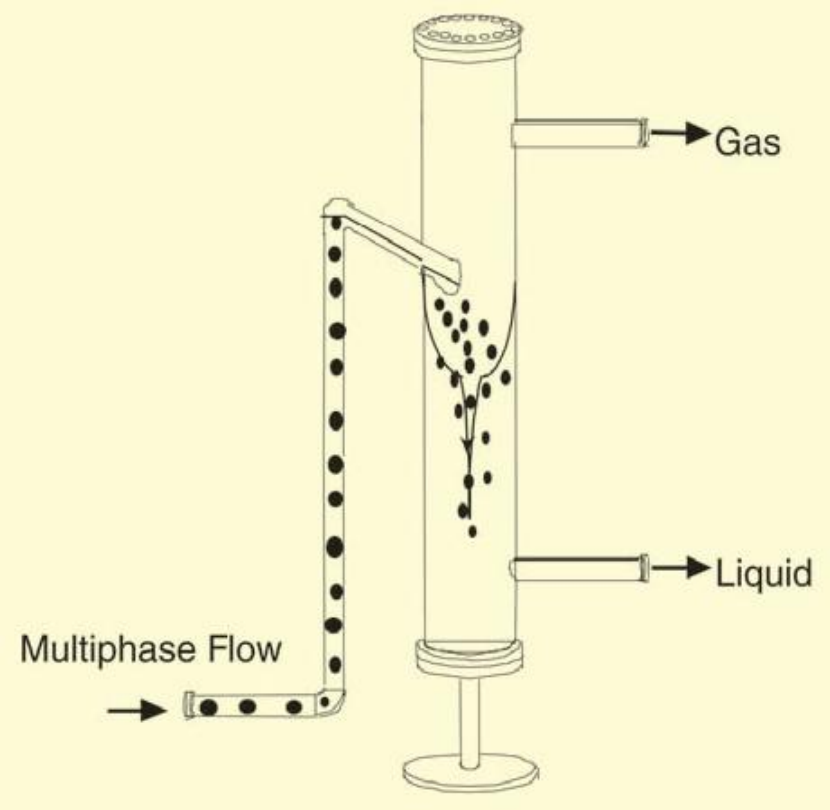


Figure 2.3 - Compact gas liquid separator by LCC

During tests, it was discovered that the gas flow rate in wet gas conditions could be inferred by measuring the rotor speed. At liquid-to-gas ratios of ≤3% the rotor speed demonstrated low sensitivity to the liquid flow rate and the gas flow rate could be estimated to within ±5% of reading accuracy using only the rotor speed for dry gas conditions. At higher liquid loadings the rotor speed dropped off due to increased fluid

drag, and at a constant gas flow rate the reduction in rotor speed was found to be proportional to the liquid flow rate.

Though, there appears some capital expenditure, weight and space saving with this class of MPFM in relation to a conventional test separator, it still does not satisfy the laid down requirements of a genuine MPFM. This equipment is still not immune from the traditional problems associated with a test separator, which are rangeability, liquid carried over in the gas leg, gas under in the liquid line, retention time, etc.

## 2.4 Phase Fraction and Velocity Measurement

These meters attempt to identify the fractions of oil, water and gas using conventional single phase flow meters to measure the phase velocities, which are not usually the same. Jamieson et al. (Jamieson et al., 1985) from Shell Exploration and Research summarised the applications of a MPFM for well monitoring, and noted that traditional flow measurement meters such as an orifice plate, turbine flow meter and displacement meter, were limited to single phase flow. However, since then numerous efforts have been made to use these meters with a compensation model to measure multi-phase flow, and in practice, manufacturers try to condition the flow so that the phase velocities are similar, and the differences in velocity are corrected using multiphase slip models.

Figure 2.4 shows a typical phase fraction meter. In practice, manufacturers try to condition the flow so that the phase velocities are similar, and the differences in velocity are corrected using multiphase slip models.

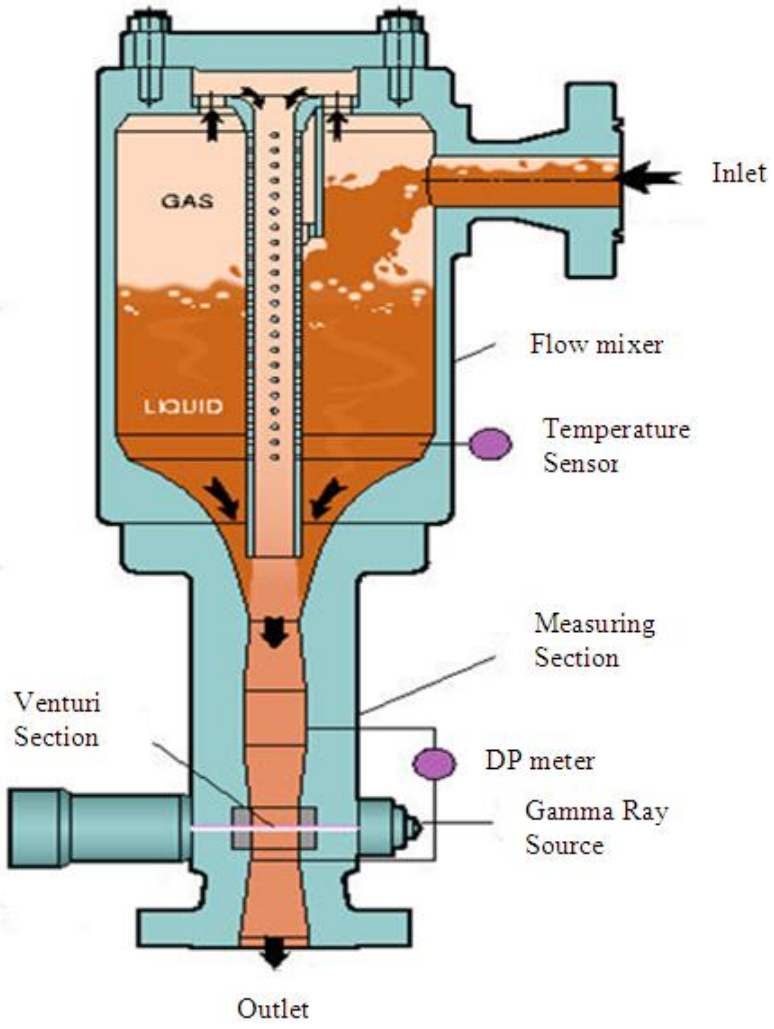


Figure 2.4 - Schematic of a typical phase velocity and phase fraction meter

This approach is rapidly being explored; however, for most of the approaches being developed the physics is underpinned but the complexity of multi phase flow metering makes it difficult to establish a validation method. Some of the approaches being utilised are as follows:

1 Positive displacement meter

2 Differential pressure measurements

3 Coriolis mass flow meter

4 Turbine meter

5 Vortex meter

### 2.4.1 Positive Displacement Meter

This meter is based on a mechanism to segregate the multiphase flow into small incremental packages (partial separation type), such that in their transit through the device the phases are temporarily confined without relative slip. By measuring the densities in packages the mass flow rate of the multiphase fluid is obtained by multiplying the package volume flow rate by the density (Spitzer, 2006). Volumetric flow rates are obtained by a pulse generating and detection system monitoring rotor revolutions. The mass flow rates of individual phase liquids can be measured from sample properties such as oil density, gas density and water-cut. Representative liquid samples are taken from the meter's central chamber.

Field tests of this class of meter showed up to 10% and 20% measurement error for volumetric and mass flow rates, respectively (Tuss et al., 1996). The main disadvantage of the meter is its intrusive nature, together with the mechanical parts of the meter which require continuous maintenance and may fail under severe flow conditions.

### 2.4.2 Differential Pressure Measurements

In instances where a multiphase flow is sufficiently mixed, differential pressure-based flow measurement techniques such as Venturi and orifice sections can be utilised to determine the flow velocity and also measure the mixture flow rate (Xie et al., 2007; Olsen, 1993). The pressure drop measured across these sections can be expressed as a function of the fluid flow rate and vice versa. The Venturi and orifice meter operating principles are well-established and well understood single-phase flow measurement methods. Full descriptions of their technical designs are detailed in ISO 5167:2003.

Figure 2.5 illustrates the geometry of the Venturi and orifice inserts and their characteristic flow profiles. In the Venturi, the reduction in the flow area results in increased fluid velocity, and consequently reduced fluid pressure. The small angle of the downstream cone facilitates large pressure recovery by minimising frictional losses. In contrast, the abrupt reduction in flow diameter in the orifice plate results in the creation of regions of fluid recirculation and the downstream pressure recovery is hindered by the disturbed flow pattern induced by the restriction (Blaney, 2008).

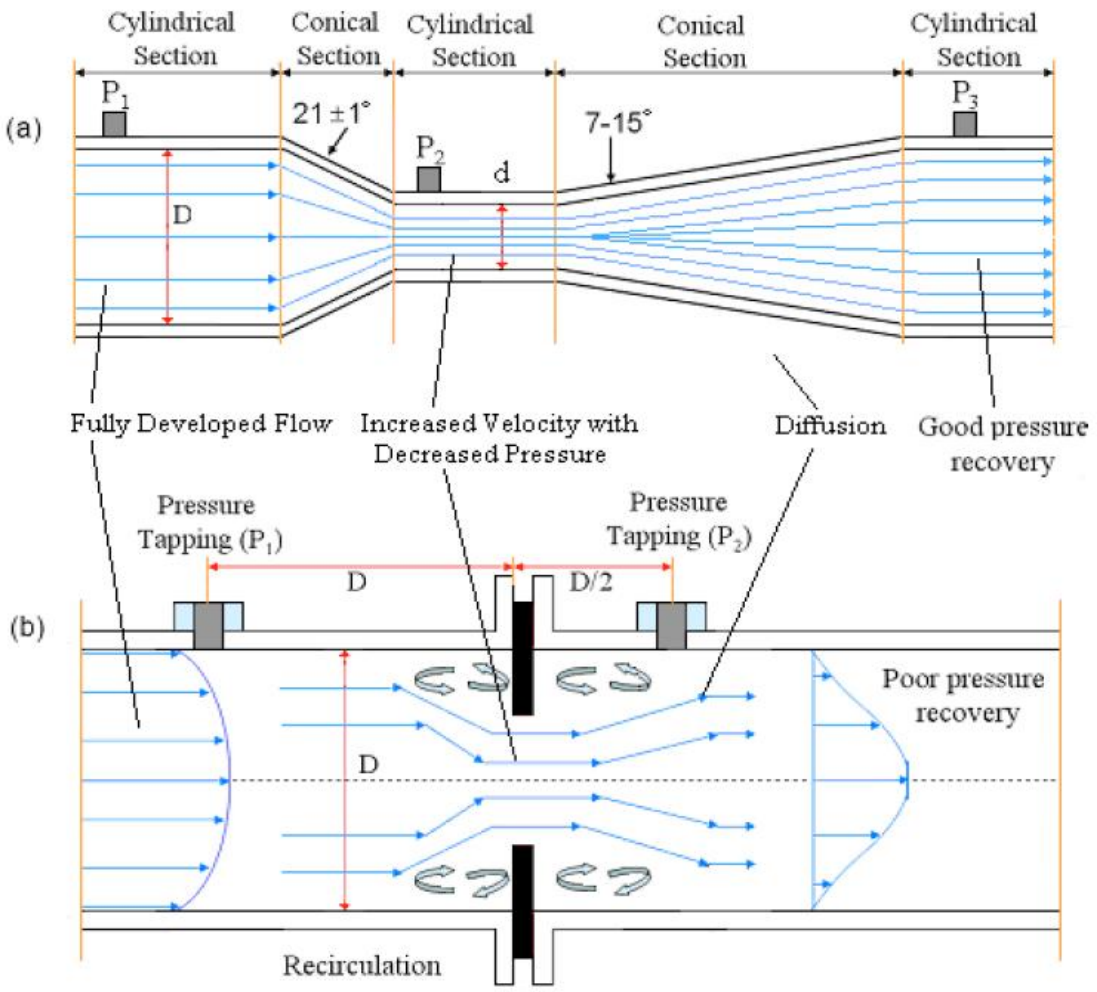


Figure 2.5 - Differential pressure measurement systems (a) venturi, (b) orifice

The use of orifice plates tends to be restricted to wet gas measurements owing to their poor pressure recovery properties. The gas phase flow rate can be determined from the two-phase mixture pressure drop through the application of either the Murdoch or Chisholm correlation. (Fang et al., 2010)

Murdoch: $$Q_g = \frac{Q}{1+1.26X_L} \quad (2.1)$$

Chisholm: $$Q_g = \frac{Q}{1+\sqrt{1+\mathrm{CX_L}+\mathrm{C}}X_L^{\,2}} \quad (2.2)$$

Where $Q$ denotes the wet gas flow rate derived from the orifice plate pressure drop, C is the Chisholm constant (Chisholm, 1967), and $X_L$ is the Lockhart-Martinelli parameter:

$$C = (\frac{\rho_l}{\rho_g})^{0.25} + (\frac{\rho_g}{\rho})^{0.25} \quad (\mathrm{X_L}<1) \quad (2.3)$$

$$X_L = \frac{Q}{Qg}\sqrt{\frac{\rho}{\rho_g}} \quad (2.4)$$

In order to determine the flow rate of the homogeneous gas-liquid mixture using a Venturi, an experimentally determined corrected differential pressure formula must be applied, such as that proposed by Hammer and Nordvedt (Hammer and Nordvedt, 1991). From this the volumetric liquid flow rate can be obtained from a measured pressure drop ($\Delta$P) for a known gas volume fraction and liquid density.

$$Q_L = \sqrt{(1-\alpha)}\frac{\Delta P}{\rho_l} \quad (2.5)$$

The Venturi method has many advantages, including low cost, good pressure recovery, familiarity, and simple operation. Furthermore, high accuracy velocity measurements (relative error <1%) can be obtained as long as the multiphase flow mixture maintains

homogeneity. In contrast, the multiphase flow requires pre-conditioning in order to induce a state of homogeneity. In addition, the differential pressure lines of the Venturi meter require regular purging and scale formation can yield excessively high pressure drops.

### 2.4.3 Coriolis Mass Flow Meters

Figure 2.6 shows the architecture of a Coriolis meter. Although there are straight pipe Coriolis flow meters, e.g. the ABB Coriolis flow meter, it is more convenient to use a U-shaped meter to explain how one functions. The main components are a U-shaped pipe and a T-shaped leaf string with a magnetic detector. When fluid passes through the meter, the momentum change causes an angular deflection of the tube proportional to the mass flow rate, which is sensed by a magnetic detector (Henry et al., 2006). The driving force, i.e. the Coriolis force causes the U-tube to oscillate at its natural frequency is proportional to the fluid mass flow rate through the U-tube (Agar, 2010). The meter is a non-intrusive instrument, but for metering multi-phase flow, due to its dependence upon the detection of vibrational amplitude, it is not suitable for use at high void fractions where mechanical vibration caused by slugs can introduce significant errors.

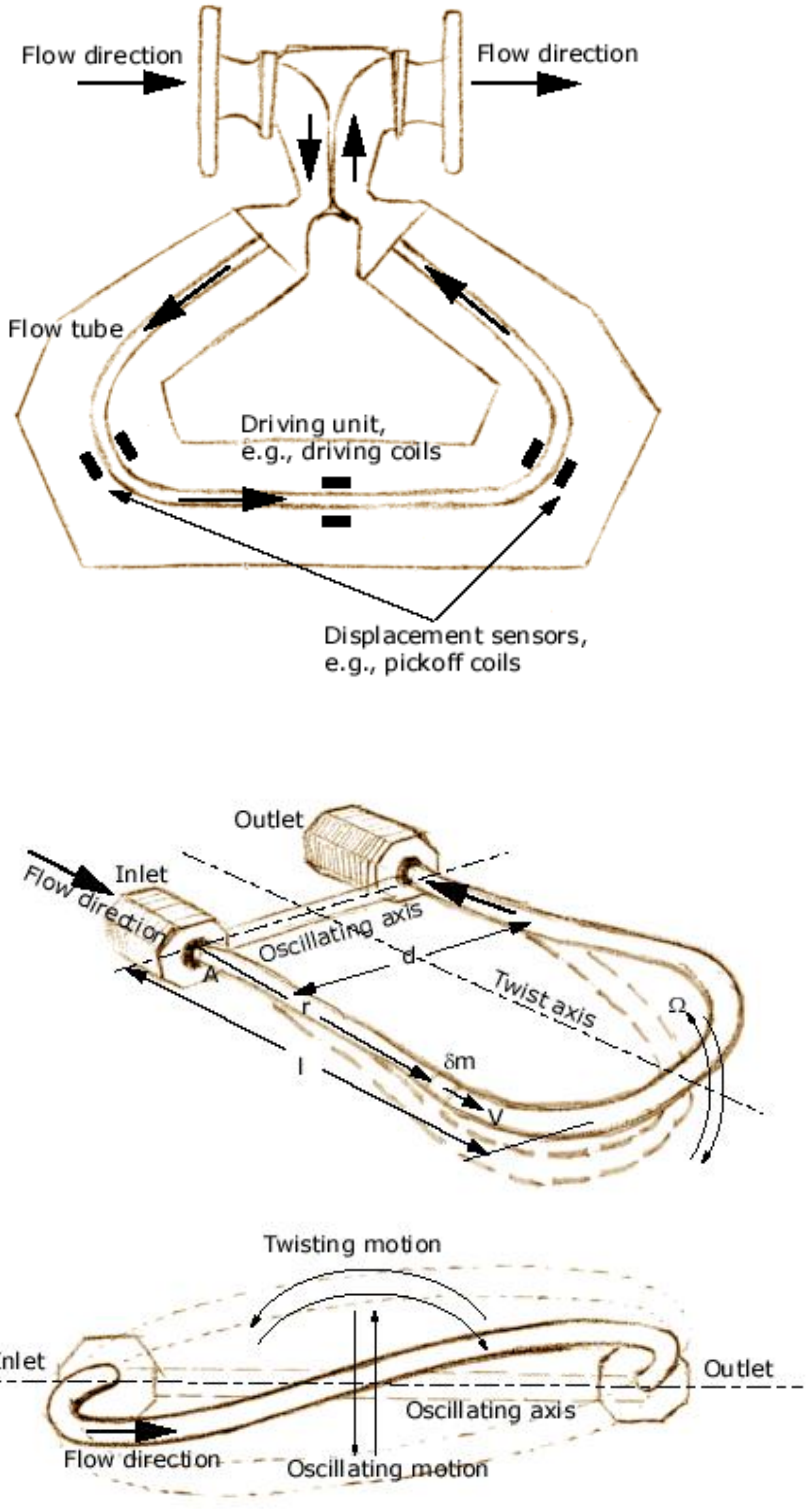


Figure 2.6 - Principles of operation of a coriolis meter

Although Coriolis meters are traditionally used for liquid flow measurements, most manufacturers now offer them for gas applications. The meter is calibrated in water and used also for gas flow.

Due to its ability to directly measure the mass flow rate, there is a particular interest in evaluating Coriolis performance in wet gas flow conditions. The results have indicated that the Coriolis meter showed a clear pressure dependency in dry gas conditions, with the error becoming increasingly negative with increasing pressure. The meter also exhibited greater errors in wet gas flow conditions. At all liquid fractions tested, the meter under-predicted the reference gas mass flow rate with measurement errors reaching as high as 50% in higher liquid loading (Agar, 2010).

According to previous work on general two-phase flow by Wood (Wood, 2002), the meter can function at up to 10% gas entrainment providing that the two-phase gas-liquid flow remains homogenised within the small vibrating tubes of the Coriolis meter. An advantage of a Coriolis flow meter is that it measures the mass flow rate directly, which eliminates the need to compensate for changing temperature, viscosity, and pressure conditions.

### 2.4.4 Turbine Flow Meters

Figure 2.7 shows the schematics of a turbine flow meter which can be used to measure the volumetric flow of a flowing fluid (liquid or gas). The unit consists of a multiple-bladed rotor housed in a non-magnetic body, mounted with a pipe perpendicular to the liquid flow. The rotor spins as the fluid passes through the blades. The rotational speed is

a direct function of flow rate and can be sensed by magnetic pick-up, photoelectric cells, or gears. These instruments operate linearly with respect to the volume flow rate and because there is no square-root relationship (as with differential pressure devices), their rangeability is greater. Extensive coverage of the considerable range of turbine designs together with a review of their principle operations was provided by Baker (Baker, 1998).

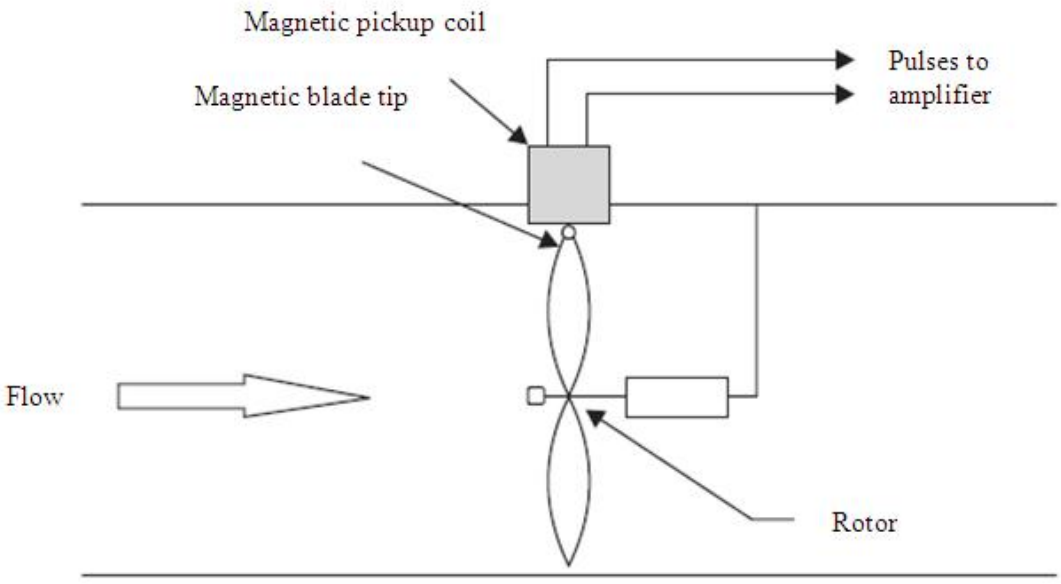


Figure 2.7 - Turbine flow meter

Stewart described (Stewart, 2002) a series of wet gas tests on a 6-inch instrument gas turbine meter at the National Engineering Laboratory (NEL). The presence of a small quantity of liquid produced a significant effect on the turbine meter readings at Reynolds numbers below $5 \times 10^6$, whilst at higher Reynolds numbers the liquid appeared to have little effect on the meter. Stewart concluded that additional testing, preferably on more

than one model of turbine meter, would be required to provide a better examination of turbine meters in wet gas conditions.

### 2.4.5 Vortex Flow Meters

Vortex meters make use of a natural phenomenon that occurs when liquid flows around a bluff object, whereby eddies or vortices are shed alternately downstream of the object. The frequency of the vortex shedding is directly proportional to the velocity of the liquid flowing through the meter (Figure 2.8). The three major components of the flow meter are a bluff body strut- mounted across the flow meter bore, a sensor to detect the presence of the vortex and to generate an electrical impulse, and signal amplification and conditioning transmitter whose output is proportional to the flow rate (Sanderson, 1998).

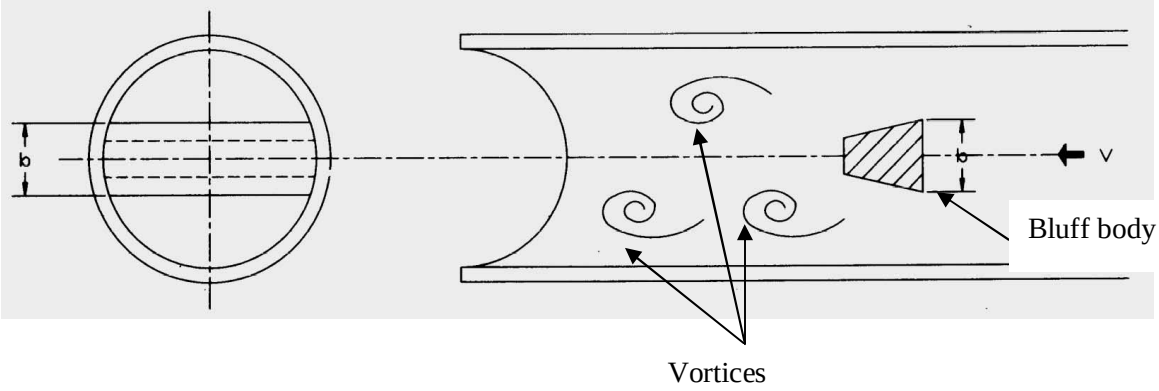


Figure 2.8 - Principle of vortex flow meter

Vortex meters are normally used for processed natural gas and steam flow. A typical quoted accuracy for these applications for an uncalibrated meter is of the order of ± 1.5% of the reading and ± 1.25% for calibrated flows (Sanderson, 1998).

Four-inch Fisher-Rosemount and Yokogawa vortex meters were tested by the NEL in a horizontal orientation in wet gas at 15, 30 and 60 Barg. The results showed that the meters overestimated the reference gas flow rates with a relative error ranging from 0 to 30%, which was dependent on liquid volume fraction and gas velocity (Stewart 2002). These results indicated that if vortex meters are used for unprocessed natural gas, then large measurement errors can be expected as the presence of liquid causes the meter to over-estimate the actual gas flow rates. Hua and Geng (Hua and Geng, 2012) in their recent publication provided measurement accuracy figures for liquid phase as ± 20%.

## 2.5 Microwave Technique

Microwave sensors are used to distinguish between water and oil in the liquid phase of a multiphase flow. Water and oil have distinctly different dielectric constants and conductivities and it is this difference that allows a microwave sensor to determine the water content of a water-oil mixture. Nyfors et al. (Nyfors et al., 1989) described three different microwave sensor operation principles:

1. Transmission sensor and measurement on a single frequency
2. Transmission sensor and measurement on a varying frequency
3. Resonator sensor

### 2.5.1 Transmission Sensor and Measurement on a Single Frequency:

A probe is used to transmit microwave radiation through the multiphase medium to a receiving probe. Caution must be exercised to prevent reflections in the pipe/sensor and a guided wave sensor may be deployed to prevent against this. The microwave-receiving

sensor may be configured to output the attenuation of or the phase change in the transmitted microwave radiation.

### 2.5.2 Transmission Sensor and Measurement on a Varying Frequency

Owing to the large amounts of water present in continuous liquid phases on high frequency microwaves, it can be beneficial to employ a varying frequency method whereby the frequency of microwave radiation transmitted is a function of the dielectric properties of the fluid. This can be implemented by monitoring the change of phase such that the meter can determine the frequency where the phase change is constant.

### 2.5.3 Resonator Sensor

This meter measures the dielectric properties of the mixture using the resonant cavity method. A resonant cavity is comprised of a metal structure which confines an electric field, causing it to reflect back and forth within the cavity. By matching one of the dimensions of the cavity to the wavelength of the electromagnetic radiation, a standing wave is produced. When this cavity is filled with a specific fluid, the resonant frequency of the cavity will shift in direct proportion to the dielectric constant of the fluid present. By measuring the resonant frequency and peak width, the dielectric properties of the fluid can be determined and the system can be calibrated to give the water-cut. In practice, microwave sensors use a combination of techniques, using the resonating cavity principle for oil continuous flows and the varying transmission frequency for in water continuous. A microwave sensor can then be used in tandem with either electrical impendence or the gamma attenuation technique to obtain the gas volume fraction of the multiphase flow.

### 2.5.4 Microwave Sensor and Positive Displacement Flow Meter by AGAR

Agar and Farchy (Agar and Farchy, 2002) suggests that flow measurement is achieved with three independent subsystems stacked in series. The positive displacement (PD) Flow meter as shown in Figure 2.9 offers total volumetric measurement and eliminates slip as all three phases exit the PD meter at the same velocity. The momentum meter determines gas void fraction using standard Venturi equations. The Agar microwave water-cut meter measures the amount of water in the combined stream. The bias produced by the amount of gas in the water-cut reading is corrected using the gas void fraction measured in the momentum meter.

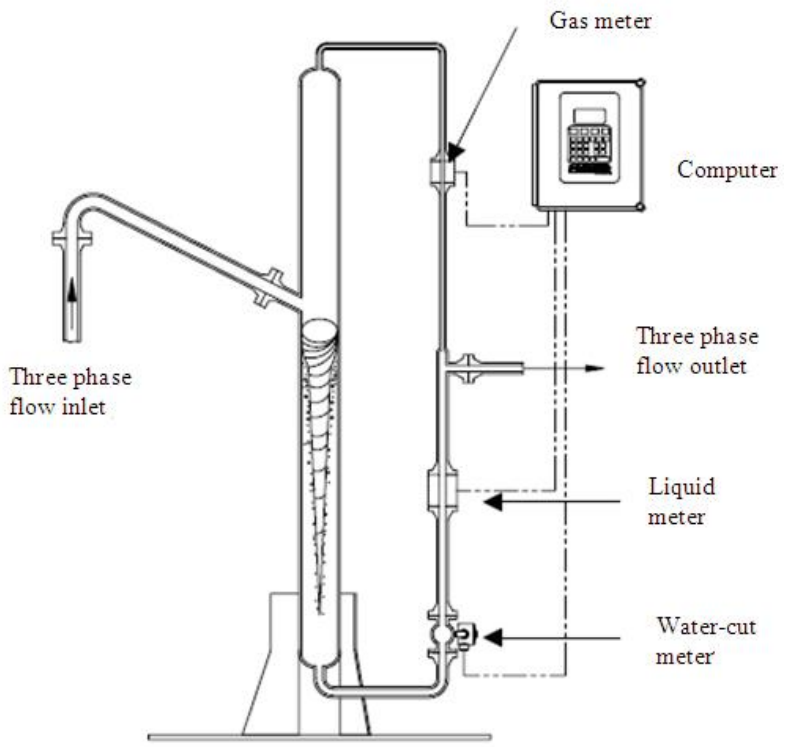


Figure 2.9 - Agar MPFM 400 series schematic

*Advantages of a PD meter:*

Every time the PD meter turns a revolution, a known volume of fluid goes through the meter, and although at this point in time it is not known if it is oil, gas, or water, the total volume is measured very accurately. This is a very important point; the PD meter measures total volume as opposed to most competitors systems which measure mass and calculate volume through mass/density equations. Therefore, the PD meter measure of total volume is always more accurate than a calculated total volume.

- By design, there is no slip through the PD meter. No matter how fast the gas or how slow the liquid is moving at the time the flow stream enters the PD meter, the entire flow stream will exit the PD meter at the same velocity, thereby reducing the slip between the phases to zero. The PD meter works over the entire GVF range of 0-100%.
- The Venturi is directly sensitive to changes in density and viscosity and losses are corrected by taking additional differential pressure measurements across the Venturi (inlet to outlet). Determination of the velocity by the PD meter, and the knowledge that there is no slip between the fluid components at the entrance of the Venturi, allows the frictional losses to be determined. The head loss at the throat is dependent on the acceleration loss, and the head loss across the Venturi is due to frictional losses and the viscosity loss. An ideal fluid will have a 99% pressure recovery, while a viscous fluid will have a much lower recovery rate. The velocity will also affect the recovery rate as well; the higher the velocity, the higher the loss for head of viscous fluids. Therefore by measuring the differential

pressure across the Venturi and knowing the velocity from the PD meter, this loss can be determined. The system measures a greater loss created by the more viscous fluids and corrects for it.

*Advantages of an Agar meter:*

- Since this MPFM is a volume based system (it measures actual total volume) and does not use mass/density equations, Agar MPFM need only be calibrated once and there is no need to calibrate multiple wells and the density of the oil, gas, and water. If the salinity or oil density changes, then the meter does not require recalibration nor is the accuracy of the unit affected. This is considered as a big advantage in wells producing from multiple zones with varying fluid densities.
- There are no mixers or fluid conditioners required with the Agar MPFM, thus reducing the pressure drop through the unit.

The Agar MPFM is said to have performed to its specifications (±10% of the reading for gas, oil and water) in numerous fields worldwide, up to 99.99% GVF (McNulty and Beg, 1997; Agar and Farchy, 2002). Conoco (USA) tested the Agar MPFM for high GVF under controlled field conditions on its Lafayette test loop and found it to be accurate to ± 12% compared with reference single-phase measurements.

Generally, the response of PD meters for multiphase flows depends on upstream flow conditions (Murugesan, 2002). Spitzer (Spitzer, 2006) stated that the effective liquid viscosity depends on the continuous phase, the dispersed-phase fraction, and the degree to which they are mixed. An increased flow viscosity increases the differential pressure through the meter and may affect the calculation of the flow velocity. There are no

general relationships for differential pressure across Venturis and other devices in multiphase flow. The best approach is to attempt to get as close as possible to a homogeneous flow, which suggests pre-mixing (flow conditioning), which is not a requirement for a genuine multiphase meter.

## 2.6 Nuclear Technique

Several methods used to measure phase volume fractions in multiphase flows involve radiation, such as neutrons, gamma rays, or x-rays, that are partially attenuated by the flow. Information about local density or phase distributions can be obtained by measuring the attenuation of radiation through the flow, or by triangulating the locations of radiation sources within the flow (George et al., 1998).

### 2.6.1 Schlumberger VenturiX Meter

Figure 2.10 shows the Schlumberger VenturiX meter whose basic concept is a Venturi measurement and a dual-energy gamma ray absorption measurement over the throat of the Venturi (Letton et al., 1997). There is no mixing conditioning unit, the meter should be installed vertically with upward flow and just upstream, and in the vertical section, a blind tee is recommended to improve mixing. The radioactive source for topside and onshore applications is a Gd-153 source which has energy levels of 41.5 and 97.4 keV. These two energy levels are used in the dual energy gamma ray absorption concept for composition measurement. Although the source is attractive from a measurement point of view (low energies give better discrimination between oil and water), the half-life of the source is relatively short (242 days).

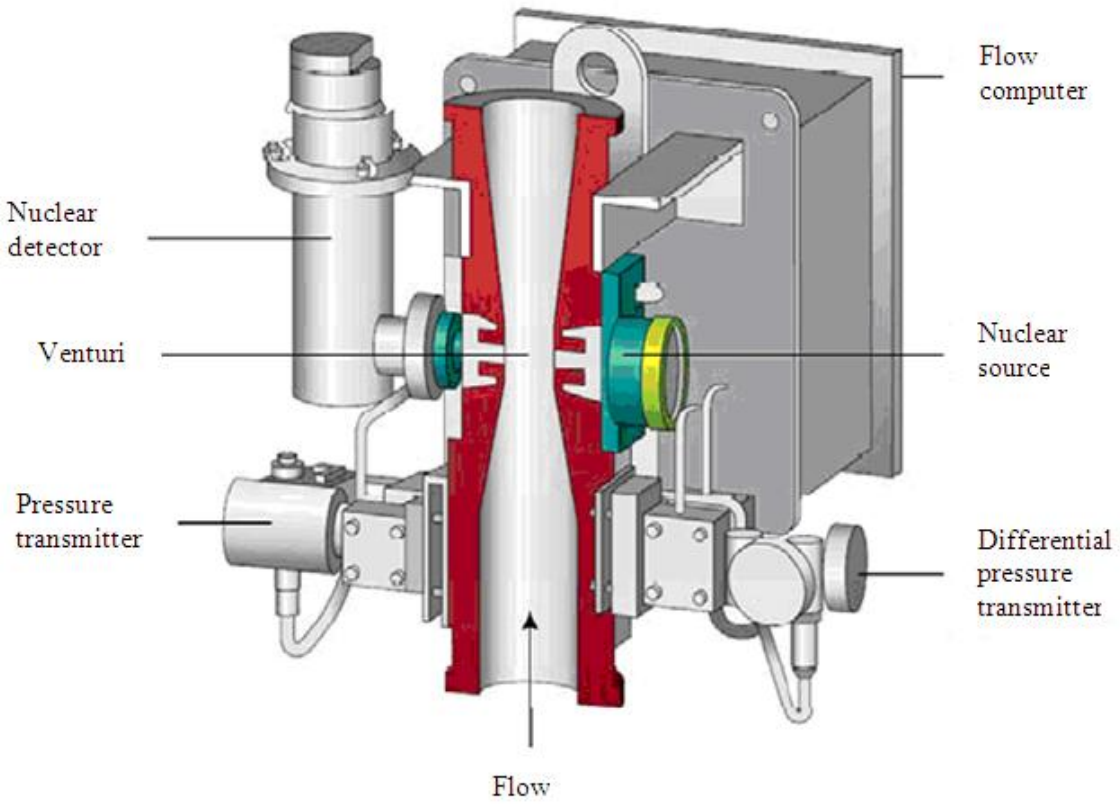


Figure 2.10 - Schlumberger VenturiX MPFM

Laboratory testing of the PhaseWatcher Vx meter was also undertaken at the NEL by Letton et al. (Letton et al., 1997). The test matrix was comprised of a number of points with GVFs ranging from 0 to 95%. Liquid phase and oil flow rate measurements were produced within a relative uncertainty band of ±10% and water-cut readings had an associated absolute error of ±6%. No quantification of the gas phase measurement performance was reported.

Al-Khafji Joint Operations installed five PhaseWatcher Vx MPFMs in the offshore-Khafji field for satellite-based monitoring and well tests were referenced against a test barge comprising of a conventional three-phase separator set up. Measurement

agreements for the PhaseWatcher Vx meters were reported to exhibit a 5-10% relative error for the oil and water flow rates and were in excess of 15% for the gas phase flow rate, with respect to the separator measurements (Al-Bourni et al., 2005).

The Schlumberger Vx meter uses a dual gamma source and has the advantage of being non-intrusive. The amount of gamma radiation absorbed by the fluid is a function of the fluid density and the attenuation properties of the fluid. A comparison of the number of gamma rays reaching the detector to the number emitted by the source reveals the fluid density. When this technique is used in multiphase flows, the resulting density is a weighted average over the length of the beam. Generally, because times in the order of minutes are required to collect statistically significant samples, radiation absorption techniques yield time-averaged results, and consequently, they are better suited for flows where the amounts of each phase are stable over long time periods. Gamma-ray methods also require that the gas and liquid phases have significantly different attenuation properties for useful quantitative results. These methods have the advantage of being non-intrusive, which is helpful if the gas and liquid phases are to remain separated and unmixed (Blaney and Yeung, 2007). However, time averaged results are a challenge for fiscal metering and flow pre-conditioning will not satisfy the requirement for a true multiphase flow meter.

### 2.6.2 Gamma Ray Densitometers by Roxar

The Roxar meter as shown in Figure 2.11 (Leggett, 1996) is another nuclear technique for measuring radioactive isotopes for multiphase measurement that uses a dual velocity method with calculated phase fractions based on capacitance and conductivity

measurements in combination with a single energy gamma densitometer, cross-correlation, and Venturi section to determine the flow rates of the individual phases. Gamma radiation attenuation techniques are used to resolve two-component mixture phase fractions based on a single-energy gamma source or for three-component mixtures using a dual-energy gamma source (Busaidi and Bhaskaran, 2003).

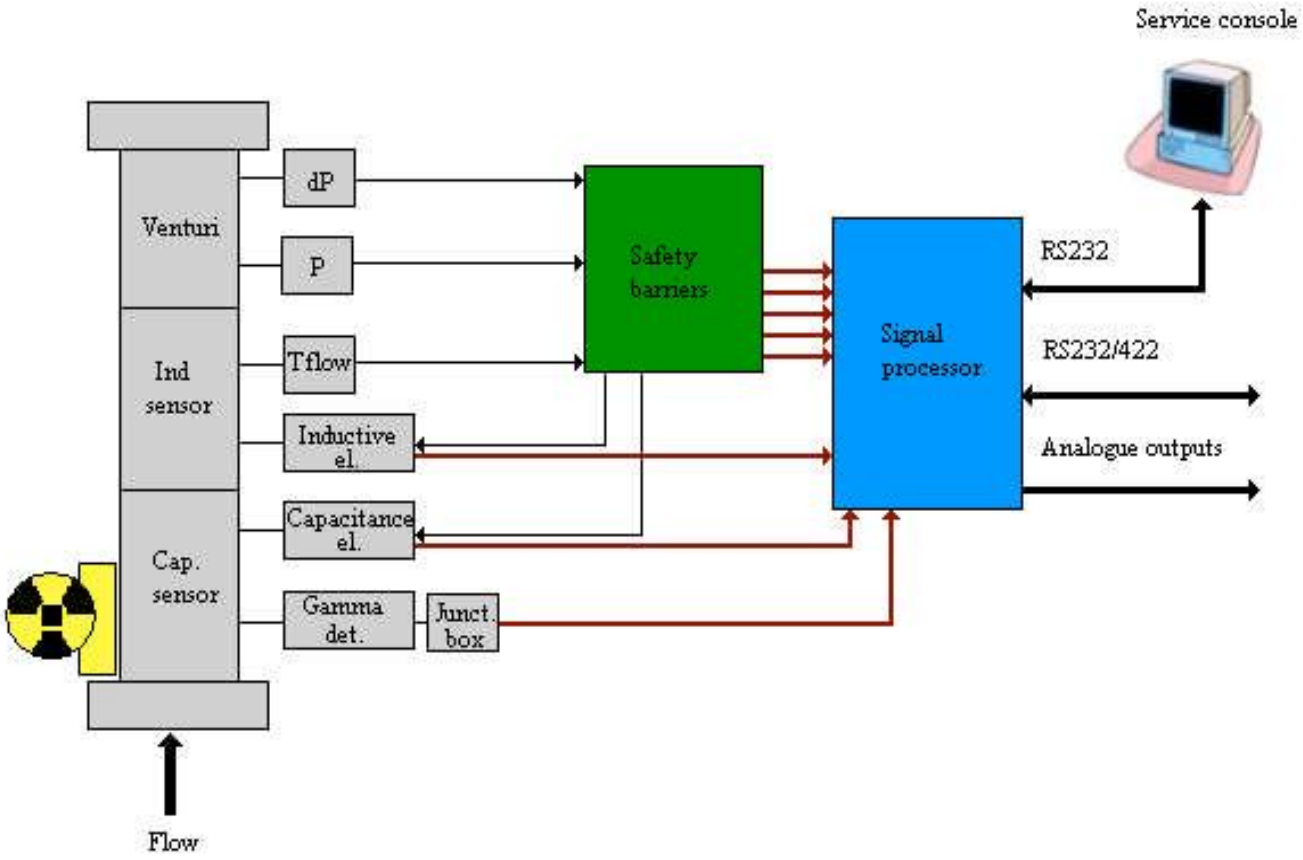


Figure 2.11 - Schematics of Roxar MPFM

A collimated gamma ray beam is directed at the pipe with a sensor placed diametrically opposite the source on the other side of the pipe. The intensity of the gamma beam

decays approximately exponentially as it passes through matter flowing in through the pipe measurement section. A gamma ray beam will be attenuated to different degrees by materials according to their density: a more dense material will attenuate the electromagnetic radiation to a greater extent than a less dense material. If the gamma source employed has two distinct energy levels, then this property can be exploited to determine the volumetric fractions of oil, water and gas in a three-phase mixture as the atomic attenuation coefficients depend not only on the density of a material but also on the energy of the gamma beam itself

The Roxar subsea multiphase meter as shown in Figure 2.12 is a compact, state of the art meter, which provides real-time, accurate measurement of hydrocarbon flow rates and water production. The meter has an operating range of 90 to 100% GVF, a quoted hydrocarbon mass flow relative uncertainty of ±5%, a water fraction measurement uncertainty of 0.1abs vol. % and water fraction sensitivity < 0, 0008 abs. vol. %. (Packman and Braaten, 2011)

Field tests of the Roxar subsea MPFM meter were undertaken by the Gulf of Suez Petroleum Company (GUPCO) in Egypt on seven wells. (Leggett et al., 1996). During testing, the flow regime observed was noted to range from severe slugging through to annular owing to the dynamics of the gas-lift production system employed (the average GVF ranged between 93 and 98%). It was reported that gas and liquid phase flow rates were measured to within ±10%, relative to the test separator, for GVFs in the range 93 – 96%. Significant errors were reported for liquid flow rate measurements in tests where the GVF was in excess of 96%.

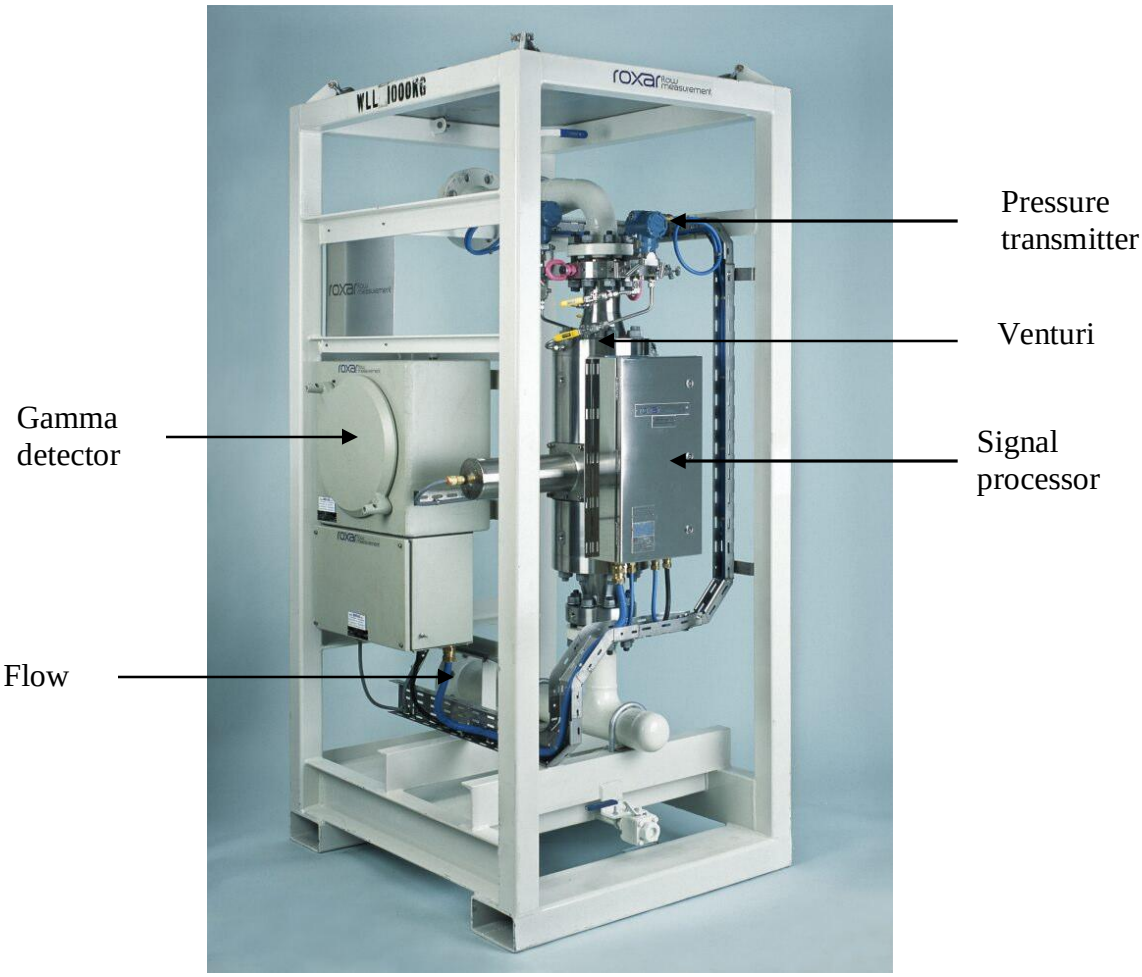


Figure 2.12 - Roxar MPFM

Roxar uses a gamma source (or sources) with different energies to determine the holdups of the three phases, and these measurements are coupled with velocity measurements to yield the required phase flow rates. Problems associated with this technique include

- shielding
- source decay
- averaging over the cross section
- fundamental statistical inaccuracies

- limitations in detection equipment
- effects of changing water salinity
- Operating sophisticated electronics for sub-sea applications.

### 2.6.3 Haimo MPFM Concept

The Haimo multiphase flow meter skid as shown in Figure 2.13 (Haimo, 2005) is another multiphase metering technique that consists of a cross correlation meter (two single gamma sensors), Venturi meter, dual gamma source sensor, gas conditioning cyclone, vortex meter and a static flow conditioner. It also includes two pressure transmitters, DP transmitter, temperature transmitter, an electric controlled control valve and a data acquisition and analysis system. Basically, phase fractions are derived from two separate independent measurements, i.e. water-cut in the liquid and gas fraction of the entire flow. Gas and liquid velocities are determined based on the cross correlation measurement and a slip relation included in the software model with the assumption that the difference between oil and water velocities can be ignored. Temperature and pressure are also measured and assumed equal in all phases. The system obtains the phase flow rates by determining the cross correlation areas occupied by each phase, and multiplying each area by the velocity of the corresponding phase. The gas conditioning cyclone reduces the amount of gas in the mixture by separating some of the gas away from the total flow and the separated gas is measured independently using the vortex flow meter. In the case of low GVF, the Venturi meter is used for measuring the total flow rate. The radioactive sources are 59.5 keV from Am-241 and the 22 keV that is created by a silver film that is irradiated by the 59.5 keV.

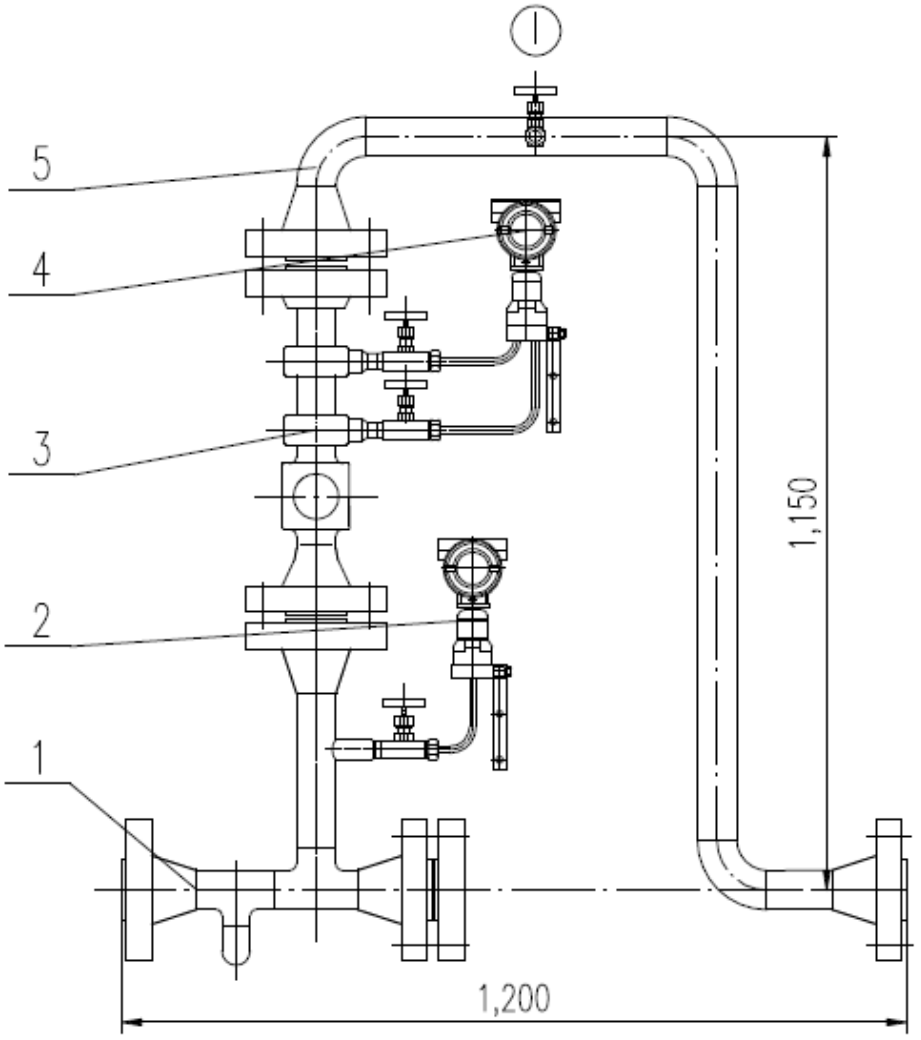


Figure 2.13 - Haimo MPFM

1: Inlet Blind T
2: Pressure transmitter (PT)
3: Venturi + single gamma sensor
4: DP transmitter
5: Outlet pipe
6: Exhaust valve
7: Junction Box (power converter board)
8: Junction Box (DAU)
9: Temperature transmitter (TT)

In the case of low GVF, the venturi meter is used instead for measuring the total flow rate. The radioactive sources are 59.5 keV from an Am-241 source and the 22 keV that is created by a silver film that is irradiated by the 59.5 keV.

In March 2005, Haimo claimed to have completed well tests on more than 1500 wells and to have over 100 MFM meters installed in onshore and offshore applications. (Haimo Newswire, 2005)

The Haimo MPFM is a combination of a gas/liquid two-phase flow meter and a full-range three-phase water cut meter. Net oil flow rate accuracy depends directly on the accuracy of the water-cut flow rate measurement. The higher the water-cut and worse the absolute accuracy of the water-cut, the poorer of the net oil flow rate in accuracy.

### 2.6.4 Accuflow MPFM

Figure 2.14 (Shen and Riley, 1998) shows the process flow scheme and major components of the Accuflow Multiphase Metering System (AMMS). This metering system consists of a vertical pipe section and a horizontal pipe section connected together. Multiphase fluid (oil, water and gas) from the production flow line enters the vertical pipe tangentially, creating a cyclonic action in the vertical pipe where the majority of the gas is separated and flows upward. The slightly downward inclination of the inlet pipe promotes liquid/gas stratification in the inlet pipe which enhances gas/liquid separation in the vertical separator pipe. The remaining gas, mostly in the form of small bubbles, is carried downward with the liquid stream and enters the horizontal pipe section

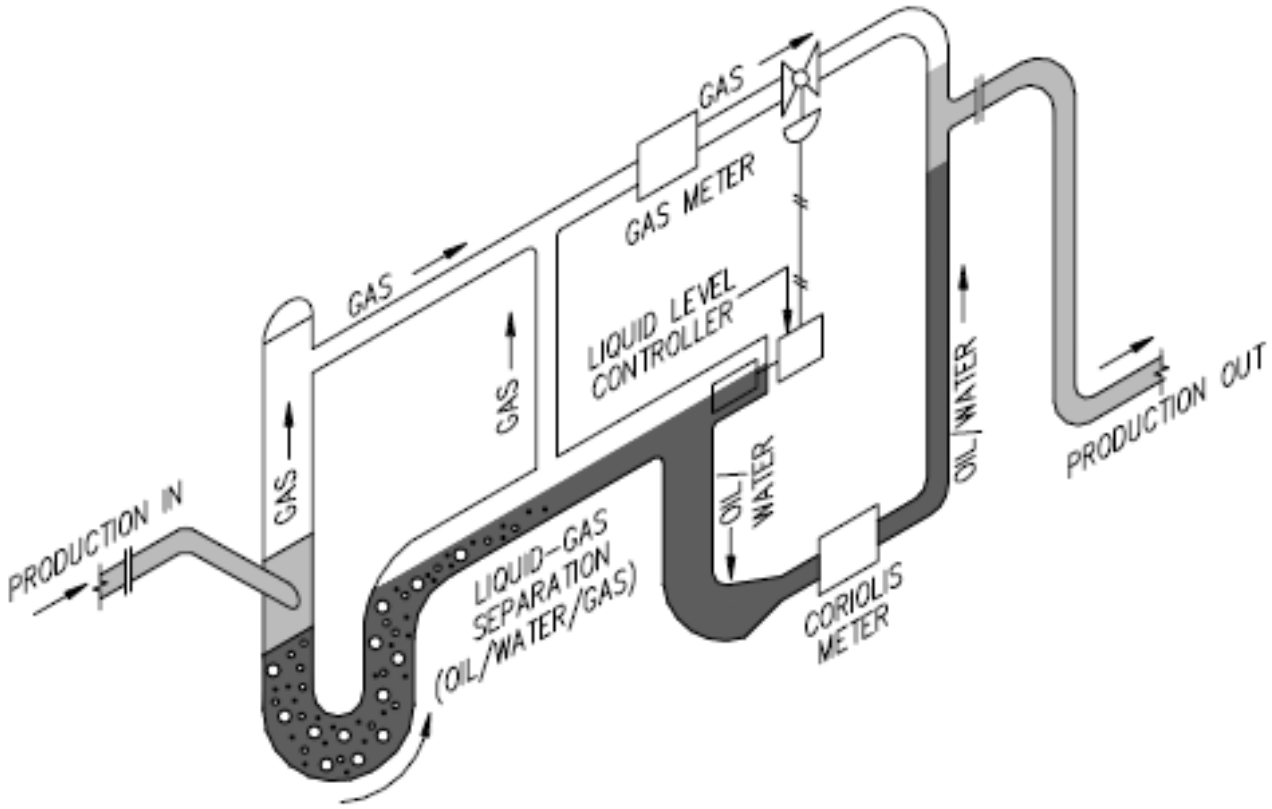


Figure 2.14 - Operating principle of the AMMS

The liquid level in the horizontal separator pipe section is controlled in the middle of the pipe using a control valve located in the gas flow line. As the liquid level in the horizontal pipe rises, a liquid level signal is transmitted to the gas control valve. This causes the control valve to "pinch" or close slightly and creates a slightly higher back pressure in the gas phase. The back pressure then "pushes" the liquid to flow at a higher-than-average flow rate that in turns causes the liquid level in the horizontal pipe to fall and stabilise to the set point. Conversely, when the liquid level falls, the control valve opens slightly to reduce the back pressure in the gas phase. This reduction of back

pressure causes the liquid to flow out of the system at a lower-than-average flow rate. Consequently, the liquid level rises and stabilises to the set point.

As the liquid stream flows through the horizontal pipe, gas bubbles rise to the gas/liquid interface and are completely separated as the liquid stream flows toward the outlet end of the horizontal pipe. The large gas/liquid interface area, thin gas-bearing liquid layer, and quiescent flow in the horizontal pipe, all contribute to the efficient removal of entrained gas bubbles from the liquid stream.

A Coriolis type flow meter is typically used to measure liquid flow rate and water cut in the liquid stream is measured with a conventional water-cut meter. A phase dynamics water-cut meter based on the microwave frequency shift principle is utilised in this application. The phase dynamics net oil transmitter receives the liquid flow rate signal from the Coriolis flow meter and is capable of performing net oil calculations and displaying net oil and water rates and volumes. For gas measurements, a conventional vortex meter is typically employed. In this particular application, a vortex meter supplied by Sierra Instruments is used. The Sierra vortex meter has built-in temperature and pressure sensors incorporated into the meter assembly. Its flow transmitter also performs temperature and pressure compensation calculations and displays the gas flow rate and volume at standard conditions. Following measurement, the gas and liquid streams are typically recombined and returned to the multiphase flow line.

*Advantages of this system:*

- Low cost, compared with multiphase meters and conventional separators.
- Compact and very portable.

- Low maintenance.
- High Efficiency > 90%

Accuflow claim that their patented pipe separator design can achieve complete gas-liquid separation and can thus employ conventional proven single-phase measurement devices to measure the separated phase streams (typically vortex or ultrasonic meters for the gas and a Coriolis meter for the liquid). The AMMS has been employed by Chevron Texaco in the Lost Hills and Cymric Oil Fields in California, USA, since 1996 (Shen, 1998). Chevron Texaco reported AMMS volumetric liquid measurements to within 2% of those of the test separator and agreement to within 3% was obtained for the liquid phase water-cut, however no gas phase measurements were performed. Accuflow reports its has installed units at 65 sites, in six countries, with similar measurement accuracies attained for flow rates of up to 30,000 bpd, and at water-cuts and gas fractions up to 99% (Dutton, 2004).

## 2.7 Pattern Recognition

Multiphase flows can distribute themselves in an infinite number of ways. Flow regimes are classifications that have been developed to describe, in general terms, multiphase flow geometry. The flow regime adopted by a multiphase flow is dictated by a number of parameters including operating conditions, fluid properties, flow rates, pipe geometry, and pipe orientation.

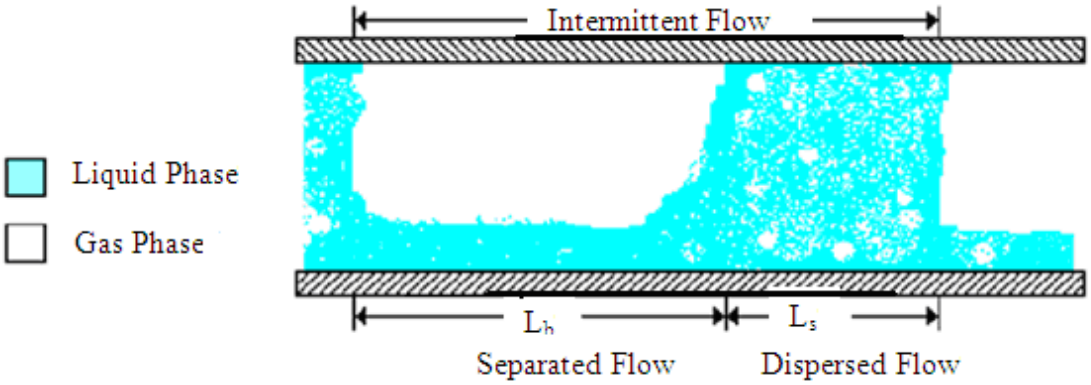


Figure 2.15 - Flow regime in a pipe

Researchers have reported a number of experimental-based methods to rationalise flow regime identification; data from sensors have been analysed using techniques such as template matching (Darwich et al., 1989), statistical analysis of signal responses (Stapelberg and Mewes, 1990), and fractal analysis (Franca et al., 1991). While these techniques enable the general classification of flows operating within particular regimes, describing the boundaries between flow regimes remains somewhat subjective as these are sensitive transitional areas rather than clear-cut boundaries.

These techniques were first developed by engineers dealing with flow abnormalities and the resulting behaviour of meter outputs. The proposed concept, described in technical briefs published by the NEL (Flow Measurement Guidance Note No. 15, 1998), uses an analysis of multiple sensor outputs and variations in sensor responses to determine the properties of the wet gas. These systems are characterised by their use of simple sensors combined with complex signal processing. Potentially they offer the cheapest hardware combined with the highest metering performance, and a major benefit of this technique is

that it is able to provide a low cost solution for specific applications, as one can use low cost sensors and available signal processing to solve the problem.

In wet gas measurement, which this project focuses on, pattern recognition techniques are also advocated as tools for identifying multiphase flow regimes and changes in the physical behaviour of the flow. Combined with appropriate sensors, a pattern recognition technique could potentially be used to notify a high-vapour sensor or high-water sensor of the presence of liquids or certain components in the flow. Combinations of sensors could then be turned "on" and "off" to gather appropriate data for the wet gas flow, depending on the pattern recognition analysis. At present, pattern recognition techniques can be used to enhance the performance of certain gas or liquid sensors. A typical "intelligent system" combines techniques for measuring phase volume fractions, such as gamma densitometry or electrical impedance tomography, with more conventional meters for measuring phase velocities or flow rates such as ultrasonic meters or Venturis. The system would then apply statistical analyses, neural networks, knowledge-based systems, or other pattern recognition (PR) techniques to objectively estimate phase flow rates from patterns in the unfiltered signals.

No standard exists for the application of such techniques to multiphase flows, and the area of wet gas flow measurement has not yet adopted pattern recognition measurement techniques. This may be due to the fact that pattern recognition tools must be customised to the sensors and the application, and cannot be treated as a "black box" that universally solves all measurement needs. This research considers the use of pattern recognition and velocity measurement as a necessary technology to provide a targeted solution to this form of metering.

### 2.7.1 Electrical Impedance Tomography

Electrical impedance tomography (EIT) is another class of non-intrusive phase fraction techniques. It relies on measurements of the variation in electrical properties of the flow to provide an image of the pipeline contents for measuring gas and liquid volume fractions in a multiphase flow. Depending on the properties of the flow, the instrumentation may actually determine the resistance, capacitance or complex impedance of the flow to locate the gas and liquid phases. The basic principle of the impedance and capacitance methods of component fraction measurement is shown in Figure 2.16 and 2.17. If the electrical impedance ($Z_e$) is measured across two electrodes, between which an oil-water-gas mixture is flowing, then the measured resistance ($R_e$) and capacitance ($C_e$) is given by:

$$R_e = \frac{1 + \omega^2 R^2 (C_m + C_p)^2}{\omega^2 R_m C_p^2} \qquad 2.6$$

$$C_e = \frac{[1 + \omega^2 R_m^2 C_m (C_m + C_p)] C_p}{1 + \omega^2 R_m^2 (C_m + C_p)^2} \qquad 2.7$$

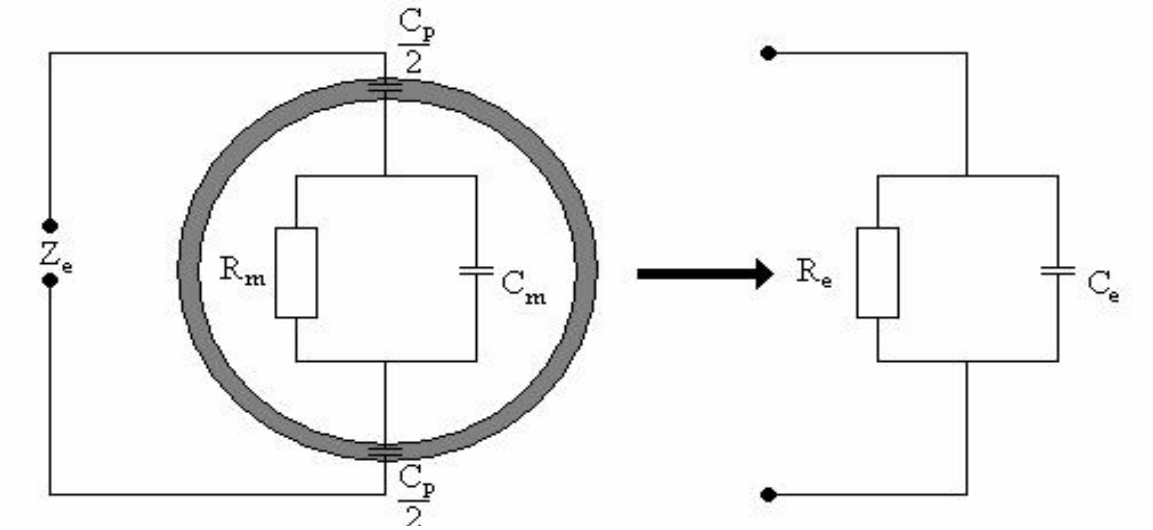


Figure 2.16 - Capacitance method of component fraction measurement

The resistance ($R_m$) and capacitance ($C_m$) of the mixture flowing through the pipe depends on the permittivity and the conductivity of the oil, water and gas components, the void fraction and the water fraction of the flow, and the flow regime. The resistance and capacitance measured across the electrode will in turn depend upon the $R_m$, $C_m$ and the excitation frequency ω of the detection electronics, geometry and material of the sensor.

In EIT, a number of electrodes are mounted to the surface of a pipe wall or other structure housing the flow as show in Figure 2.17. Applying between an electrical reference ground and each electrode, separately, an input electrical signal which, while applied to any one of the electrodes, causes the respective output electrical signals to be generated between the reference ground and each other one of the electrodes, measuring the output

electrical signals and processing the resulting measured data to provide a representation of the distribution, within the said material, of its electrical impedance (Wang et al., 2005)

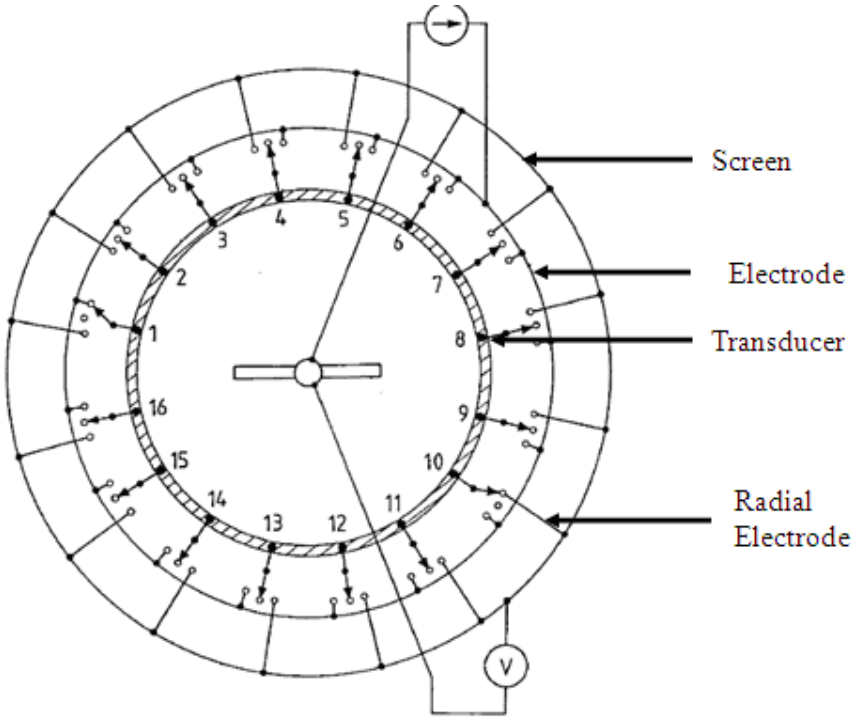


Figure 2.17 - Multi-electrode ECT in a circular sectional vessel

Finally, the phase distribution is inferred from the computed impedance distribution. The equations that relate the impedance and voltage distributions in the flow must be solved iteratively to obtain the impedance distribution that corresponds to the measured boundary voltages. In some applications, a controlled voltage is applied to the electrodes and the current is measured, but the same iterative process is followed to arrive at the phase distribution of the flow.

The resolution of the image of the phases is strongly related to the number and size of electrodes present. As the number of electrodes and the resolution increases, the sensitivity to noise also increases. Currently, some systems are capable of real-time imaging of the phase distribution, but this is an eventual goal of every EIT system. More information on EIT theory and the development of EIT systems for the study of multiphase flows can be found in articles by Dickin et al. (Dickin et al., 1993) and Ceccio and George (Ceccio and George, 1996).

Hall (Hall, 2000) carried out several studies assessing the accuracy of EIT in gas-liquid flows which were conducted at the Sandia National Laboratories. The Sandia system was initially used to measure air-water distributions in a vertical column resembling a chemical reactor. Rather than concentrate on imaging the phase distribution, this work sought to improve the accuracy of measured gas and liquid volume fractions at different locations in the column. For flows with gas volume fractions from 0 to 15%, the average values and radial gas distributions determined by EIT agreed with the measurements from a gamma densitometry system to within 1% of the volume fraction. Though these bubble column flows differ from wet gas pipeline flows, the tests suggest that EIT may be capable of accurately measuring volumes of gas and liquid in such flows. Work has also begun on an EIT system capable of operating in an electrically conducting column, which would enable the concept to be applied in pipeline environments.

More relevant tests of EIT technology were conducted at NEL with a mixture of crude oil, water and nitrogen. In the NEL tests (NEL, 2001), an electrical capacitance tomography (ECT) system was installed around a perspex spool piece through which the horizontal three-phase flow could be videotaped. While the system successfully visualised the

various flow regimes, quantitative measurements of the gas volume fraction showed significant errors of the order of 20% of the reading when the water-cut of the three-phase flow exceeded 5% by volume. However, volume fractions of two-phase oil and water flows could be more accurately measured with ECT, particularly at low flow rates. Improvements in the reconstruction algorithm, or the use of ECT with other measurement techniques, may be needed to improve the accuracy of volume fractions determined by this method. Improved accuracy will also be needed for EIT to become acceptable for oil and gas allocation, and eventually for the identification of wet gas flows.

The Flowsys meter is a capacitance and inductance based meter that comprises of a Venturi with the standard differential pressure and temperature sensors. In the throat of the Venturi an array of permittivity and conductivity sensors are used to measure both the liquid and gas velocities by means of cross correlation, hence, the velocity (flow rate) measurements are not performed by the Venturi. Instead, the Venturi is used to measure the fluid density which is an indication for the GVF. The permittivity and conductivity measurements are used to split the liquid into water and oil. The key features are that the equipment is very simple and thus the manufacturing costs can be kept to a minimum. No separation devices, flow conditioners, mixers, by-pass lines or radioactive sources are used in the TopFlow concept. A picture of the FlowSys TopFlow meter as installed in Shell's Rabi field in Gabon is presented in Figure 2.18 (Hall, 2000) and the principle of operation can be summarised in the block diagram of Figure 2.19. The $\Delta P$ is measured across the inlet and throat of the Venturi insert and the electrodes inside the Venturi throat measure the capacitance or conductance of the mixture flowing through the Venturi insert. The velocity is found from cross-correlating the high resolution time

signals from pairs of electrodes within the Venturi insert. Unlike most other meters, as there is no gamma densitometer, the FlowSys meter does not measure the fluid mixture density directly. Instead, the density is determined indirectly through the momentum equation of the Venturi. The set of equations utilised in the calculations of the fractions are listed below (Hall, 2000):

$$Cap/Con = f(\alpha_{oil}, \alpha_{water}, \alpha_{gas}/\sigma_{water}) \quad 2.8$$

$$Density = f(\Delta P, Velocity) = f(\alpha_{oil}, \alpha_{water}, \alpha_{gas}, \sigma_{water,} \rho_{oil}, \rho_{water}, \rho_{gas}) \quad 2.9$$

$$\alpha_{oil} + \alpha_{water} + \alpha_{gas} = 1.0 \quad 2.10$$

Note that capacitance and oil permittivity ($\varepsilon_{oil}$) is applicable for oil-continuous mixtures while conductance and water conductivity ($\sigma_{water}$) applies for water-continuous mixtures. The capacitance or conductance, $\Delta P$ and velocity are the input measurements and are measured by the electrodes and $\Delta P$ transmitter. The permittivity of the oil ($\varepsilon_{oil}$), water conductivity ($\sigma_{water}$) and densities of oil, water and gas ($\rho_o$, $\rho_w$, $\rho_g$) are input parameters entered into the user interface. The fractions of oil ($\alpha_{oil}$), water ($\alpha_{water}$) and gas ($\alpha_{gas}$) are calculated from the equations above.

Figure 2.18 - FlowSys MPFM during test

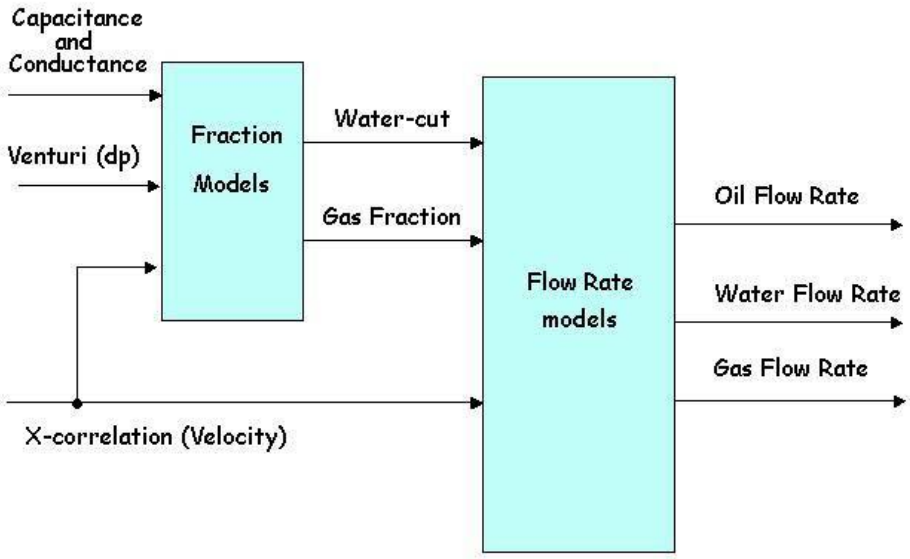


Figure 2.19 - Schematic diagram of FlowSys meter

The Water-in-Liquid Ratio (WLR) or water-cut is defined as:

$$WLR = \alpha_{water} / (\alpha_{oil} + \alpha_{water}) \quad 2.11$$

The set of equations for the calculation of flow rates $Q_{oil}$, $Q_{water}$ and $Q_{gas}$ are listed below:

$$Q_{oil} = AV\alpha_{oil} \quad 2.12$$

$$Q_{water} = AV\alpha_{water} \quad 2.13$$

$$Q_{gas} = AV\alpha_{gas} \quad 2.14$$

The cross sectional area of the pipe ($A$) is based on the geometry of the Venturi, the velocity ($V$) is measured by cross-correlating the electrical signals from the electrodes, and finally, the fractions of oil, water and gas are found from the set of three equations above.

Laboratory testing of the FlowSys meter was undertaken at NEL (Hall, 2000). The test matrix was comprised of a number of points with liquid and gas flow rates ranging between 0-60 $m^3/h$ and 0-340 $m^3/h$, respectively. Liquid phase and oil flow rate measurements obtained were within a relative uncertainty band of ±5%. However, for test points with a GVF greater than 70% or water-cuts in excess of 75%, large deviations from the reference values were observed. The gas flow rate measurements were found to be within ±20% across a large proportion of the operating envelope.

Further laboratory testing of the TopFlow MPFM was carried out by Christian Michelsen Research (CMR) (Klepsvik et al., 2000). The test matrix was comprised of a number of points with liquid and gas flow rates ranging between 15-40 $m^3/h$ and 20-90 $m^3/h$, respectively. It was reported that 99% of the liquid flow rate measurements were within a

relative deviation of ±10% from the reference values, 78% of oil flow rate measurements were within ±10% and 84% of the gas flow rate measurements were within ±15%.

In 2001, a FlowSys TopFlow meter was field tested by Eni in Trecate, Italy (Mazzoni et al., 2001). It was documented that the FlowSys meter gave phase flow rate measurements within ±10% for GVFs up to 92-93% for the gas flow rate and GVFs of up to 86-87% for the liquid flow rates. Liquid and gas flow rates ranged between 6-35$m^3$/h and 35-145 $m^3$/h, respectively. However, at GVFs in excess of 92-93%, the liquid flow rate measurement accuracy deteriorated to approximately ±20%. Owing to the limitations imposed by the test wells, the water-cut was only examinable between 41-51%, and for this range it was reported that the meter was able to classify the majority of the test points to within ±5%.

The FlowSys meter has been extensively tested and the results reveal that within the operating envelope of the meter, relative errors in the order of ±10% for liquid could be achieved. For water-cut measurements a distinction between oil continuous and water continuous emulsions needed to be made. For oil continuous emulsions the water-cut measurement is within ±5% (absolute) while for the water continuous emulsions ±10% (absolute) is a more realistic figure. The test programme has shown that the FlowSys meter is robust with no operational problems of any kind or failure of any parts having been experienced, and the meter is an attractive candidate in the low cost MPFM market.

## 2.8 Particle Image Velocimetry

Particle image velocimetry (PIV) is a non-intrusive technique measuring the velocity of particles entrained in a flow of interest (Meinhart et al., 2000). PIV is accomplished by

introducing seed particles into a flow field, and if properly sized, these particles will accurately follow the flow field. To determine the particles' velocity they are illuminated, typically by a laser sheet at least twice within a known short time interval. The light scattered by the particles is then captured as a series of images timed coincident with the laser pulses and software is used to correlate reflections from different frames to estimate particle paths. The differential of each particle's displacement is then taken in order to estimate the velocity based on the time between laser pulses.

Successful PIV is largely dependent on having the correct seed particles, in the area of interrogation. These seed particles must be small enough to accurately follow the flow and large enough to be accurately recorded and processed for velocity determination. Furthermore, there must be a sufficient number of particles within each interrogation region to yield adequate spatial resolution of the flow. The measurement is indirect, via the displacement of moving particle groups within a certain time interval. For this purpose the flow is seeded homogeneously with appropriate particles. It is assumed that the particles are small enough to move with the local flow velocity.

Figure 2.20 and 2.21 (Wieneke, 2005) presents a flow chart and pictorial representation of the PIV evaluation process which it attempt to step through the sequence and stages of the analysis to the point where flow rate is outputted.

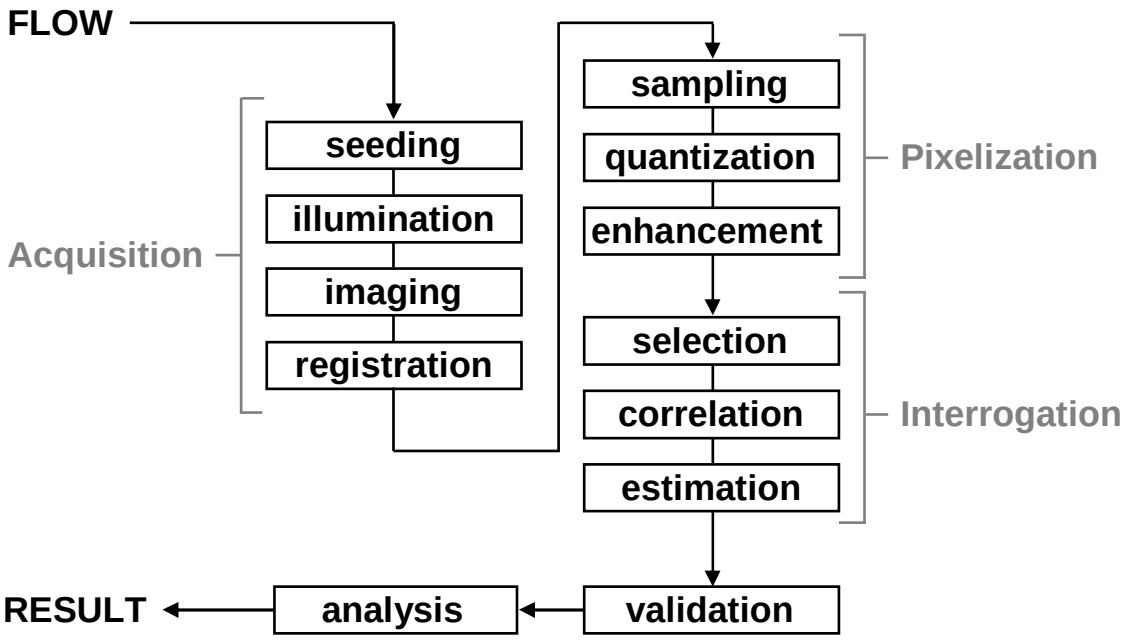


Figure 2.20 - Flow chart of PIV process

As represented in Figure 2.20, the basic requirements for a PIV system are an optically transparent test-section, an illuminating light source (laser), a recording medium (film, charge coupled device (CCD), or holographic plate), and a computer for image processing. This review addresses the basics of the PIV technique such as PIV algorithms, optical considerations, tracer particles, illuminating lasers, recording hardware, errors in PIV measurements, and PIV vector processing.

A plane within the flow is illuminated twice within a short time interval by a laser sheet. The duration of the illumination light pulse must be sufficiently short that the motion of the particle is frozen during the pulse exposure in order to avoid blurring of the image. The light from each pulse scattered by the seed particles is recorded by a CCD sensor on separate frames. The time delay between the illumination pulses must be long enough to

be able to determine the displacement between the images of the tracer particles with sufficient resolution, whilst short enough to avoid particles with an out-of-plane velocity component leaving the light sheet between subsequent illuminations. Analysing one image pair it is possible to identify the path a particle has travelled, and knowing the time delay between the two pulses, allows the velocity to be calculated. The time interval between two pulses has to be adjusted according to the mean flow velocity and the magnification of the camera lens, and the particle displacement must be small relative to the nest flow scale to be resolved.

After determining the displacement, Δx, of each interrogation spot using equation 2.15, the quantity is divided by the magnification factor M of the image system to calculate the first order approximation of the velocity field, u, equation 2.16 as follows:

$$\int_{t}^{t+\Delta t} u(t')dt' \approx \Delta x \qquad 2.15$$

Hence

$$\frac{\Delta x}{\Delta t} = \frac{\Delta X}{M\Delta t} \approx u \qquad 2.16$$

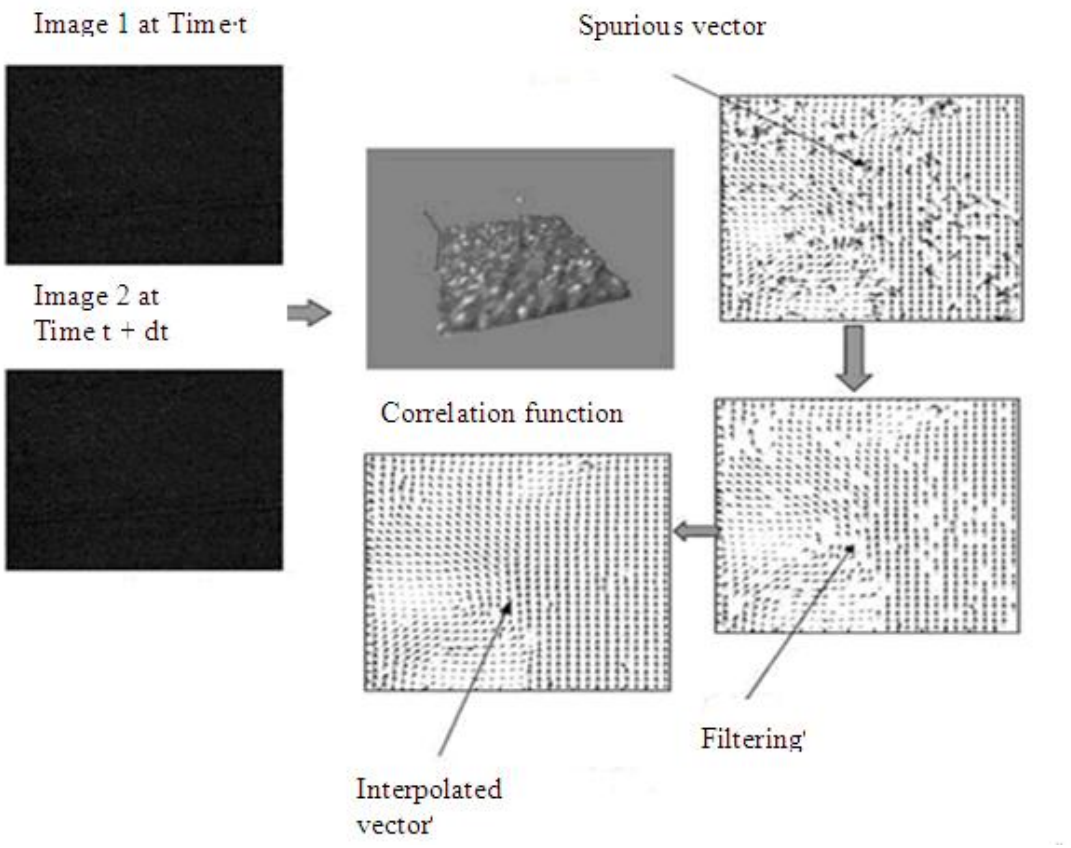


Figure 2.21 - Schematic of image process flow

## 2.9 Cross Correlation

Cross-correlation is a computational technique commonly used in signal processing to compare the similarity of two signal samples and for a given spatial shift (Lindken and Merzkirch, 2002). For this work, cross correlation function is defined as a measure of how closely the two image maps (these two image maps were recorded at a fixed time interval) or regions within the two image maps correlate with one another when offset by a number of pixels (m, n). The highest value for R (m, n) is taken as the true correlation, where 'm' and 'n' are the number of pixels defining the vector by which the image was shifted. This vector is the output of the cross-correlation function, and it is multiplied by

a scale factor in order to calculate an average displacement. The scale factor utilised is the ratio of distance in the image plane to distance on the CCD, also known as pixel pitch. It is a function of the distance from the experimental plane to the CCD, as well as the magnification of the camera's lens.

Although the cross-correlation technique seems straightforward and relatively simple, and there exists many correlation algorithms, there is a major pitfall: the correlation here is of disturbances and not fluid velocities. In a fully developed turbulent flow the larger eddies exist longer, and thus contribute preferentially, to the cross-correlation function. It would be expected that in a gas-continuous flow, the velocity of the larger droplets is measured (provided the timing between the two frame is not too large), ignoring the liquid at the wall, and to a lesser extent the velocity of the small droplets. As water and oil in such a flow tend to have different velocities and different size distributions (the surface tension of water is significantly higher than that of hydrocarbon liquid in a hydrocarbon gas), this easily gives rise to bias (systematic error). In a gas-continuous flow, measurement of the gas can only be achieved using seed particles, which would generate only small signals (compared to the droplets) and thus easily be missed or drown in the contribution of droplets. In addition, the calculation of the superficial gas velocity requires an accurate number for the hold-up. In bubbly flow, the above mentioned problems are less severe (as the mass of a bubble is small and the forces acting on it are large), so a better result would be obtained; however, the optical problems do not disappear. The problems anticipated and encountered with respect to correlation method will now be further elucidated.

Considering a small time scale, the signals within an interrogation region of the image map will shift in proportion to its velocity, but remain relatively unchanged. Therefore, if the first image is offset in proportion to the true flow velocity, the interrogation regions within the two image maps should line up and correlate with one another. That shift, combined with the knowledge of the elapsed time between signals, corresponds to velocity. In digital PIV, the two image maps are the signals and the shift must be determined in the two dimensions that the camera is observing. The shift determines the average displacement vector between samples of two image pairs and the cross-correlation function for two discretely sampled images of the same size m (i,j) and n(i,j) is defined as:

$$R(m,n) = \sum i \sum I_1(i,j) I_2(i+m, j+n) \qquad 2.17$$

In direct cross-correlation, the image maps are shifted by every possible value to determine the highest cross-correlation value. This makes direct cross-correlation computationally intensive. For a given interrogation region of area N, the number of operations which must be computed is of the order of N4. By introducing the Fast Fourier Transform (FFT) into the cross-correlation algorithm, the computational effort is of the order of 2Nln (N), a considerable decrease compared to N4. In this technique, the Fourier transform is taken of each image map, next, instead of performing a sum over all the elements in the sampled interrogation region, the complex conjugates of each corresponding pair of Fourier coefficients from the transform of each image map are

multiplied. The products are then inversely transformed, resulting in the cross correlation function in Cartesian coordinates.

## 2.10 Inferential Method of Multiphase Determination

The fundamental function of a multiphase flow meter in the oil and gas industry is to supply the user with information on the mass flow rate of oil, water and gas components in a flow. Ideally, a flow meter should simply take direct measurements of each of these three quantities; unfortunately, direct mass flow meters for multiphase flow measurement do not exist.

As direct mass flow rate measurement in multiphase flow is yet to be achieved, the approaches mentioned above use inferential methods instead, and multiphase flow metering systems are dependent on primary variables:

- Phase Fractions
- Phase Velocities
- Phase Density

Together with to some extent secondary variables such as:

- Flow Regime
- Phase Viscosity
- Phase Salinity

Evaluation of the primary variables is a prerequisite in applying the inferential method for multiphase flow measurement. Determination of the secondary variables is not strictly required and is not considered in this thesis, but could facilitate more accurate measurements if taken into consideration. The flow regime parameter may be considered

a primary variable if a flow regime dependent sensing technique is used in the determination of the core primary variables.

The inferential method requires the resolution of the instantaneous velocity, cross-sectional fraction, and density of each component in order to be able to calculate the individual flow rates and the total mixture flow rate as shown in Figure 2.22.

Density data for all three components is readily available from other parts of the production process or can be estimated using phase diagrams. Thus, the problem the measurement of the component velocities and two of the three component volume fractions, usually the gas phase and the liquid phase water fractions, in order to calculate the total mass flow using the following expression:

$$G_t = \alpha V_g \rho_g + \beta V_w \rho_w + (1 - (\alpha+\beta)) V_0 \rho_0 \qquad 2.18$$

Where it is assumed that:

$$\alpha+\beta+\gamma = 1 \qquad 2.19$$

Where:

$G_t$ is the total mass flow rate of hydrocarbon gas and liquid under measurement.

$\alpha$, $\beta$ and $\gamma$ are the phase fraction of gas, condensate and water respectively.

$V_g$, $V_w$ and $V_o$ are the flow velocities of gas, water and condensate respectively.

$\rho_g$, $\rho_w$ and $\rho_o$ are densities of gas, water and condensate respectively.

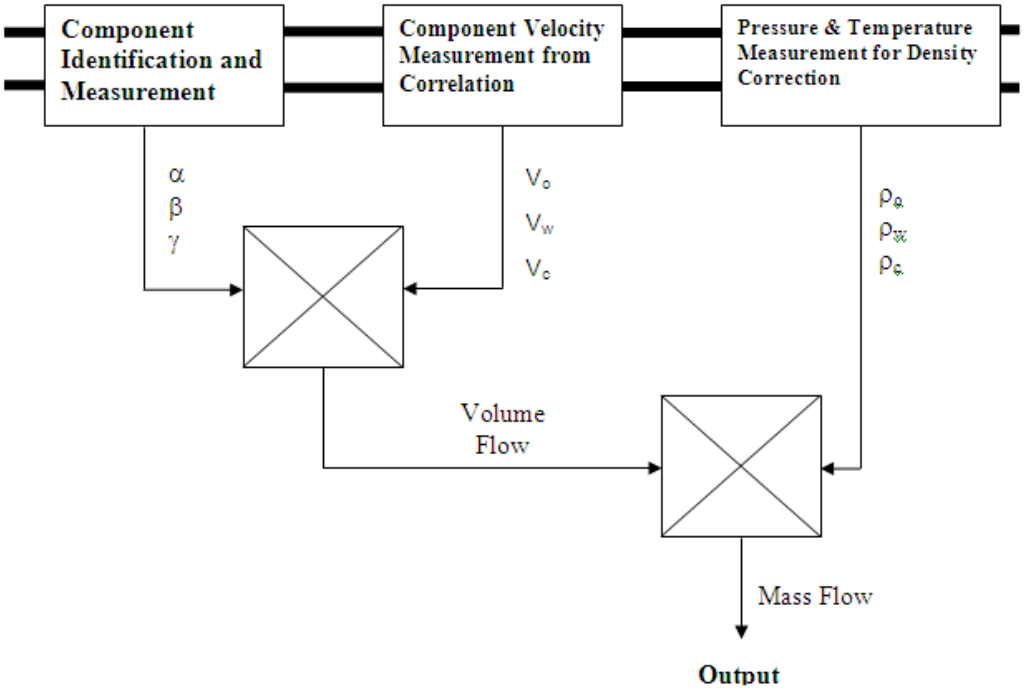


Figure 2.22 - Flow determination process

It is common practice to simplify the problem by assuming that the liquid phase velocity parameters are equal, thereby reducing the number of unknown variables to five, and homogenisation of the multiphase mixture may be employed to reduce the velocity parameters to a single uniform mixture velocity (Hewitt, 1989).

## 2.11 Conclusions

Although to date a generic solution to MPFM does not exist, adequate methodologies are emerging for specific applications. The quality of the results achievable using existing commercial MPFM solutions depends on the appropriateness of the work that operators must undertake during the pre-engineering phase of an MPFM application.

Each project in the oil and gas industry has specific requirements for production measurements, which are driven by the hardware costs and the value of the information obtained by the measurements (this includes the uncertainty of the measurement). MPFMs can contribute significantly to cost savings if they are used as a replacement for conventional test separators. The need for a MPFM on a per well basis results from other than production facility layout considerations, for example where sub-surface or production optimisation considerations are more dominant.

# Chapter 3: METHODOLOGY

In this section, the work of a temporal MPFM entitle Uletech is presented. Analysis of the current technologies, as summarised in Table 3.1 suggests that only the Flowsys multiphase meter meets all the conditions of a true MPFM. The ideal multiphase meter should be non-intrusive, have no form of phase separation, should require no flow conditioning like pre-mixing, and should not use radioactive isotopes due to adverse environmental and possible health impacts.

Table 3.1: Summary of some existing multiphase meter technologies

| | Agar | FlowSys | Roxar | Haimo | Schlumberger Vx |
|---|---|---|---|---|---|
| **Flow Condition** | In-line separation | Leave-as–it-is | Leave-as–it-is | In-line separation | Leave-as–it-is |
| **Gamma Source** | Not used | Not used | Used | Used | Used |
| **Intrusive** | Yes | No | No | No | No |
| **Cross Correlation** | Yes | Yes | Yes | Yes | No |

The solution proposed by this researcher, like other image based systems, stems from what has been used within hospital for many decades - ultrasound. Doctors have been able to use ultrasound scan technology to view the foetus in the womb without causing harm or known distress of any kind through image reconstruction. Through the use of an

ultrasound scanning machine doctors have been able to accurately predict sex, age and the weight of a foetus.

PIV is a technique, which by placing high resolution laser cameras within the pipeline, allows graphical images of the flow to be obtained, and it is possible to 'count' the flow particles through a pipeline (Waelchli and Rudolf, 2006). This may be considered as point measurement and can also be viewed as non-continuous, but the fact that the camera is capable of capturing so many image frames per second of the flow through the measurement spool makes it possible to produce accuracies of custody transfer quality almost continuously with sufficient resolution for industrial applications.

The design philosophy is based on the following facts:

- All matter is composed of discrete elements or a combination of elements called a compound, which can be distinctly identified.
- Via the use of a powerful light source such compounds can be made visible and be accounted for.
- By injecting tracers at known rates and then analysing a sample of the multiphase flow sufficiently far downstream of the injection point, liquid phase flow rates can be determined by measuring the dilution of the tracer in the sample.

However, the phases (gas and liquid) move with different velocities due to liquid hold-up at the wall (slip), and the "correlation" to an "overall" flow rate is only possible if the velocities of both phases are known. This is one of the elementary, but essential, problems of multiphase flow metering (Fries et al., 2007).

## 3.1 The Uletech Meter Scheme

The proposed multiphase flow meter is based on a combination of particle recognition in the form of PIV for the gas phase and tracer dilution for the liquid phase. PIV basically uses seed particles which are supposed to follow the gas phase but require excitation by a source light. A high resolution digital camera capable of identifying/recognising the particles within the flow is required.

Figure 3.1 provides a schematic of the proposed Uletech flow meter. Upstream of the camera, micron-sized particles are injected from the tracer bottle by a metering pump and become entrained in the flow. The flow is then illuminated with a sheet of monochromatic light from a pulsed laser generated by a laser light. This light reflects off the particles and is sensed and recorded by a CCD digital camera timed to be coincident with the laser pulses, and both the laser source and the camera are controlled by a computer to achieve synchronous flashing and data recording. Software is then used to correlate the reflections from two consecutive frames in order to estimate particle paths based on cross correlation.

The differential (spatial displacement) of the particles is then determined to estimate the velocity via the displacement and the time taken between laser pulses. This process is performed for each pixel across the illuminated area of the flow, thereby creating a 2-D map of the particle velocity distribution. The resulting velocity measurements are therefore indirect measurements of flow velocity, as they are the velocity of the particles entrained in the flow.

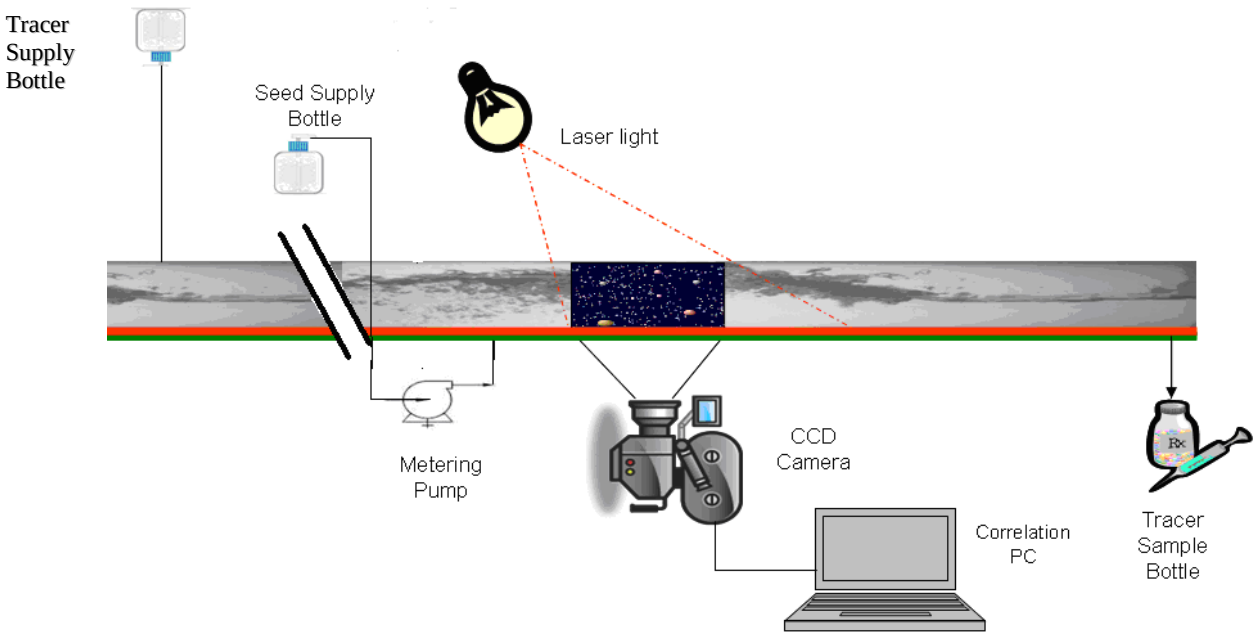


Figure 3.1 - Schematic of proposed "*Uletech*" multiphase flow meter

A simple algorithm that correlates the particle displacement to the volume within the pipes internal diameter has been developed based on the fact that each phase occupies a fraction of the total cross sectional area of the pipe. The superficial phase velocity is defined as the flow velocity of one phase, assuming the phase (gas or liquid) occupies the whole conduit.

For a single-phase gas travelling through a pipe of cross sectional area **A** at an average velocity **V**, the volumetric flow rate *Q* can be calculated by:

$$Q = AV \qquad 3.1$$

When an oil and gas mixture is flowing through the same pipe, then the calculations of the volumetric flow rates are more complicated. A simple approach to estimate the volumetric flow rates for each phase is to establish the distribution of each phase (as illustrated in Figure 3.2) by assuming that each phase is occupying a fraction of the total cross-sectional area at any instant, which can be determined by the following relationships:

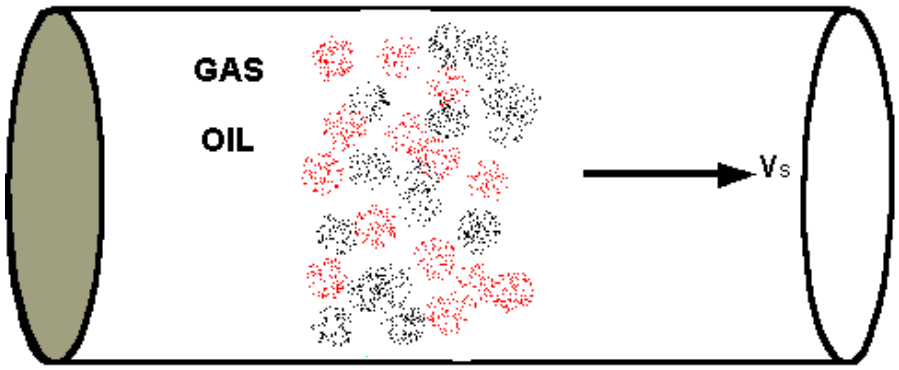


Figure 3.2 - An approximate model of the multiphase flow

$$\alpha = A_o/A \qquad 3.2$$

$$\beta = A_g/A \qquad 3.3$$

$$\alpha + \beta = 1 \qquad 3.4$$

Where $\alpha$ and $\beta$ are the volume fractions - fraction of cross sectional area A occupied by the oil and gas phases in the mixture.

The volumetric flow rate ***Q*** of each phase and the total (mixture) flow rate are then determined by:

$Q_{oil} = A\ \alpha\ V_{oil}$ 3.5

$Q_{gas\text{-}pr} = A\ \beta\ V_{gas}$ 3.6

Where the area A of the pipe is defined as $\pi r^2$

Where $Q_{oil}$ and $Q_{gas,}$ are the volumetric flow rates for oil and gas phases in the mixture. For the work on PIV, only the gas flow velocity is determined and consequently, the compensated gas flow rate $Q_{gas}$ is given by the following algorithm:

$$Q_{gas} = Q_{gas-pr} * \frac{P_f}{P_b} * \frac{T_b}{T_f} \quad 3.7$$

Where $Q_{gas\text{-}pr}$ is the volume flow rate under prevailing conditions of pressure and temperature; $P_f$ and $T_f$ represent the prevailing conditions of pressure and temperature, respectively, and $P_b$ and $T_b$ represent standard conditions of pressure and temperature, respectively.

$P_b$ = 1 atm (14.7 psia)

$T_b$ = 20°C (68)

The condensate flow is measured by injecting the tracers (e.g. fluorescent dyes) at a known flow rate, which mixes only with the liquid phase. By analysing a sample of the multiphase fluid taken sufficiently far downstream of the injection point, and combining this with the injection rate, the individual phase flows can be determined using the following equation:

$$Q_p \approx \frac{C_i}{C_p} Q_i \quad 3.8$$

Where:

$Q_i$ is the volumetric flow rate of tracer solution into the flow line, $m^3/s$

$Q_p$ is the volumetric flow rate of condensate phase in the flow line, $m^3/s$

$C_p$ is the concentration of fluorescent tracer in the flow line, $mol/m^3$

$C_i$ is the concentration of fluorescent tracer in the injected solution, $mol/m^3$

The compensated liquid flow rate is given by:

$$Q_{oil} = Q_p * \frac{P_f}{P_b} * \frac{T_b}{T_f} \quad 3.9$$

The experimental setup for this work is in two parts the first for gas flow measurement using the PIV technique, and the second for liquid flow measurement using tracer dilution, which will be discussed in Chapter 4.

## 3.2 Measurement of Gaseous Phase

The average gaseous phase velocity is measured using PIV. As mentioned above, PIV has the ability to capture the spatial velocity distributions for a whole field simultaneously with high resolution. This technique is also non-intrusive as there is no probe disturbing the flow. The PIV system setup consists of two major functional units: the control unit and the measurement unit for the imaging technique, as shown in Figure 3.3. The control unit is further divided into two sections or sub-units – the synchroniser and the computer. The measurement unit, otherwise called the transducer, is sub-divided

into three units; the flow imaging block, the image capture block and the image analysis block. Each of these five functional blocks is described in detail in the following sections.

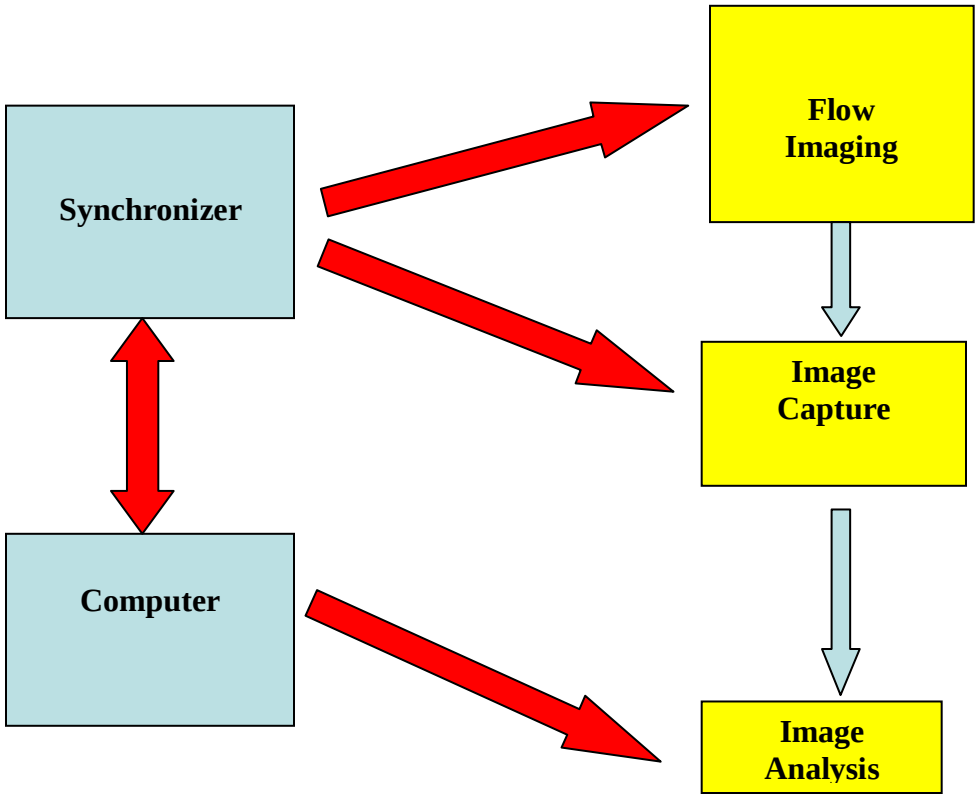


Figure 3.3 - PIV system block diagram

### 3.2.1 Seed Particles (Flow Imaging)

For the gas flow to be made visible it has to be seeded. The choice of seed particles is important, as the measured displacement velocity is not a direct measurement of the flow velocity, but of the particles entrained in the gas phase. Therefore, the accuracy of the measurements is directly limited by how closely the entrained particles follow the gas flow. The ideal seed particles should be inert, neutrally buoyant, and small enough to

accurately follow the flow of the hydrocarbon gas phase. Smaller particles are preferred for such applications because their relatively low inertia allows them to more accurately follow the flow. To illustrate this point consider two particles of the same substance and shape but of different sizes entrained in the same flow. The smaller particle will experience higher viscous and pressure forces, with respect to its own inertia, compared to a larger particle. The primary reason is as overall size decreases, the ratio of surface area to internal volume, and therefore mass, will increase. A simple example can be illustrated by taking the ratio of surface area to volume for a sphere:

$$\frac{SurfaceArea}{Volume} = \frac{4\pi r^2}{\frac{4}{3}\pi r^3} = \frac{3}{r}\alpha\frac{Surface}{Mass} \qquad 3.10$$

Assuming constant density, volume can be replaced by mass in the denominator. This illustrates how the ratio becomes a comparison of the area over which sheer forces act for a given amount of inertia, and explains why smaller particles will follow a turbulent or quickly changing flow more closely than larger particles. Although larger particles have the ability to scatter more lights, smaller particles are still preferred due to their ability to more closely follow turbulent flow, making the measured variable more representative of the sample.

In addition, it was also thought beneficial to match the density of the seed particles to that of the hydrocarbon gas flow. This is because when the particle density is not matched to the flow, the particle is expected to experience a body force due to gravity, as well as different loading in a turbulent or turning flow.

***Selection of seed particles***

Traditionally, seed particles for gas flows have included solid particles such as polystyrene, aluminium oxide, magnesium oxide, titanium dioxide and dioctylphathalate, as well as atomised liquids such as glycol, silicone oil, etc. Successful PIV measurements have been achieved in gas flows using a variety of seed material and Raffel et al. (1998) provided a summary of common seeding materials for gas flows, as presented in Table 3.2.

Table 3.2: Common Seed Materials

| Class | Examples |
|---|---|
| Irritant | Ammonia, Sulphur Dioxide |
| Asphyxiant | Nitrogen Dioxide, Carbon Monoxide and Dioxide |
| Anesthetic | Aliphatic Hydrocarbons, Ethyl Alcohol |
| Systemic Poison | Heavy Metals, Carbon Tetrachloride |
| Sensitizer | Isocyanates, Formaldehyde |
| Fibrotic Agent | Silica, Coal Dust |
| Mutagens and Carcinogens | Arsenic, Asbestos |
| Nuisance | Alumina, Kaolin, Magnesia |

Although this is not a comprehensive list of all seed materials, it provides further substantiation that seed particles of the order of 1 to 10 microns are widely used and suitable for the purposes of PIV. As noted earlier, smaller particles are more appropriate for high-speed flow fields.

Reeder et al. (Reeder et al., 2010) suggested two seeding systems that have the potential to provide such a solution. The first system is a new concept which uses liquid carbon dioxide that can be made to form discrete particles as it expands from a high-pressure tank. PIV measurements have been demonstrated in several flows, including supersonic

and subsonic tunnels, using these residue-free seed particles. The second system utilises a combination of steam and liquid nitrogen to produce an aerosol or fog that serves as flow seeding. Water- or steam-based seeding has been previously demonstrated for flow visualisation in subsonic tunnels; however, here it is utilised as the seed material for PIV measurements, as well as for flow visualisation in a large supersonic tunnel.

***Health and Safety Impact of Seed Materials***

In addition to selecting a proper seed material for accurate PIV purposes, it is also important to assess the potential impact on health and safety. The health and safety concerns of various seed materials were presented at a NASA conference on PIV (Brown, 1985). Many traditional seed materials are potentially harmful to personnel using them and increase the difficulty of employing them in a large-scale facility. This hazard is compounded when working around seeding material, because for seeding material to be useful it is required to be in a particulate form which is easily respirable. The American Conference of Governmental Industrial Hygienists (ACGIH) publishes a size distribution guide describing how respirable particulates may be, and this is summarised in Table 3.3 (Brown, 1985).

Table3.3: Respirable Particulate Size Distribution

| Particulate Size (μm) | % Respirable |
|---|---|
| < 2 | 90 |
| 2.5 | 75 |
| 3.5 | 50 |
| 5.0 | 25 |
| 10 | 0 |

In addition to health concerns, particulate seed materials also present an explosive hazard. A commonly referenced property that adequately describes the volatility is vapour pressure, and this is often expressed as a material's lower explosive limit. The lower explosive limit is the minimum air concentration at which a homogeneous mixture can burn when subjected to an ignition source of adequate temperature and energy. A synopsis of the health and safety hazards for common seed materials is provided in Table 3.4.

Table 3.4: Health and hazard properties of seed materials

| **Seed Material** | **Density** | **Effect** | |
|---|---|---|---|
| Aluminium Oxide | 10 mg/m$^3$ | Nuisance, carcinogen | N/A |
| Kaolin | 10 mg/m$^3$ | Nuisance | |
| Silicon Carbide | 10 mg/m$^3$ | Nuisance | |
| Polystyrene Latex | 10 mg/m$^3$<br>50 ppm | Nuisance, carcinogen<br>Anesthetic, irritant | 15 g/m$^3$<br>1.1% |
| Vinyl Toluene | 10 mg/m$^3$<br>50 ppm | Nuisance<br>Anesthetic, irritant | 0.1% |
| Propylene Glycol | | Nuisance | 2.6% |
| Kerosene | 14 ppm | Irritant | 0.9% |
| Ethyl Alcohol | 1000 ppm | Anesthetic, Irritant | 3.3% |
| Methyl Alcohol | 200 ppm | Anesthetic, Irritant | 6.7% |

Following the above considerations, Aluminium Oxide particles were chosen because they have a small nominal diameter, a lower density, and present none of the environmental hazards that must be considered when utilising titanium dioxide particles. Aluminium Oxide is used as an industrial abrasive due to its low reactivity, hardness, and

its ability to withstand high temperatures. It is a crystalline solid with a rating of 9.25 on the Mohs' scale of relative hardness and has a refractive index of 2.65

### 3.2.2 Light Source:

Lasers are used almost universally in flow imaging (Kirby, 1999), and was favourably considered for this work owing to it has:

- High brightness
- Coherence
- Excellent focusing properties
- Monochromatic range of wavelengths

Lasers can be either pulsed or continuous wave (CW); however, pulsed lasers are more commonly used because they provide high-energy pulses that are sufficiently short (e.g. 10 nS) to freeze the motion of nearly any flow. Most lasers used in flow imaging operate at visible or UV wavelengths. The reason for this is that there are few low-noise imaging arrays that operate outside of the UV-visible to near-IR wavelength range. Furthermore, some techniques such as Rayleigh and spontaneous Raman scattering, increase in scattering efficiency as the frequency of the incident light increases, and therefore UV and visible lasers have a large advantage over IR sources. Finally, PIV as used in this research involves the excitation of atomic/molecular electronic transitions, which occur at UV and visible wavelengths. The predominance of techniques in the visible/UV range is by no means absolute, as recent advances in laser and camera technology have enabled the development of PIV techniques that rely on the excitation of vibrational transitions at IR wavelengths (Willert et al., 2010).

The most widely used laser utilised in flow imaging is the flash lamp-pumped Neodymium: Yttrium–Aluminum Garnet (Nd:YAG) laser, which emits in the infrared range (1.06 μm), but whose output is usually frequency-doubled (532 nm), tripled (355 nm) or quadrupled (266 nm), using nonlinear crystals. Due to the above analysis, for this project a frequency doubled Nd:YAG laser was selected.

### 3.2.3 Image Capture Block

Obtaining particle images demands the use of cameras that have the ability to record sequential images in separate frames, in order to achieve high spatial resolution, and to capture multiple frames at high speeds, all with high sensitivity. This is a non-trivial matter, and depending on the diameter of the pipeline to be viewed, this may be particularly difficult. If for example the internal diameter of the pipe is 50 mm and the tracer particles have a diameter of 10 microns (μm), then one-dimensional resolution is equal to 50/0.01 = 5000. For a square camera image, this would mean 25 Mpixel - are such cameras available in the market with this kind of resolution? The most commonly used cameras in quantitative imaging techniques are mostly based on CCD arrays or image-intensified CCD arrays.

Appendix C provides additional information on the comparison between a CCD and CMOS based camera. There are however a few applications where film may be preferred to a digital camera, such as large field-of-view PIV and high framing-rate PIV. Nevertheless, CCD arrays have largely supplanted film and other detectors, including TV tubes, photodiode and charge-injection device (CID) arrays (Adrian, 2011), owing to their:

- Low noise
- Excellent linearity
- Uniformity
- Resistance to blooming

Figure 3.4 - PIV cameras

Table 3.6: Technical comparative analysis of CCD against CMOS Cameras

| | **CCD** | **CMOS** |
|---|---|---|
| **Sensitivity** | High Sensitivity | Lower Sensitivity |
| **Resolution** | High Resolution (11 M pixels!!) | Normal Resolution (0.5 - 2 Mpixel) |
| **SNR** | Low Noise level | Higher noise level |
| **Sample Rate** | Low sample rate (~10Hz) | High sample rate (~1 – 10 KHz!!) |
| **Others** | Needs frame grabber boards | Easy integration (USB, Ethernet ) |

Table 3.6 presents a summary of a comparative analysis of CCD versus CMOS based cameras. The CCD camera (Figure 3.4) was elected for this project owing to its unique advantages over CMOS based cameras as enumerated above and in Appendix C. Added

to this, is that it is relatively cheaper and it was available in the laboratory for free. Funds were not available to allow for a performance comparison with other CCD cameras types.

***Principle of Operation of CCD***

The operation of a CCD is based on the fundamental principle that a photon incident on the CCD produces an electron–hole pair in a region of silicon that is biased to some potential. The electrons generated are called "photoelectrons" and these migrate to the "potential well" of the CCD pixel where they are stored for later readout. Because the CCD stores charge, it is essentially a capacitor whose charge is proportional to the number of incident photons. The quantum efficiency, $\eta$ is the ratio between the number of photoelectrons generated and the number of photons incident. Front illuminated CCDs have quantum efficiencies of 10–50% at visible and near-IR wavelengths (peaking near 700 nm) but are virtually zero at UV and mid-IR wavelengths. Back-illuminated CCDs, although more expensive, provide quantum efficiencies of up to 90% in the visible and can maintain a good response (e.g., $\eta$ = 20%) well into the UV. CCD arrays can be of the full frame, frame transfer, or interline transfer type (Mulleners et al., 2009).

Full frame CCD arrays read out the charge by shifting it down through the entire array (like a "bucket brigade") into an output register where it is then read out serially. Because the array is used to shift the charge, the image will be blurred if the CCD is exposed during readout, and as readout can take several seconds, a mechanical shutter must be used. In contrast, frame transfer CCD arrays use a photosensitive array and an identical array that is masked off from any incident light. Following an exposure, the charge of each pixel is shifted down through the array into the masked array, and the masked array

is then read out in the same manner as a full frame CCD array. Frame transfer CCD arrays offer some level of electronic shuttering, but this is limited to a few milliseconds. The pixel area for both full frame and frame transfer CCD arrays is 100% photosensitive, thus the pixel width is the same as the pixel pitch (spacing) (Vogel and Lauterborn, 1991).

Interline transfer CCD arrays have non photosensitive storage registers located adjacent to the photo sensors. This enables the rapid transfer of charge (in parallel) from the pixels into the storage registers, thus making it possible to rapidly shutter the array electronically, and allowing exposure times of the order of microseconds or less. The interline transfer arrays also enable "frame straddling" whereby two frames can be captured in rapid succession. For example, standard RS-170 format video cameras based on interline transfer arrays can acquire two video fields in less than 10μs between frames. More expensive scientific grade interline transfer cameras report interframe times as short as 200 ns. Frame-straddling by video cameras is useful for double-pulse imaging in high-speed flows (Clemens et al., 1996), whereas frame-straddling by higher resolution scientific/industrial cameras (e.g. FlowSense 4M and ES4.0) is now becoming the norm for PIV because it enables the use of cross correlation processing algorithms. The main drawback of interline transfer imagers is that they tend to be noisier than either full frame or frame transfer imagers. The main reason for this is that the storage registers are located adjacent to the photosensitive sites; therefore the photosensitive area of the pixel is substantially smaller than the physical area of the pixel.

The fraction of the pixel area that is photosensitive is called the "fill factor" and is typically 20–30% for an interline transfer CCD. As will be discussed later, the signal

scales with the number of photons collected per pixel and so low fill factors result in low signals. Some manufacturers mitigate this problem to some extent by using micro lenses over each pixel to collect light across a larger area and this can increase the fill factor to about 60%. If neither electronic shuttering nor frame straddling is required, then full frame or frame transfer imagers are desirable to maximise the signal-to-noise ratio (SNR). Generally, the relatively long shutter times are not a problem when pulsed lasers are used because the laser pulse duration acts as the exposure time. Intensified CCD cameras (ICCD) are used for low light level imaging and for very short exposure times.

The requirements for the illumination source are that the pulses must be able to provide sufficient energy, be close together in time, and short enough in duration that the particle reflections are discrete and not blurred together. Although these requirements do not exclude other light sources, lasers are almost exclusively used for digital PIV, and Nd:YAG is the most commonly used laser because of its high output, short pulse duration, and emission which can be frequency doubled to within the visible spectrum: 532 nm wavelength. This frequency doubling is useful for three reasons. This frequency doubling is useful for three reasons:

- 532nm electro-magnetic radiation is visible as green light making laser alignment relatively simple, and
- Digital CCD cameras are available with high quantum efficiency at 532 nm,

Electromagnetic energy is emitted from most lasers in the form of a low divergence beam in wavelengths ranging from infrared down to ultraviolet. Laser energy is coherent and monochromatic (Lin and Rockwell, 1994); that is, it is comprised of a single wavelength or a narrow band of wavelengths. In the case of the Nd:YAG laser used in the Flow Lab,

the laser energy is passed through a dichroic mirror allowing the 532nm light to transmit while reflecting any 1064 nm light remaining from the frequency doubling crystal. It then exits the laser housing and is passed through sheet-forming optics. These usually consist of mirrors to orient the beam, a half-cylindrical lens to make the beam diverge at a constant angle, and a spherical lens to focus the beam so that the sheet is thin when it illuminates the test area. There is a trade off with sheet thickness, as a thin sheet provides the maximum power density and only illuminates particles in both frames that have relatively two-dimensional velocity. This characteristic is beneficial because a higher power density increases the SNR and less out of plane motion will be recorded, thereby minimising the error due to the parallax effect. However, if the sheet is too thin, it will illuminate too few of the same tracer particles in both frames, leading to a loss of pairs.

### 3.2.4 Synchronizer

The laser timing and camera timing needed to be aligned, and these are controlled through a synchronisation unit that is linked to the computer and controlled by appropriate software. In order to effectively "freeze" the micron-sized particles in an image, the laser burst must be short in duration. Releasing the laser energy in short pulses also increases the peak power without requiring more energy. Energy is released over a shorter amount of time, thus increasing the peak power.

The PIV laser setup in the Flow lab uses a dual cavity laser with a *Q*-Switch on each cavity. The two lasers can fire with a much shorter delay between pulses than would be possible with only one laser cavity. The PIV laser in the Flow Lab can deliver two pulses with as little as 300ns separation between pulses, but the delay between pulses must be

matched to the expected velocity of the flow. The reflections from the two pulses are sufficiently close together in the acquired image pairs to be successfully correlated.

The *Q*-Switch refers to the quality of the reflector, which is quickly changed to control the laser emission. Energy pumped into the gain medium can be stored, but is not amplified when the quality of the reflector at the end of the lasing medium is low. During this phase, light leaving the gain medium is not reflected and lasing does not occur. However, the energy being pumped into the gain medium causes a population inversion to develop and stores energy up until the saturation point is reached, whereupon the quality of the optical resonator is switched to a high value and the stored energy is stimulated into emission. This emission results in concentrated pulses of laser energy released at controlled intervals

### 3.2.5 Image Analysis

One of the most critical issues in flow imaging is obtaining an adequate signal to noise ratio (SNR). Imaging measurements that use laser light scattering are particularly susceptible to a low SNR because the laser beam must be spread out into a sheet, thus signal strength is lower by 100 to100-fold compared to a point measurement with the same laser energy. The image is usually inverted in flow imaging, and after the magnification there is typically less than unity, meaning that the object is minified.

Assuming that a camera uses an array sensor and has a lens of known focal length $f$ and limiting aperture diameter $D$, each pixel of the camera, of width $\partial x$ and height $\partial y$, transforms to a region in the flow of dimensions:

$$x = \frac{\delta x}{m} \quad 3.11$$

$$y = \frac{\delta y}{m} \quad 3.12$$

Where $m = \frac{y_i}{y_o}$ is the magnification.

The main drawback of this technique was the risk of damage to the array by the focused laser beam.

### 3.2.6 Implementation in MATLAB (Computer):

The process of determining the velocity can be classified into the following discrete steps, which are shown in the software flow diagram in Figure 3.5. These are:

1. Load an image pair
2. Parse the images to interrogation areas with a given initial shift.
3. Load an interrogation area pair.
4. Calculate the cross correlation for both frames
5. Find the cross-correlation for the field maximum
6. Calculate the mean displacement.

All the PIV images were analyzed using MatPIV the MATLAB based toolbox. The software is designed to analyze images taken by the digital camera that was used. It uses a two-pass analysis algorithm to improve spatial resolution, and image shifting to improve signal to noise ratio.

Step 1: This step was to make sure that the folder containing the PIV Software is in the MATLAB path.

Step 2: Was to initialize global variables by running the startup script in the PIV software folder.

***>startup***
***>load('MATLAB.mat')***

Step 3: The images were read into MATLAB

***>im=imread(***'F:\uleh\Research\PIV data\sampleA', ***image.tif');***

The array 'im' was a very large array, so it was necessary to use the semicolon ';' to avoid a very, very long list of data values being displayed.

Step 4: The 'setpivana.m' code was used to set up the interrogation window, the search window, and to do a preliminary test of the PIV image.

***>setpivana(im,[100*16 1000*16]);***

The seed density values were selected (arbitrarily) to obtain reasonable contrast in the image displayed. After entering the PIV processing parameters, **'setpivana.m'** displays the PIV image. By positioning the cursor and left clicking the mouse the first and second exposures of the PIV image are displayed as well as the cross correlation. The complete program from this point is in Appendix A.

The algorithm used in this application tracks the seed particles only in the gas phase in the images to calculate the displacement between two frames, and the displacement is measured using cross correlation analysis. The displacement between frames is divided by the time between the two frames to yield the velocity in pixels per second. The resulting velocities are then orthonormalised to yield velocities in metres per second.

The test results confirm that the proposed technique is plausible. However, this is only for the gas phase and seeding the liquid phase was not successful. It is envisaged that the biggest obstacle could be the reflection of water film on the inner pipe wall which can blur the tracer particle images. For multiple phases the system has to work in sequences, so that the flow profile needs to be stable over the measurement period, which is around a few second.

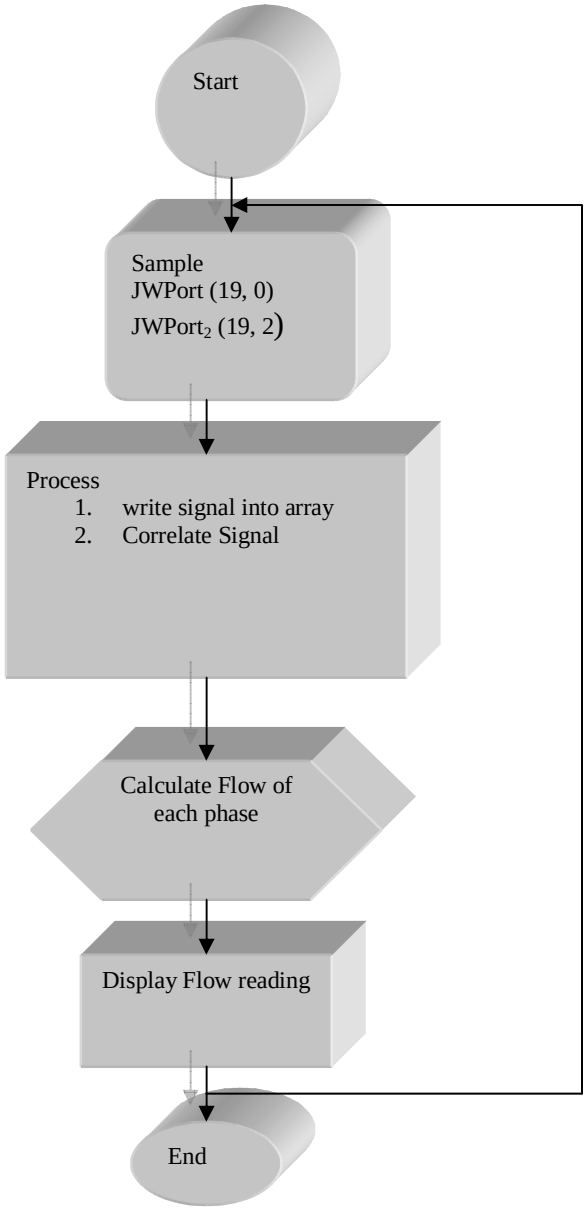

Figure 3.5 - "*Uletech"* Software flow scheme

## 3.3 Liquid Flow Measurement

The hydrocarbon condensate will be measured through the use of the tracer dilution technique. The tracer dilution method as shown in Figure 3.6 consists of adding a known, strong concentration of tracer solution $C_i$ at a constant rate to the flow, then, by chemical analysis, the downstream diluted uniformly mixed concentration $C_p$ is measured. For condensate, the option is to use soluble florescent tracers which are hydrophobic and stay with the condensate. There is a hydrophilic tracer for water, but this was not investigated here, because the process sample available had been striped of water. Care must be taken to ensure that the tracer injection rate is very low or insignificant relative to the process flow rate.

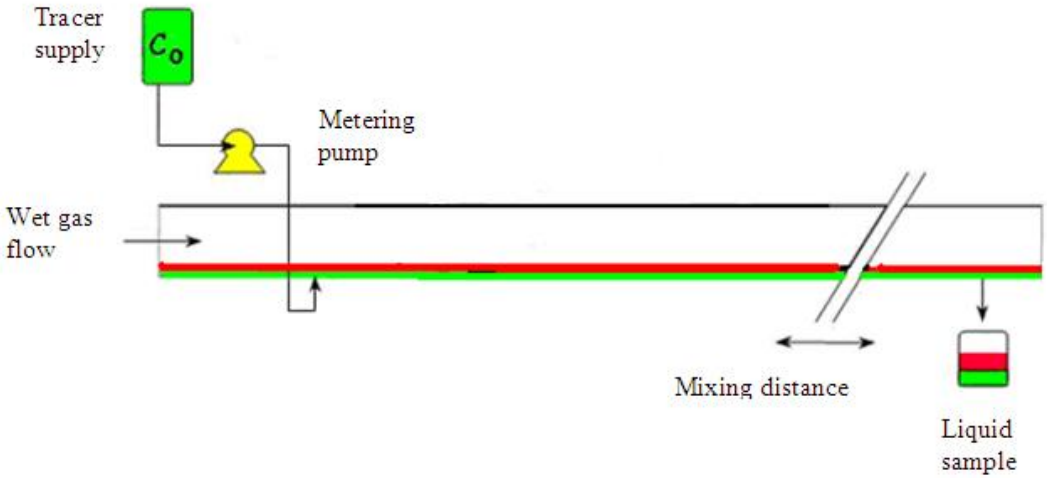


Figure 3.6 - Schematic of tracer dilution methodology

When a tracer is dissolved in a liquid (heptane) and then injected into the flow line with a specific constant flow rate, the tracer will mix with the liquid in the pipeline and will become diluted. When the injected tracer and hydrocarbon condensate are completely mixed (i.e. the tracer is homogeneously mixed in the condensate) and provided that the tracer solution flow rate is far smaller than the liquid flow rate in the pipeline, the concentration of the tracer in the pipeline is equal to:

$$Q_p \approx \frac{C_i}{C_p} Q_i \qquad 3.14$$

This is derived using the basic equation for the tracer dilution technique:

$$Q_p C_0 + Q_i C_i = (Q_p + Q_i) C_p \qquad 3.15$$

In which:

$Q_i$ is the volumetric flow rate of tracer solution into the flow line, $m^3/s$

$Q_p$ is the volumetric flow rate of target phase in the flow line, $m^3/s$

$C_p$ is the concentration of fluorescent tracer in the flow line, $mol/m^3$

$C_i$ is the concentration of fluorescent tracer in the injected solution, $mol/m^3$

$C_0$ is the natural or background concentration of the tracer of the flow, $mol/m^3$

Solving for $Q_p$ assuming $C_0$ is zero (0) in the basic equation results in:

$$Q_p = \frac{c_i}{c_p} Q_i - Q_i \qquad 3.16$$

As $Q_i \ll Q_p$ in most cases, this can be approximated by:

$$Q_p \approx \frac{C_i}{C_p} Q_i \qquad 3.17$$

Thus, by the determining the concentration of the tracer in the injected solution in the pipeline, the liquid flow rate in the pipeline can be determined. Figure 3.7 by Murdock (Murdock, 1992) provides a pictorial representation of the tracer dilution process. Using this method the water and condensate flow rates can be determined.

Fluorescent tracers are suitable for this task and both hydrophobic and hydrophilic tracers are available. Fluorescent tracers have the advantage that they do not require special licences (compared to radio-active tracers) since they are harmless to the environment. In addition, the small amounts that end up in the product cause no problems at all during the processing of the hydrocarbons.

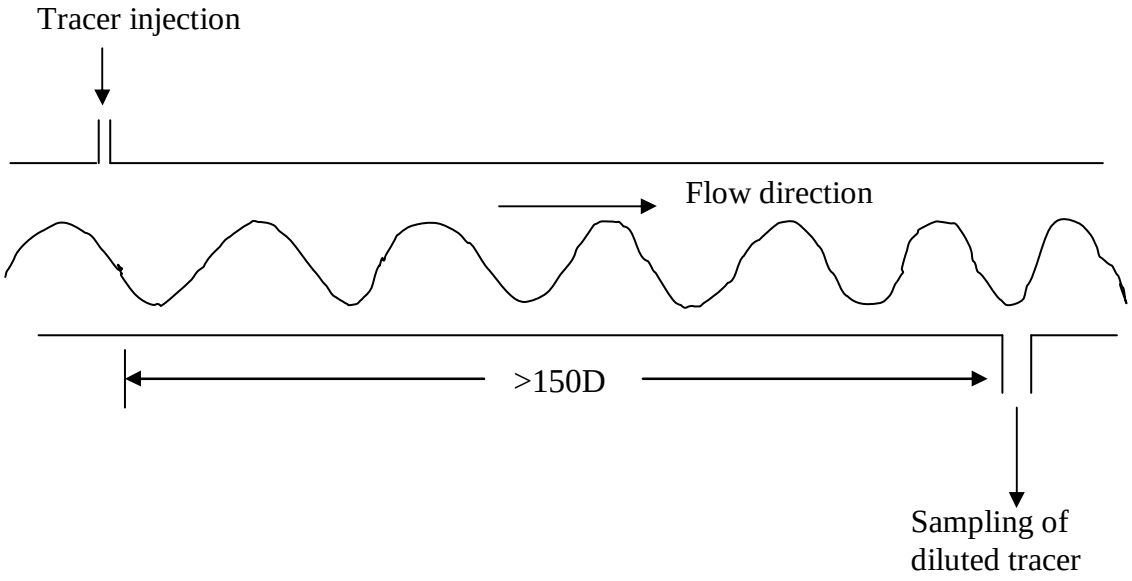


Figure 3.7 - Setup of tracer dilution technique

Although tracer dilution is basically straightforward, the technique has some specific requirements for its correct implementation. These are related to the following aspects:

1. Choice of solvent for the tracers.
2. Homogeneity of the tracer solutions.
3. Injection flow rate accuracy and stability.
4. Mixing with the target liquids in the flow line.
5. Stability of the target liquid flow rate.
6. Configuration of the flow line.
7. Mixing using short distances or limited available space.

The implementation of the tracer dilution technique consists of several main stages, starting with the tracer solutions and their injection into the flow line (the upstream part), followed by the transportation and mixing in the flow line (the middle part), the sampling of the liquids (the downstream part) and finally the processing in the laboratory.

### 3.3.1 Choice of Solvent for the Tracers

The solvent used to dissolve the condensate tracer should be miscible with the condensate (or oil) in the flow line and should be a hydrocarbon (mixture) with a density similar to the condensate, both at line conditions. This is primarily because the condensates can be significantly less dense at line conditions than after stabilisation due to the loss of light components. If there is a significant difference in density between the tracer solution and the target liquid then stratification might occur, and additional turbulence (and mixing length) is required to overcome the density difference.

### 3.3.2 Homogeneity of the Tracer Solution

Tracer solution which is to be injected into the flow line should be completely homogeneous, and water tracers are usually available as a solid. The prepared solution is filtered shortly before injection or given ample time (12 to 24 hours) to ensure that all solids have been dissolved, followed by thoroughly mixing the injection solution. The condensate tracer is usually available as a viscous liquid, which can be dissolved by thorough mixing with the solvent.

### 3.3.3 Mixing with the Target Liquids in the Flow Line

The mixing needs to be done by turbulence, for the very simple reason that no other mechanism is able to achieve this in the short time and distance available. Hence, the flow conditions are important for the quality of the mixing.

The minimum distance between tracer injection and extraction shall be 150 D, unless it can proven that mixing will be complete within a shorter, specified distance.

### 3.3.4 Types of Tracers

The most commonly used tracers are:

- *Silicon Carbide:* Suitable for measurements in liquids and gases, silicon carbide particles have a narrow particle size distribution (mean diameter of 1.5μm). Their high refractive index is useful for obtaining good signals in water, even in backscatter operations and they can also be used in high temperature flows. Supplied as a dry powder, the particles can be mixed into a liquid to form a suspension before dispersing.

- *Titanium Dioxide:* These particles (mean diameter of 0.2μm) are usually dispersed as a dry powder for gas flow measurement applications. The smaller particle size makes titanium dioxide attractive for high-speed flows and it can also be used for high temperature flows.
- *Polystyrene Latex:* With an extremely narrow size distribution (nominal diameter of 1.0μm), polystyrene latex (PSL) particles are useful in many different measurements. They are supplied in water, but are not recommended for high temperature applications.
- *Metallic coated:* These particles (mean diameter of 9.0μm) are normally used to seed water flow measurements due to their lower density and higher reflectivity. They cannot be used where salt is present as salt reacts with the metal coating, causing the particles to aggregate and drop out of the flow.

Following the above analysis Silicone carbide was considered more suitable and used for this experiment

## 3.4 Challenges

The problems anticipated and tackled in the course of the project can be classified into two categories: general and transducer specific issues.

Under the general issues are:

- The programming platform upon which to implement this work
- Signal sensing with special attention being paid to prevention of aliasing
- Signal degradation and the possible reconstruction of degraded or distorted images

Under the transducer specific issues are:

- Visibility of the camera (resolution)
- Calibration of the camera view
- Possible issues concerning the cross-correlation technique

### 3.4.1 Loading Analogue Signal into MATLAB Environment

The initial problem in executing this project was the importing of the signal into the MATLAB environment. It was thought that importing the signal into a PC would provide an excellent means of being able to store the signal and carry out off-line analysis of the stored signal.

Having successfully imported the signal into MATLAB the next problem was determining the sampling rate of the computer, and this proved to be problematical since the laboratory PC that was being used for the project was not a standalone system dedicated to running MATLAB. The sampling rate varied enormously from minute to minute depending on what activity was going on, e.g. system health checks, network interrogation, synchronisation, automatic data saving procedures, and so on, which the computer was performing. It was very important to know the sampling rate in order to determine when aliasing was likely to set in. Another very obvious problem was that as the number of program codes increased, the computer took more time to execute the commands, which would inevitably introduce more error into the sampling rate.

### 3.4.2 Signal Sensitivity

The problem on the Uletech sensor was mainly the consideration of the reflection from the pipe wall. The transducer sensitivity was greatly hampered and distorted if the signals

did not come strictly from the reflective seeds injected into the flow. Reflection from the pipe surface had to be identified and filtered out or better, the pipe wall of the measurement spool should be coated to prevent reflections.

The next question is whether the sensor signal in terms of the SNR is strong enough to carry out any statistical analysis, and if not, how can it be enhanced/improved, and how can the anticipated noise be suppressed without distorting the original sensor signal? Possible solutions to these questions are discussed later.

### 3.4.3 Aliasing

The Nyquist-Shannon sampling theorem defines the minimum sampling interval one can apply without losing a wavelet's identity. The maximum frequency component a sampled data system can accurately handle is termed its Nyquist limit, and the sample rate must be greater than or equal to two times the highest frequency component in the input signal. When this rule is violated, unwanted or undesirable signals appear in the frequency band of interest and this is called aliasing. For example, to digitize a 1 kHz signal, a minimum sampling frequency of 2 kHz is required. In actual practice, sampling is usually higher to provide some margin and make the filtering requirements less critical.

To help understand aliasing, suppose a visible mark is placed on a bicycle wheel, the wheel is spun and snapshots are taken in time (or samples). Since a movie camera captures motion by taking a certain number of snapshots per second, it is inherently a sampled data system (Figure 3.8). Just as the film takes discrete images of the wheel, an analogue-to-digital converter (ADC) takes a sequence of snapshots of a moving electrical signal. When the wheel is first accelerating, the sample rate (the frame rate of the movie

camera) is much higher than the revolution rate of the wheel, so the Nyquist criterion is met. The camera's sample rate is greater than twice the rate of the revolution of the wheel.

At the Nyquist limit, the two points are 180 degrees apart (Figure 3.8c) and these two points typically, are indistinguishable from each other in time by the human eye; they appear simultaneous and the wheel appears to stop. At this wheel speed, the rate of the rotation is known (based on the sample rate), but the direction of the spin cannot be ascertained. As the wheel continues to accelerate, the Nyquist criterion is no longer met, and there are two possible ways to view the wheel. It can be seen as spinning forward or in the reverse direction (Figure 3.8d).

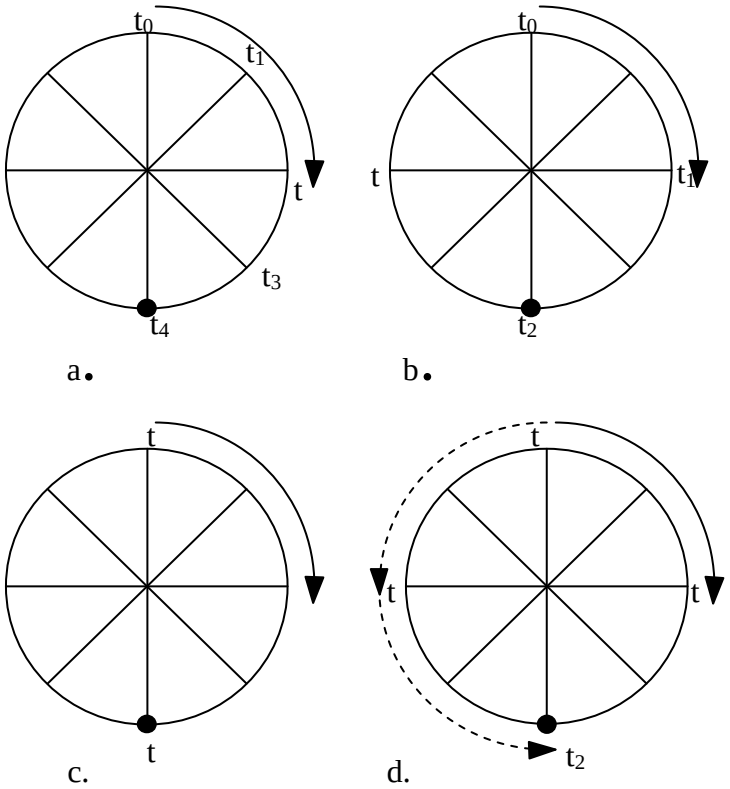


Where $T_N$ is the mark of time

Figure 3.8 - Wheel example to illustrate Nyquist theorem

Both can be viewed as the correct direction depending on how the wheel is seen, but now the signal is aliased. That is, there is a frequency component in the system that is unwanted and cannot be distinguished from the real value: both the forward and backward motion information is present. Typically, it appears to be the backward component or sub-multiple or image of the forward component, because the primary forward component becomes unnoticeable due to the manner in which the eye/brain combination processes the data. Another interesting observation is that at the point where the sample rate is exactly equal to the rate of the revolution of the wheel, the data obtained gives little useful information because the mark will always appear at the exact same point on the wheel. In this case it cannot be told whether the wheel is spinning or stationary.

Assuming the wheel is a unit circle with sine and cosine coordinates. If one samples at the positive and negative peaks of the cosine values (which are 180 degrees out of phase), then the Nyquist criteria are met and the original cosine values can be reconstructed from the two sampled data points. Thus the Nyquist limit is essential in reconstructing the original signal. As more and more points are added, the ability to replicate the original signal improves. In general, no information is lost by regular sampling provided that the sampling frequency is greater than twice the highest frequency component in the waveform being sampled. In practice, the sampling frequency is generally set to three times the highest frequency component.

In practice, analogue anti-aliasing filters are implemented in data acquisition signal conditioning systems so that frequencies above one-third the sampling rate are removed from the trace and aliasing effects are minimised. In other applications, to prevent aliasing an anti-aliasing filter has to be introduced, but these filters also present the following problems:

- *Time Response:* In designing an anti-aliasing filter, there is a temptation to have its attenuation roll-off extremely quickly and the way to achieve this is to increase the order of the filter. A so-called brick-wall filter (one with an infinitely high order), however, causes a sine function time response that decays proportionally to 1/t. What this means is that an extremely high order filter that eliminates all signals above the cut off frequency will cause signals that change rapidly to ring on for a long time - a highly undesirable effect.

- *Phase Distortion/Time delay:* Most analogue filters have a non-linear phase response. This is a problem since non-linear phasing causes an unequal time delay as a function of frequency. The higher frequency signals will arrive later than low frequency signals and this can especially be a problem when multiple sensor outputs are compared. As higher order filters have more severe nonlinear phase shift characteristics, this distorts the output signal.
- *Amplitude Distortion:* By definition, the filter will modify the frequency structure of the sensor signal which is usually not desired, however, they have been applied carefully to remove unwanted noise in the original signal.

Signal aliasing was an important consideration in the design of this measurement system, particularly when considering the effect of the scatter in the radiation that was anticipated due to the irregularity in the pipe surface.

**Transducer Specific Challenges**

A major problem is the visibility of the injected seed particles. Just to give a flavour to the extent of this problem, imagine using 50 mm as the internal pipe diameter of the process pipe and the central part of the pipe to be viewed. The image has to be detected through a mist of droplets or bubbles of 25 mm and this is only possible at low concentrations of droplets or bubbles. As the refractive index of the fluids in the pipe are different from the refractive index of the pipe material (especially when gas is the continuous phase), the pipe wall will act as a cylinder lens, thus distorting the picture. Although it is in theory possible to correct the picture, some information will be lost.

The next problem to be anticipated was how to correctly calibrate the camera view and develop an algorithm that translates the camera view to volume within the pipes internal diameter, keeping in mind that in a horizontal flow line, the distribution of either droplets or bubbles is not homogeneous over the cross sectional area of the pipe due to gravity. This obviously makes the interpretation of the picture non-trivial when translating it to flow rates (integration in cylindrical coordinates, liquid flowing at the wall).

### 3.4.4 Signals to Noise Ratio (SNR)

One critical issue considered within this flow imaging is obtaining an adequate SNR. Imaging measurements that use laser light scattering are particularly susceptible to a low SNR because the laser beam must be spread out into a sheet; thus signals are 100-1000

fold lower compared to a point measurement with the same laser energy. The image is usually inverted in flow imaging, and the magnification is typically less than unity, that is the object is minified.

### 3.4.5 Image Correction

In order to ensure that the measured signal relates to the flow property of interest and to ensure that the spatial structure of the object is faithfully represented by the image, several correction steps were required for the signal measured at each pixel of the array. Uletech, like most other image visualisation techniques, involves only relative measurements of signal intensity, from which absolute measurements can be obtained by calibrating a single point within the image. To obtain an image that represents quantitatively accurate relative intensity measurements requires making several corrections to the measured image.

For example, let $S_e(x, y)$ represent the desired signal level at a given pixel or location on the array $(x, y)$. By "desired" it is meant that $S_e(x, y)$ is proportional to the number of photons incident on that pixel originating from the scattering process of interest. The signal $S_e$ can be related to the total signal ($S_{tot}$) recorded at that pixel by the imaging system through the relationship:

$$S_{tot}(x, y, t_i, t_{ro}) = w(x, y)\,(L(x, y)\,Se(x, y) + S_{back}(x, y, t_i) + S_{dark}(x, y, t_{ro})) \quad 3.18$$

Where $L(x, y)$ is a function that is proportional to the laser sheet intensity (or fluency) distribution function,

$S_{back}$ is the signal resulting from unwanted background light

$S_{dark}$ is the fixed pattern signal that occurs with no light incident on the detector

$t_i$ is the exposure time

$t_{ro}$ is the array readout time (which includes the exposure time)

The function $w(x, y)$ is the "white-field" response function, which accounts for variation in the signal across an image of a uniformly white object. It has been assumed that a pulsed laser is used as the light source, in which case the signal $S$e is not a function of the exposure time.

In general, all of the functions involved in the correction may vary from shot to shot. The desired scattering signal is obtained by solving for $S_e$ in equation 3.18:

$$S_e(x, y) = S_{tot}(x, y, t_i) - (w(x, y)S_{back}(x, y, t_i) + S_{dark}(x, y, t_{ro}))\, w(x, y)L(x, y) \quad \ldots \quad 3.19$$

Equation 3.19 provides a means of obtaining the desired scattering signal image by arithmetic processing of the signal and correction images. $S_{dark}(x, y, t_{ro})$ is not noise because it is an offset that is nominally the same for each image that has the same exposure and readout time. The dark image is obtained by acquiring an image when the shutter is closed (or when the lens cap is on) and using the same integration and readout times as in the experiment. The background signal $S_{back}(x, y)$, is due to reflections of the laser from walls/windows, natural flow luminosity (as in combustion), fluorescence from windows or species not of interest, and external light sources. For non-luminous flows, a good approximation to the background can be obtained by acquiring an image when the laser beam is present but without the scattering medium (e.g. without the fluorescent species seeded into the flow). This is only an approximation of the actual background because the light itself that is scattered from particles/molecules in the flow can reflect from the walls and windows; therefore, an image obtained when the scattering medium is omitted may not have the same background signal as during an actual experiment.

### 3.4.6 Measurable Velocity

Theory suggests that the maximum measurable velocity is a function of the size of the camera's plane of focus and the pulse delay. For example, velocities of up to 2,000 m/s could be resolved in a 1mm region of interest with image pairs taken 0.5 inch apart. However, there are competing interests between dynamic range, spatial, and temporal resolution. In order to measure the maximum velocity, the delay between pulses should be as short as possible. Conversely, the pulse delay must be long enough to accurately determine an image displacement. The optimal pulse delay is short enough that the majority of the signals remains in the same interrogation region from one image to the next, but long enough in time that there is a measurable shift. With these considerations and the Nyquist sampling criterion associated to the discrete Fourier transforms of the image maps, a maximum displacement of one quarter of the window size is recommended.

## 3.5 Validation Method

The cross correlation technique used for PIV is quite robust; however, it can find invalid correlation peaks due to camera noise, out of plane velocity, lighting variation, etc. This invalid peak results in erroneous velocity vectors which have to be filtered. The raw data was processed with the cross-correlation algorithm, and the resulting velocity vector maps were processed with two validation techniques. These validation techniques are designed to filter inconsistent data and they require the user to estimate what values to accept and which to reject. This involves an iterative approach whereby the user applies the validation technique to a set of vector maps and observes the results. The technique is then adjusted to be less or more aggressive to ensure that obviously inconsistent data is

filtered. Because a high degree of user input can shape the data, the specified same set of filters and validation techniques were applied for all data.

The first technique applied was range validation. This is a basic filter rejecting any vectors outside the user-specified limits. The limits applied in this filtering in m/s, were:

(1) 0 - 140 for the overall vector length

(2) -100- 10 for the stream wise component

(3) -25 -25 for the span wise component.

Any velocity vectors outside this region were rejected.

The second technique applied was peak-to-peak validation. This filter rejects any vectors formed by correlation peaks less than a specified amount larger than the next highest peak. Cross-correlation will always result in an output of the highest peak correlation, even when there is poor correlation. On average, cross-correlation will result in several random peaks of similar magnitude when measuring noise. The underlying concept of this validation technique is that when the correlation peak is not significantly higher than the next largest peak, it is more likely to have resulted from correlating noise instead of valid signal pairs. All vector maps were filtered with this validation technique to reject any velocity vectors generated from correlation peaks that were not at least 20% higher than the next highest peak.

## 3.6 Conclusions

The Uletech MPFM design philosophy offers an inferential technically non-intrusive and cost effective method of phase detection through the use of seeds and tracers. The flow does not require pre-conditioning neither does it require physical phase separation nor the

use of radioactive isotopes, meeting most of the requirement for a genuine multiphase flow meter.

For HC measurement the tracer proposed still needs to be recovered, although this is not the subject of the current investigation. However, there are developments attempting to explore the use of carbon dioxide ice cubes as tracers, which will vaporise into the process and can be released safely into the environment without constituting any environmental or health hazards.

# CHAPTER 4: EXPERIMENTAL RESULTS AND ANALYSIS

In this section the experimental set-up is discussed and modifications to the project rig that were necessary are enumerated. The data acquisition process relies mainly on photographic film double-exposed to create a picture with pairs of signals. A cross correlation algorithm determines which signals are likely pairs and then average displacements are calculated for partitioned regions. The displacement vector is then multiplied with the phase concentration as determined by a chromatograph to obtain the gas flow rate. The results from the PIV and tracer dilution techniques are presented.

## 4.1 Experimental Rig Setup

As stated previously, there is no single instrument, which will measure the flow rates of the different phases that makes up a multiphase flow directly. Therefore it is necessary to combine several devices in an instrument package and calculate the specific flow rates from the combined readings.

To compute the flow rates of each phase, the basic parameters of phase velocities and phase fractions, i.e. phase concentrations (or quantities that can be unequivocally related to these) are measured. The phase velocities and fractions are then combined to provide the phase flow rate.

In the flowing experiments, the wet gas was comprised of two phases; the gaseous phase and the liquid phase (hydrocarbon condensate). The density data for both components is readily available from other parts of the production process or can be estimated using PVT diagrams. From the density data, the phase mass flow rate can be obtained. Thus,

the problem is to measure the component velocities and the two component volume fractions-(the gas phase fraction and the liquid phase fraction).

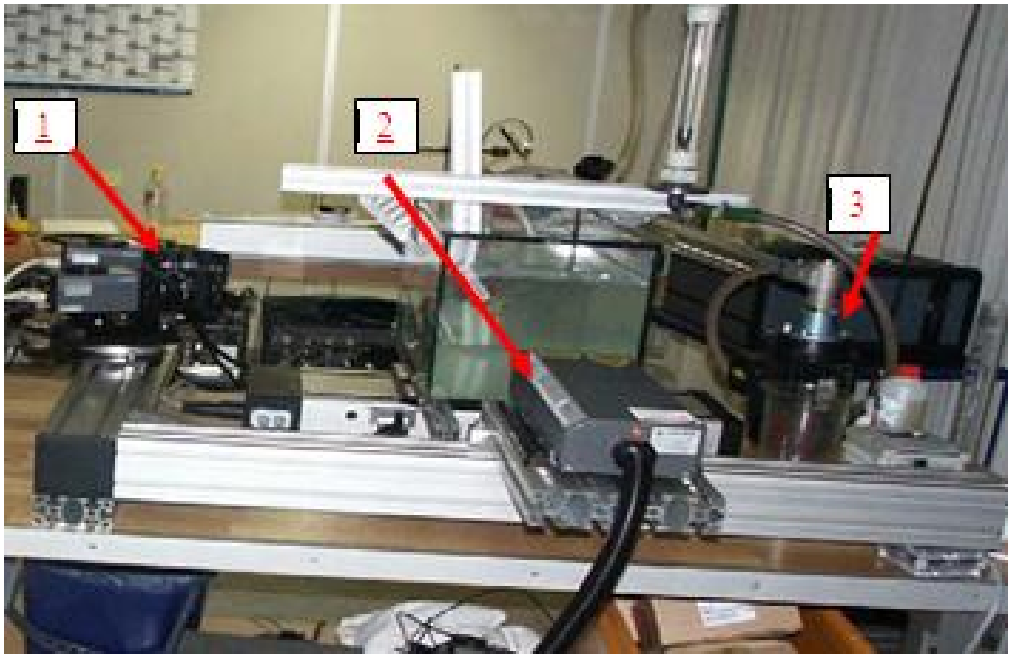


Figure 4.1 - Experimental set-up showing laser module

1. CCD Camera with fitted Nikon lens
2. Laser light
3. Synchronizer

In order to validate the proposed technique and check its viability, the experiment facility has been designed as shown in Figure 4.1. It is comprised of the following:

- NIKON lens 60mm F1.4
- Hi-Spec 4 camera (2048 x 2048 pixels)
- Field of View : 85mm (each pixel is approximately 50um)
- Laser, 532nm, 2W with Analog / TTL modulation
- Exposure time: 80μs

As shown in Figure 4.1, the rig is comprised of a CCD camera fitted with a 60mm NIKON lens, the seed generating pump, synchroniser, a computer data acquisition system and a transparent pipeline.

The flow sample collected from a three phase separator with known phase fractions was injected into the rig, synchronously with the seeds, and the light source was controlled to flash at a time interval of 20 μs. The data containing the seeds' reflection were recorded simultaneously by the computer-based DAQ system.

The image acquisition hardware that was used in this PIV study included a Hi-Spec 4 camera coupled with Nikon 60mm lens. This camera uses a CCD which comprises of a 2048 x 2048 matrix of metal-oxide semiconductor (MOS) elements. The incoming light is focused through the camera's lens onto the CCD and when the light hits these MOS elements or pixels, it is converted into a voltage. The camera has an 8-bit data resolution capability, meaning that the voltage magnitude from each pixel can be stored as one of $2^8$ (256) possible values. The camera's quantum efficiency ($\eta$), which is a measure of how effectively the incident photons are converted into electrons, is approximately 55% at 532nm.

Figure 4.2 shows the Hi-Spec 4 digital camera in its testing configuration, with an optical filter attached to the end of the Nikon 60 mm lens. This band-pass filter has a 75% transmission band from 530 nm to 540 nm, and although it does block some of the signal at 532 nm, it blocks out 99.99999% of all light below 490 nm and above 570 nm. The underlying concept is that the majority of the 532 nm light passing through the filter will be light reflected from the seed particles in the gas (which are the desired signal). The filter will block the majority of the background noise, which will be composed of the

wavelengths of light outside the transmission window. Using this method, the 532 nm band-pass filter effectively lowers the noise floor.

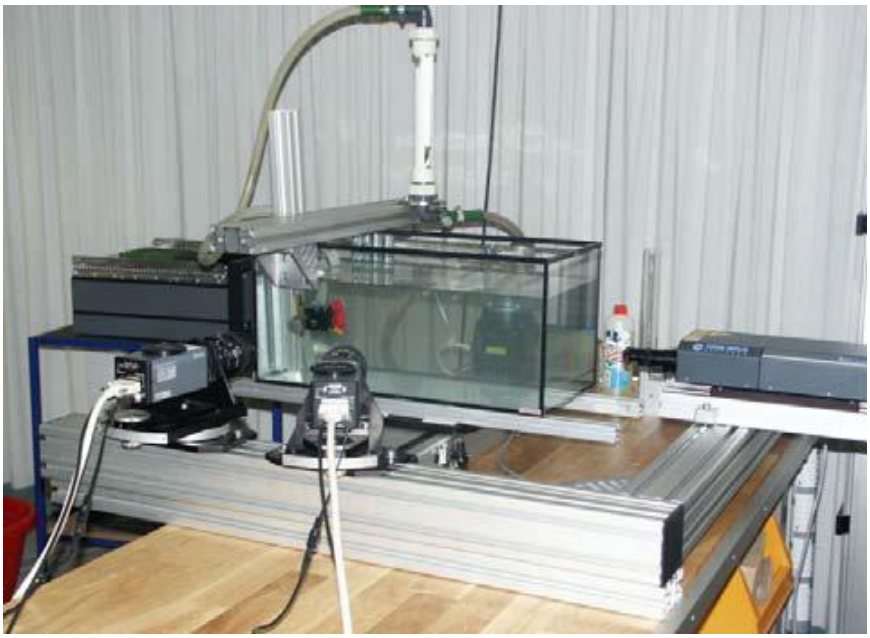

Figure 4.2 - Hi-Spec 4 camera showing filter, lens, and CCD

The Hi-Spec 4 camera has an image buffer of interlaced pixels allowing it to take a second picture before the camera has stored, transferred and processed the first image. The shutter exposes the CCD to the first image in the same manner as with any digital camera, then the image is quickly transferred to a storage buffer, allowing the CCD to be exposed to a second image. After the second exposure, the image stored on the buffer (image 1) and the image currently on the CCD (image 2) are both processed and sent to the computer. To illustrate the advantage in timing, consider the fact that a Hi-Spec 4 camera has a maximum frame rate of 15 Hz; that is, it can take 15 images per second continuously. However, with the use of the image buffer, it can take 7.4 image pairs per

second where the image pairs are spaced as little as 0.5μm apart. Overall, the camera is still limited to capturing and processing no more than 15 images per second, but pairs of images can be taken with much shorter delays between them.

## 4.2 Calibration of the Camera View:

The Hi-Spec 4 camera which was used for all data acquisition, as enumerated previously, has 2048 x 2048 pixels, which is a little over four mega pixels. It has 8-bit data resolution and quantum efficiency ($\eta$) of 55% at 532 nm. It is equipped with an optical band-pass filter with a centre wavelength of 532 nm. The camera uses Nikon 60mm lenses for focusing incoming light onto its CCD. These lenses do not have a zooming facility, requiring the camera to be as close as possible to the flow rig to enhance the detail of the particle images. The aperture on this lens, which is similar to an iris, is controlled by changing the f-stop setting. The f-stop is not a direct measurement, rather a ratio of the focal length of the lens to that of the aperture. Therefore, lower f-stop values allow more light to pass than higher f-stop. Lower f-stop values result in a narrow depth of focus, which is a disadvantage, whilst a higher f-stop value allows less incoming light, but has a deeper depth of focus. This means that "closing down" the f-stop (increasing the f-stop number) reduces the overall light captured; however, the depth of focus (the range of distances in sharp focus) will increase. A lower f-stop setting is considered advantageous because the signal energy captured on the CCD will be higher. However, the higher signal energy is predicated on the assumption that the dual laser sheets are coplanar and the illuminated experimental plane and the camera are translated in unison.

As data was acquired over several months, the camera setup was dismantled and reassembled many times in between runs. In each setup, the camera was no more than 30 cm away from the flow rig, and each time the camera was setup, it had to be aligned and focused. This involved setting the camera on "free run" mode and manually shifting the focus with the f-stop with the lens fully opened. The Nikon lens has f-stops from f/2.8 to f/32.35. An f-stop of 2.8, the most open setting, was initially used for focusing the camera on the experimental plane. However, the aperture had to be closed down two settings to an f-stop value of 5.6 for data acquisition. At this higher f-stop setting, the camera was more easily focused as it was translated. The camera and laser sheet were then translated through four experimental planes to verify that the camera was focused on both the laser pulses. The target contained calibration markers in known positions, and comparing known marker positions with corresponding marker positions on each camera image (as shown in Figure 4.3), model parameters could be adjusted to give the best possible fit. This alignment and focusing was perhaps the most time consuming part of the PIV setup procedure.

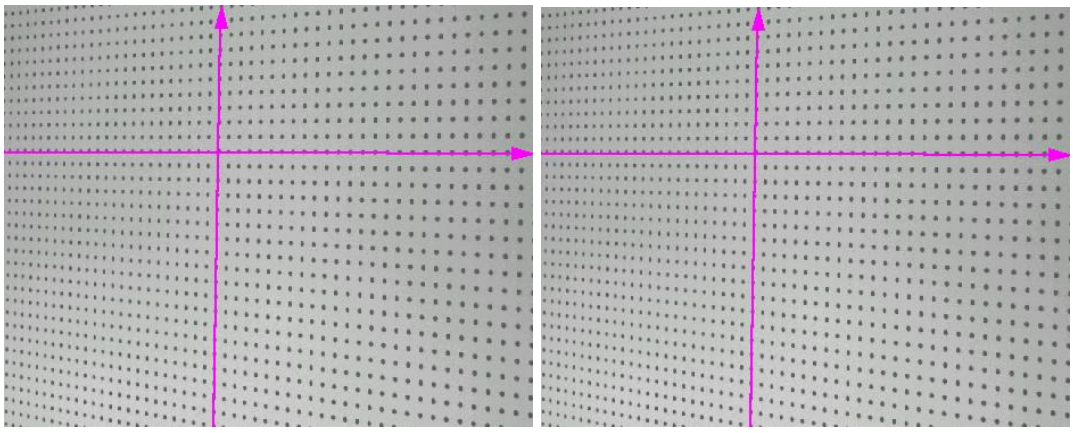

Figure 4.3 - Approximate camera field of view on the flow rig

The PIV laser is effectively two lasers in one package, as there are two Nd:YAG rods producing laser light that is then sent through the same optical path. Ideally, these two lasers appear to be a single double-pulsed laser. A small misalignment between the pulses was verified by firing each laser independently and observing the difference in their locations. Particles would appear to be in focus in one image but out of focus in the second image. Although the camera lens allows less light onto the CCD, the f-stop was closed down to 5.6 for the majority of the runs and the laser power had to be increased to compensate for the higher f-stop setting. With a more meticulous and exact experimental setup, a lower f-stop could have been used even with the more narrow depth of focus and the slight non-coplanar nature of the laser sheet. However, the camera's focus was more forgiving at the higher f-stop setting. Consequently, more corresponding particle pairs were found in the cross-correlation resulting in higher quality data. Once the cameras were properly focused, a calibration picture had to be taken to set the scale factor in the software. MATLAB has no knowledge of the distance between the camera and the experimental plane. Instead, it has pictures of particle reflections in the form of 2048 × 2048 pixel light intensity maps, which it processes and outputs the average particle displacement for each interrogation region in terms of camera pixels. The scale factor allows the velocity vectors to be converted from pixels per second to meters per second.

The process used to set the scale factor is relatively straight forward. A picture was taken of an object (i.e. meter rule) of known dimension and stored as a calibration image as shown in Figures 4.4 and 4.5. Then, two points are plotted on the image through MatPIV's "Measure Scale Factor" function. The software then takes the coordinates of the input points and determines the scale factor by dividing this input distance by the

pixel pitch multiplied by the number of pixels by which the two points were separated. This scale factor is then used to map the coordinate system in the CCD pixel plane to the coordinate system in the experimental plane.

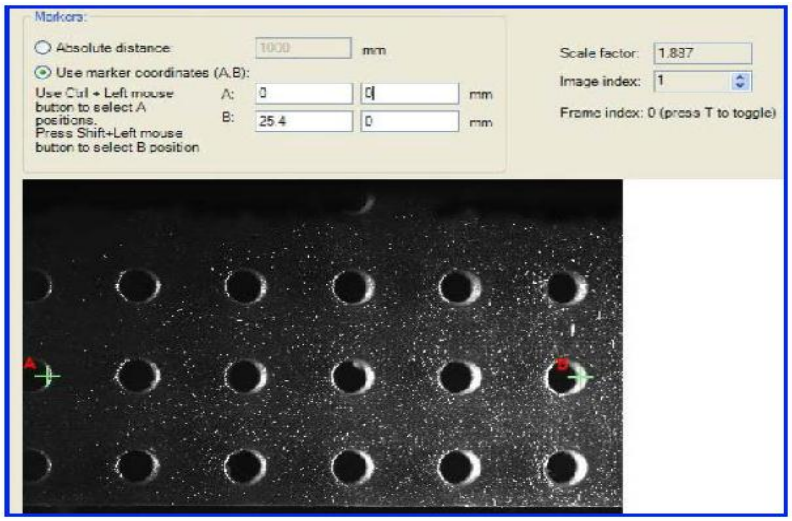


Figure 4.4 - Measurement of scale factor from MatPIV

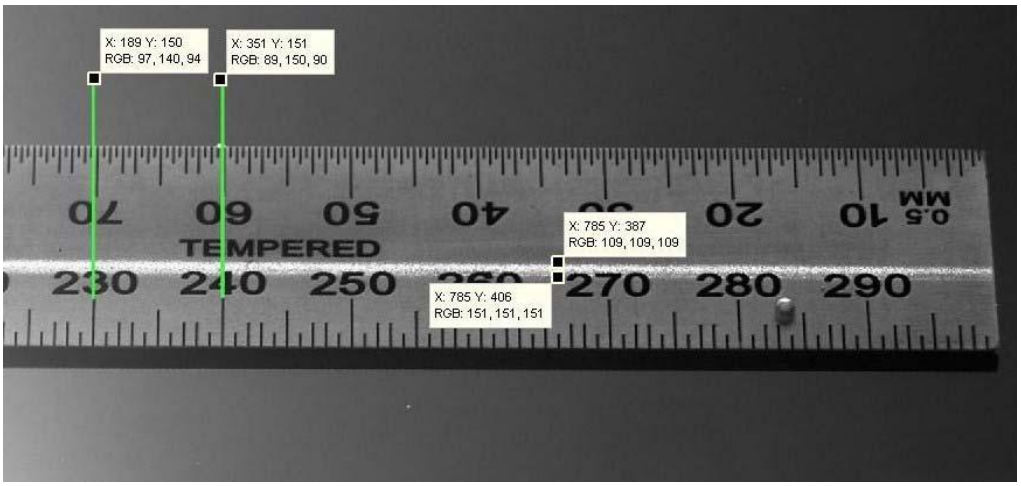


Figure 4.5 - Measurement of scale factor using meter rule

## 4.3 Gaseous Phase Velocity Measurement

The experiment was carried out using process sample of three different Gas Volume Fractions. The bottles were labelled Sample A, B and C.

- Sample A has a GVF of 96% (0.96)
- Sample B has a GVF of 92% (0.92)
- Sample C has a GVF of 88% (0.88)

A steady volume flow rate of 125 $m^3$/h was chosen for this investigation and the pulse delay $\Delta T$ was set at 20μS. The control flow rate was set using a rotameter, which gives a good feel of the combined volumetric flow rate but it is unable to distinguish between the phases, hence can not be used to estimate phase velocities.

### 4.3.1 Cross Correlation and Average Velocity at a Steady Volume Flow Rate of 125$m^3$/h

***Sample A - With steady volumetric flows set at 125$m^3$/h, for heavy seeded density***

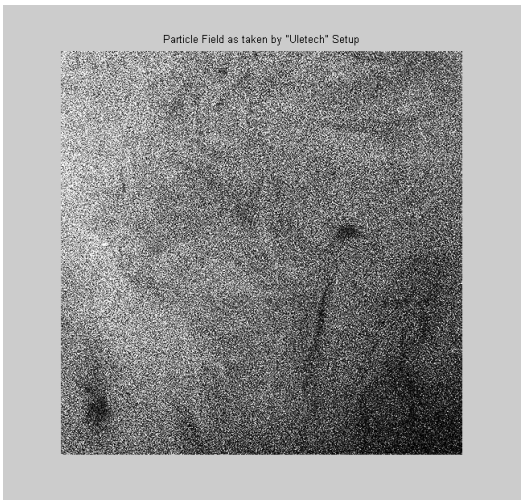


(a)

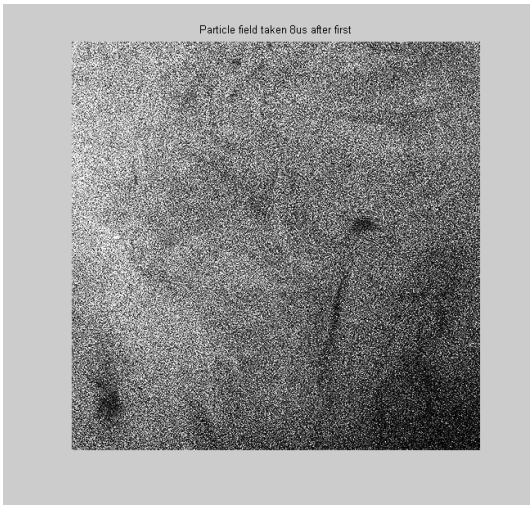


(b)

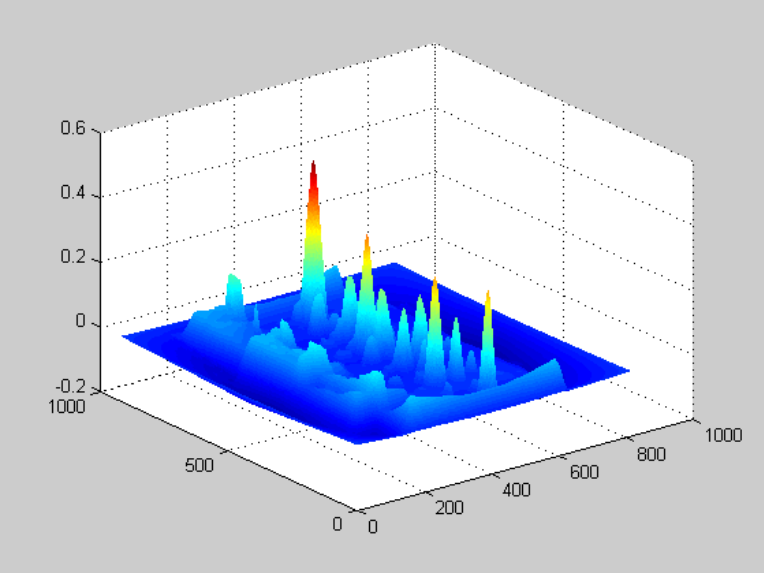


(c)

Figure 4.6 - Correlation of Sample A with GVF of 0.96 and heavily seeded

Figure 4.6 (a) and (b) are the raw pictures of seeded gas flow taken 20μS apart. The correlation of the whole field gives Figure 4.6 (c) in camera dimensions, where the vertical coordinate indicate the cross correlation value at a pixel, and the horizontal coordinates represents the pipe cross-sectional area viewed by the camera The crests of the correlation values in the correlation plane indicates the displacement of the particle. Following the calculation the flow velocity is estimated as follows, and this process is repeated all through the experiments.

*Calculations:*

The particle displacement recorded = 0.348mm = $34.8e^{-5}$ m

A pulse delay = 20μS

The velocity from $Speed = \frac{displacement}{time} = \frac{34.8*10e^{-6}}{20*10e^{-6}}$

Gas Flow Velocity, $V_{gas}$ = 17.4m/s

Volumetric flow of gas, $V_{FRG,}$ is the product of phase velocity, phase fraction and internal diameter of pipe. Represented as:

$V_{FRG} = \alpha * \pi r^2 * V_{gas}$

Where:

$\alpha$ represents the gas phase fraction = 0.96

$\pi r^2$ represents the area of the pipe and

$V_{gas}$ represents the gas velocity

From $V_{FRG} = \alpha * \pi r^2 * V_{gas}$

$V_{FRG}$ = 0.96 * 3.142* $(0.0254)^2$ * 17.4

= 0.03385$m^3$/s $\approx$ 121.86 $m^3$/h

***Sample A - With steady volumetric flows set at 90$m^3$/h, for lightly seeded density.***

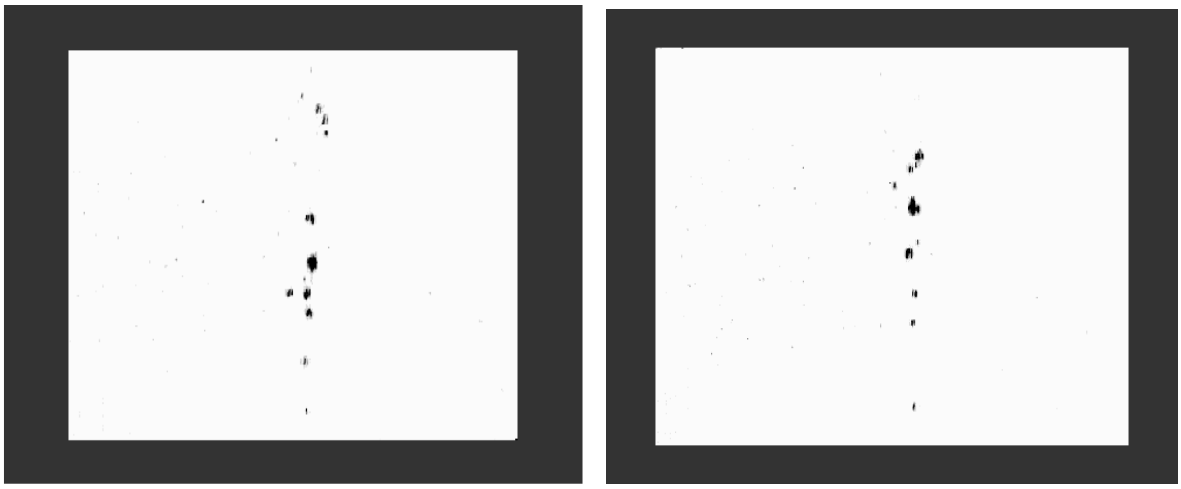

(a) (b)

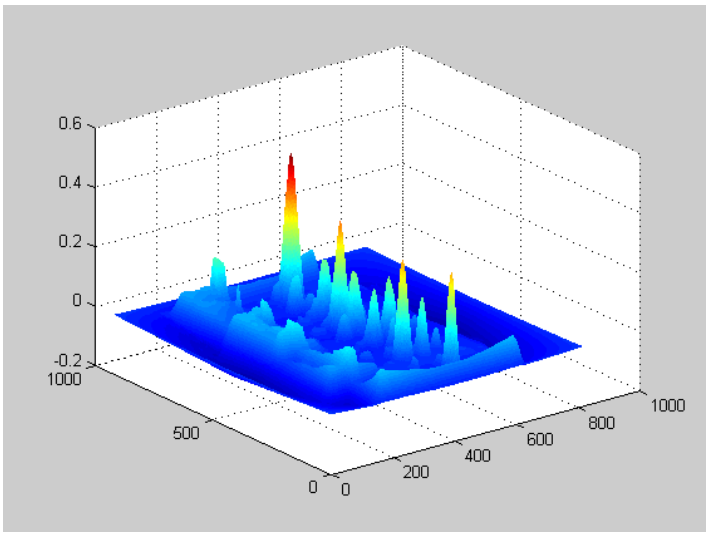


(c)

Figure 4.7 - Correlation of Sample A seeded lightly

*Calculations:*

The particle displacement recorded = 0.362mm = $36.2e^{-5}$ m

The velocity from $Speed = \frac{displacement}{time} = \frac{36.2*10e^{-5}}{20*10e^{-6}}$

Gas Flow Velocity, $V_{gas}$ = 18.1m/s

Using:

$V_{FRG} = \alpha * \pi r^2 * V_{gas}$

$V_{FRG} = 0.96 * 3.142* (0.0254)^2 * 18.1$

$= 0.03521 m^3/s$

$\approx 126.76\ m^3/h.$

***Sample B - With steady volumetric flows set at 90m$^3$/h, for heavy seeded density***

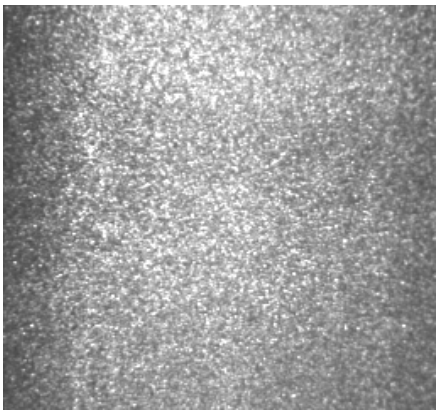

(a)

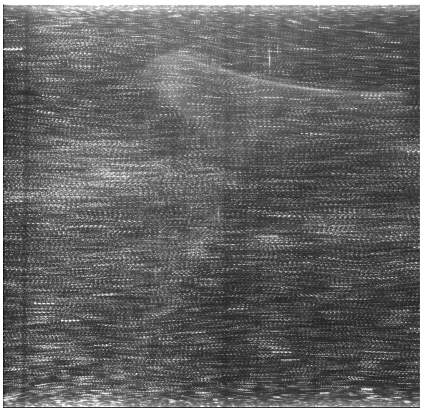

(b)

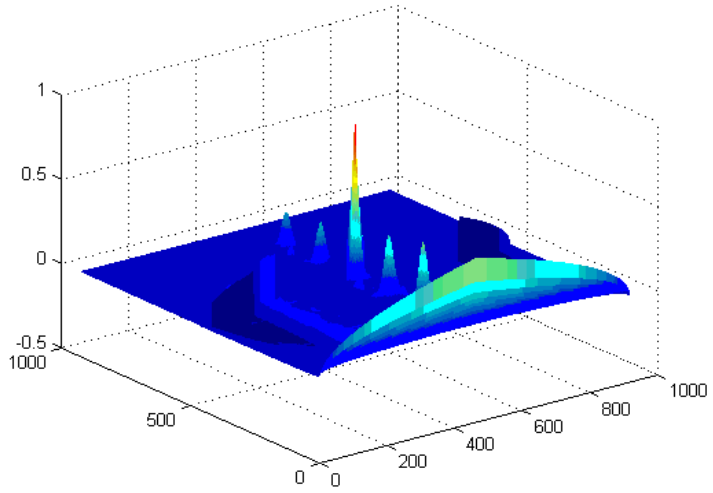


(c)

Figure 4.8 - Correlation of Sample B with GVF of 0.92 and heavily seeded

*Calculations:*

The particle displacement recorded = 0.451mm = 45.1e$^{-5}$ m

The velocity from $Speed = \frac{displacement}{time} = \frac{45.1*10e^{-5}}{20*10e^{-6}}$

Gas Flow Velocity, $V_{gas}$ = 22.55m/s

From $V_{FRG} = \alpha * \pi r^2 * V_{gas}$

$V_{FRG} = 0.92 * 3.142* (0.0254)^2 * 22.55$

$= 0.04205 m^3/s \approx 151.38\ m^3/h.$

***Sample B - With steady volumetric flows set at 90m$^3$/h, lightly seeded density***

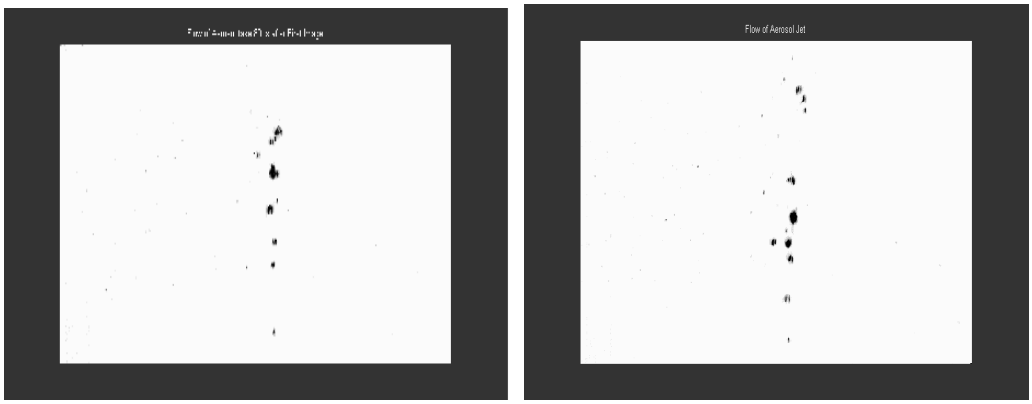


(a) (b)

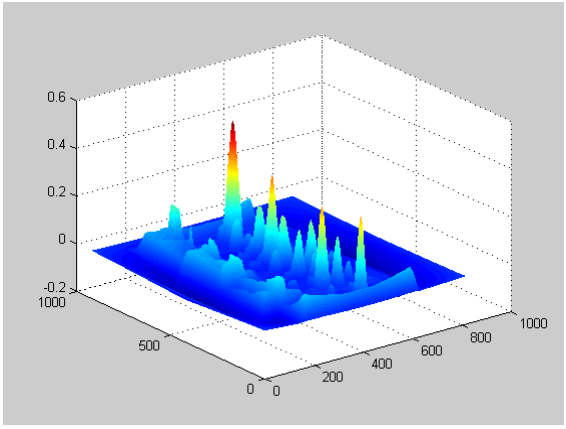


(c)

Figure 4.9 - Correlation of Sample B with GVF of 0.96 and lightly seeded

*Calculations:*

The particle displacement recorded = 0.352mm = $35.2e^{-5}$ m

The velocity from $Speed = \frac{displacement}{time} = \frac{35.2*10e^{-5}}{20*10e^{-6}}$

Gas Flow Velocity, $V_{gas}$ = 17.6m/s

From $V_{FRG} = \alpha * \pi r^2 * V_{gas}$

$V_{FRG} = 0.92 * 3.142* (0.0254)^2 * 17.65$

$= 0.03281 m^3/s$

$\approx 118.15 m^3/h.$

***Sample C - With steady volumetric flows set at 125m$^3$/h, heavily seeded density.***

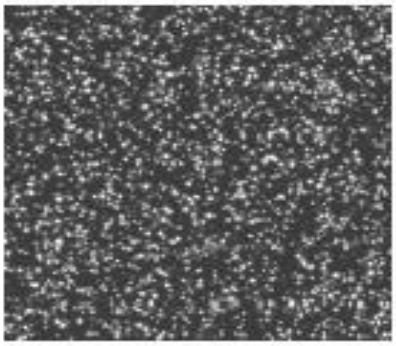

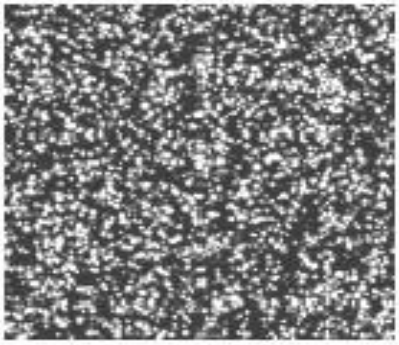

(a) (b)

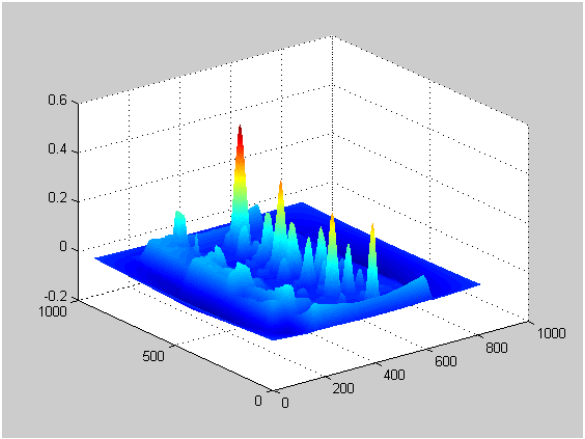

(c)

Figure 4.10 - Correlation of Sample C with GVF of 0.88 (heavily seeded)

*Calculations:*

The particle displacement recorded = 0.358mm = $35.8e^{-5}$ m

The velocity from $Speed = \frac{displacement}{time} = \frac{35.8*10e^{-5}}{20*10e^{-6}}$

Gas Flow Velocity, $V_{gas}$ = 17.9m/s

From $V_{FRG} = \alpha * \pi r^2 * V_{gas}$

$V_{FRG} = 0.88 * 3.142* (0.0254)^2 * 17.9$

$= 0.03193 m^3/s$

$\approx 114.93\ m^3/h.$

***Sample C - With steady volumetric flows set at 90m$^3$/h, lightly seeded density***

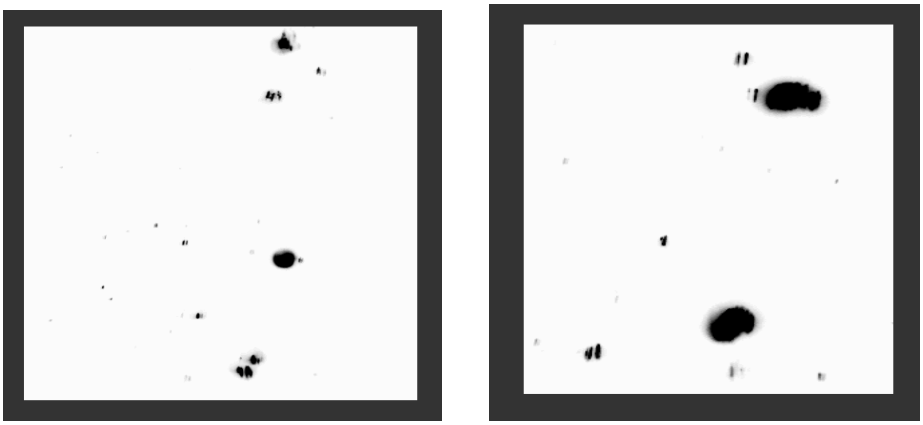

(a) (b)

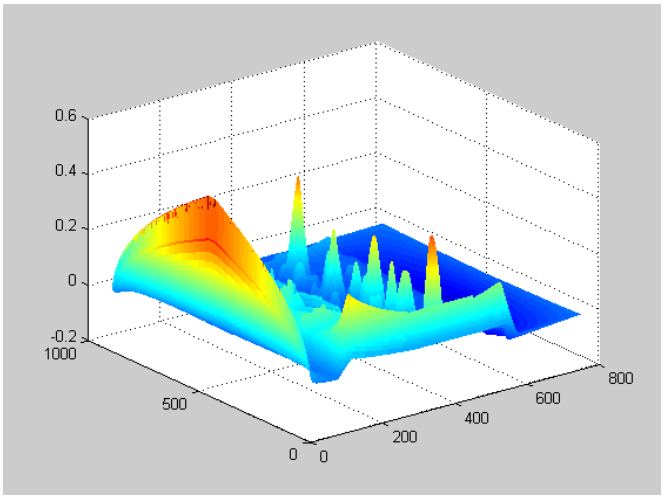


(c)

Figure 4.11 - Correlation of Sample C with GVF of 0.88 (lightly seeded)

*Calculations:*

The particle displacement recorded = 0.194mm = $19.4e^{-5}$ m

The velocity from $Speed = \frac{displacement}{time} = \frac{19.4*0e^{-5}}{20*10e^{-6}}$

Gas Flow Velocity, $V_{gas}$ = 9.7m/s

From $V_{FRG} = \alpha * \pi r^2 * V_{gas}$

$V_{FRG} = 0.88 * 3.142* (0.0254)^2 * 9.7$

$= 0.01730 m^3/s \approx 62.8 m^3/h.$

### 4.3.2 Discussion of Preliminary Results

Table 4.1 is a tabulation of the results obtained from the experimental analysis of flow for the three sample bottles at the flow of 125$m^3$/h (Rotameter reading) and heavily and lightly with seeding of the flow.

Table 4.1: Results of Heavily and Lightly seeded flow for a steady flowrate of 125m3/h

| **Name** | **Rotameter flowrate ($m^3$/h)** | **PIV Flowrate ($m^3$/h)** | **Absolute error/ (% Error)** |
|---|---|---|---|
| **Sample A - heavy seeded** | 125 | 121.86 | -3.14 (-2.512%) |
| **Sample A - Lightly seeded** | 125 | 126.76 | 1.76 (1.408%) |
| **Sample** B **- heavy seeded** | 125 | 151.38 | 26.38 (21.104%) |
| **Sample B - Lightly seeded** | 125 | 118.15 | -6.85 (-5.48%) |
| **Sample** C **- heavy seeded** | 125 | 114.93 | -10.07 (-8.056%) |
| **Sample C - Lightly seeded** | 125 | 62.8 | Outlier |
| **Average** | **125** | **126.616** | **1.616 (1.293%)** |

From the measurements obtained, the measured average flow rate bears a true resemblance to the flow rate. The maximum deviation obtained was for sample B (high seed density) with an absolute error of 26.38$m^3$/h (21.1%). The result from Sample C (lightly seeded) is an outlier. This is one of the deficiencies of MatPIV. The only explanation for this type of result is that the programme momentarily freezes whilst the PC undertakes health checks or something similar. This result was expunged from the calculation of average velocity and error.

### 4.3.3 Cross Correlation and Average Velocity for Varying Flowrates

Following the experiment on a steady flow rate of 125m$^3$/h for both lightly and heavily seeded flows for all three samples (A/B/C), it was considered that the effect of seeding density was understood and it was decided to go with the medium seeding density. For the rest of the experiments only Sample B was used.

***A: Flow rate set at 110m$^3$/h***

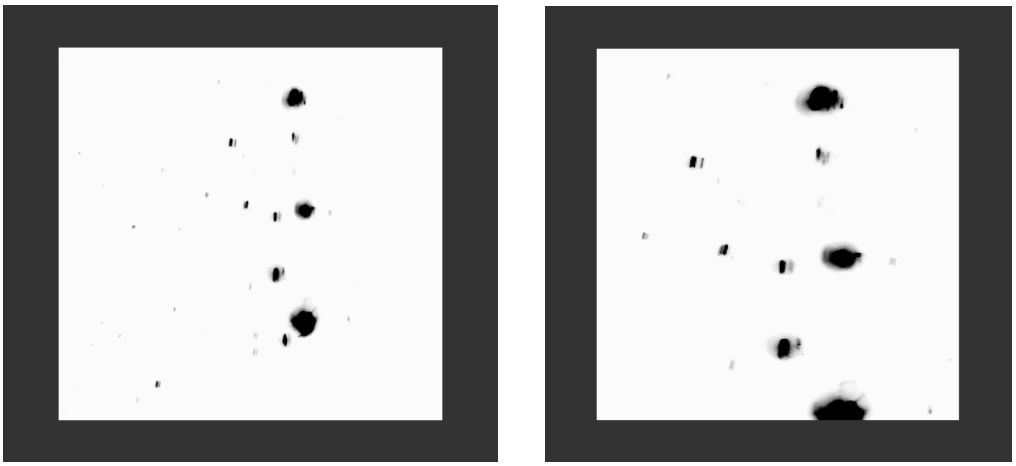

(a) (b)

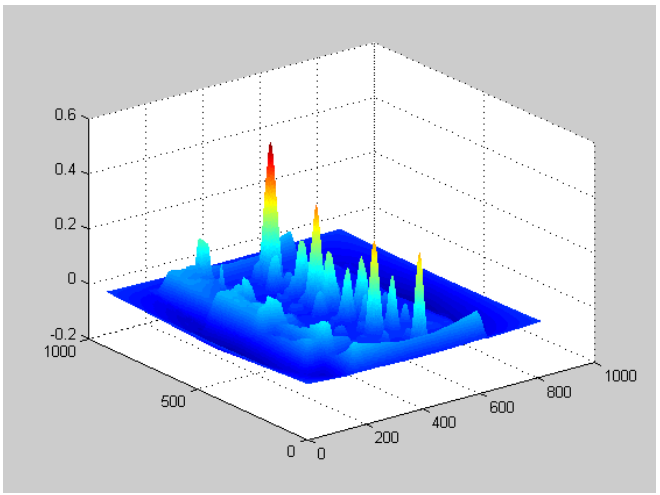


(c)

Figure 4.12 - Correlation of Sample B at a steady volume flow of

110m3/h

*Calculations:*

The particle displacement recorded = 0.363mm = $(36.3 * 10^{-5})$ m

The velocity from $Speed = \frac{displacement}{time} = \frac{36.3*10e^{-5}}{20*10e^{-6}}$

Gas Flow Velocity, $V_{gas}$ = 18.15m/s

Volumetric flow of gas, $V_{FRG,}$ is the product of phase velocity, phase fraction and internal diameter of pipe. Represented as:

$V_{FRG} = \alpha * \pi r^2 * V_{gas}$

$V_{FRG} = 0.92 * 3.142* (0.0254)^2 * 18.15 = 0.03384 m^3/s$

$\approx 121.824 m^3/h$

***B: Flowrate set at 120m$^3$/h***

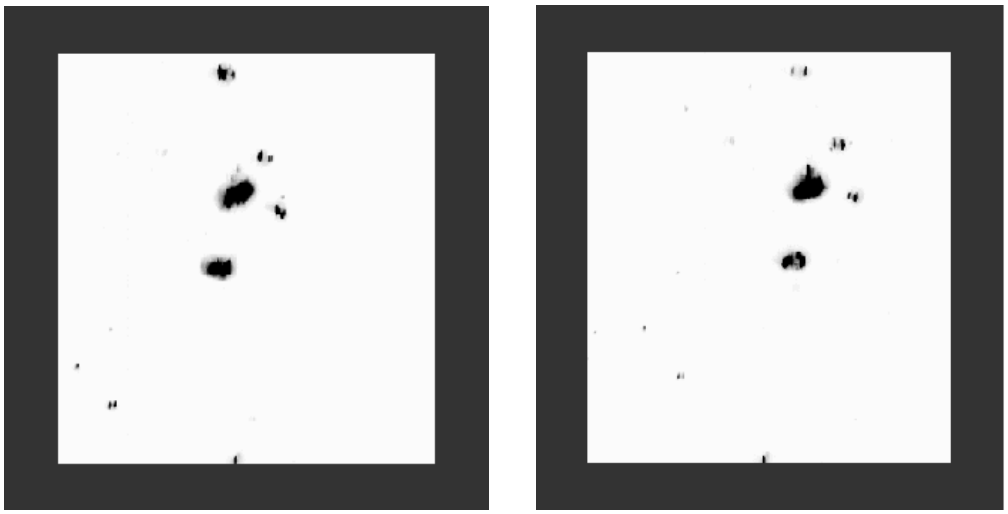

(a) (b)

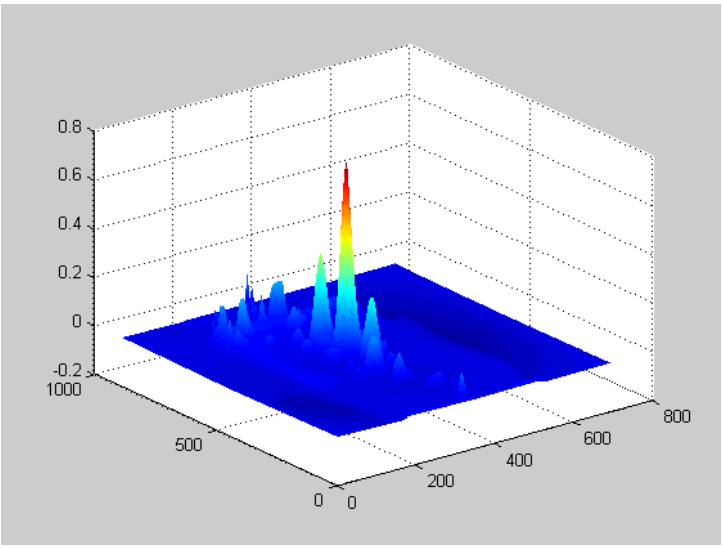


(c)

Figure 4.13 - Correlation of Sample B at a steady volume flow of 120m³/h

*Calculations:*

The particle displacement recorded = 0.399mm = $(39.9 * 10^{-5})$ m

The velocity from $Speed = \frac{displacement}{time} = \frac{39.9*10e^{-5}}{20*10e^{-6}}$

Gas Flow Velocity, $V_{gas}$ = 19.95m/s

Volumetric flow of gas, $V_{FRG,}$ is the product of phase velocity, phase fraction and internal diameter of pipe. Represented as:

$V_{FRG} = \alpha * \pi r^2 * V_{gas}$

$V_{FRG} = 0.92 * 3.142* (0.0254)^2 * 18.15 = 0.03720 m^3/s$

$\approx 133.92 m^3/h$

***C: Flowrate set at 130m$^3$/h***

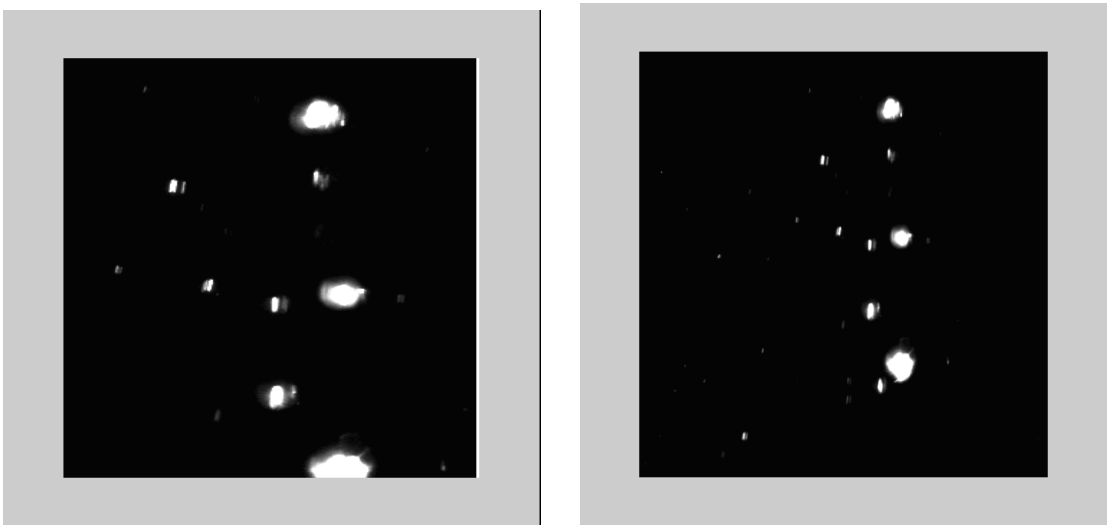

(a) (b)

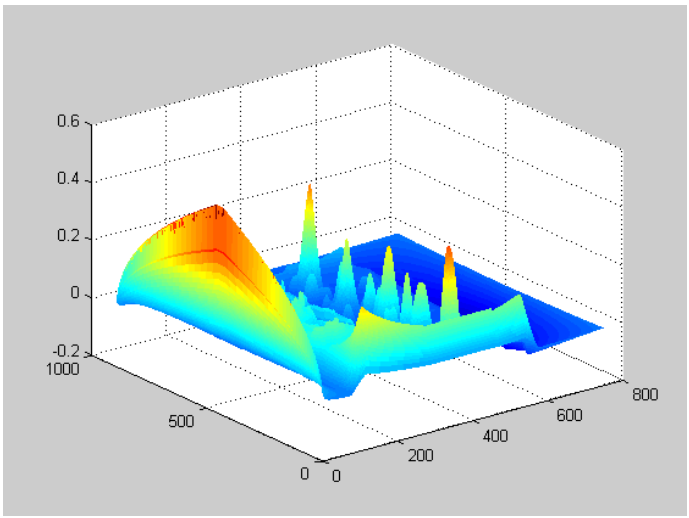


(c)

Figure 4.14 - Correlation of Sample B at a steady volume flow of

130m³/h

*Calculations:*

The particle displacement recorded = 0.2mm = $(2.0* 10^{-2})$ m

The velocity from $Speed = \frac{displacement}{time} = \frac{20.0*10e^{-6}}{20*10e^{-6}}$

Gas Flow Velocity, $V_{gas}$ = 1.0m/s

Volumetric flow of gas, $V_{FRG,}$ is the product of phase velocity, phase fraction and internal diameter of pipe. Represented as:

$V_{FRG} = \alpha * \pi r^2 * V_{gas}$

$V_{FRG} = 0.92 * 3.142* (0.0254)^2 * 1 = 0.001865 m^3/s$

$\approx 6.714 m^3/h$

***D: Flowrate set at 130m$^3$/h (Repeat)***

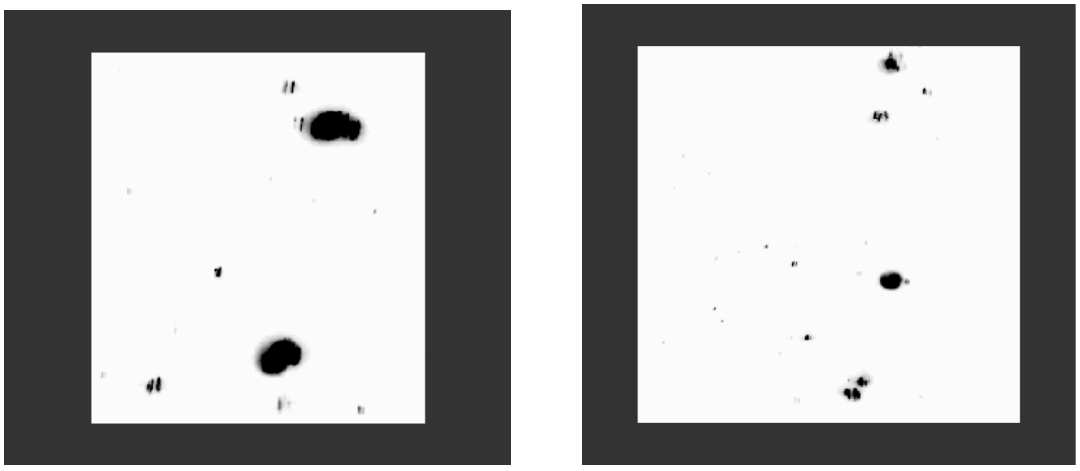

(a) (b)

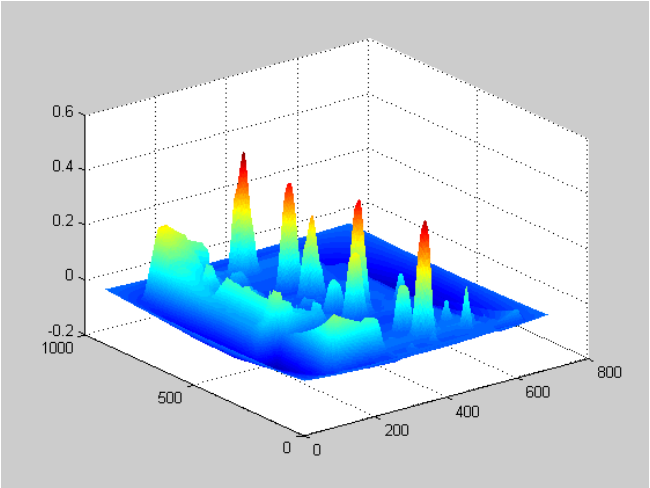


(c)

Figure 4.15 - Correlation of Sample B at a volume flow rate of 130 $m^3/h$

*Calculations:*

The particle displacement recorded = 0.344mm = $(34.4 * 10^{-5})$ m

The velocity from $Speed = \frac{displacement}{time} = \frac{34.4*10e^{-5}}{20*10e^{-6}}$

Gas Flow Velocity, $V_{gas}$ = 17.2m/s

Volumetric flow of gas, $V_{FRG,}$ is the product of phase velocity, phase fraction and internal diameter of pipe. Represented as:

$V_{FRG} = \alpha * \pi r^2 * V_{gas}$

$V_{FRG} = 0.92 * 3.142* (0.0254)^2 * 17.2 = 0.03207 m^3/s$

$\approx 151.45 m^3/h$

***Discussion of results:***

Three more run of sample B was done this time at three different flowrates 110$m^3$/h, 120$m^3$/h and 130$m^3$/h. The results is as tabulated in Table 4.2.

Table 4.2: Results of Sample B using three different flow rates.

| **Name** | **Rotameter flowrate ($m^3$/h)** | **PIV Flowrate ($m^3$/h)** | **Absolute error/ (% Error)** |
|---|---|---|---|
| **PIV A** | 110 | 121.824 | 11.824 (10.749%) |
| **PIV B** | 120 | 133.92 | 13.92 (11.6%) |
| **PIV C** | 130 | 6.714 | -94.84 %(Outlier) |
| **PIV D** | 130 | 151.45 | 21.45 (16.5%) |
| **Average** | **120** | **135.73** | 15.73 (13.108%) |

Test C again gave a poor result which was considered an outlier because the computer had switched from MatPIV to perform other health checks.

***E. Seeding the liquid phase:***

Further experiments were carried out to verify if the liquid phase would yield useful result if seeded. The results as shown in Figure 4.16 proved to be unsuccessful, as the liquid quickly covered the injected seed and then a clear view was impossible. It was decided at this point that liquid flow tracers would be used. Once the velocity of each phase can be identified, the flow rate of each phase can then be measured with higher accuracy.

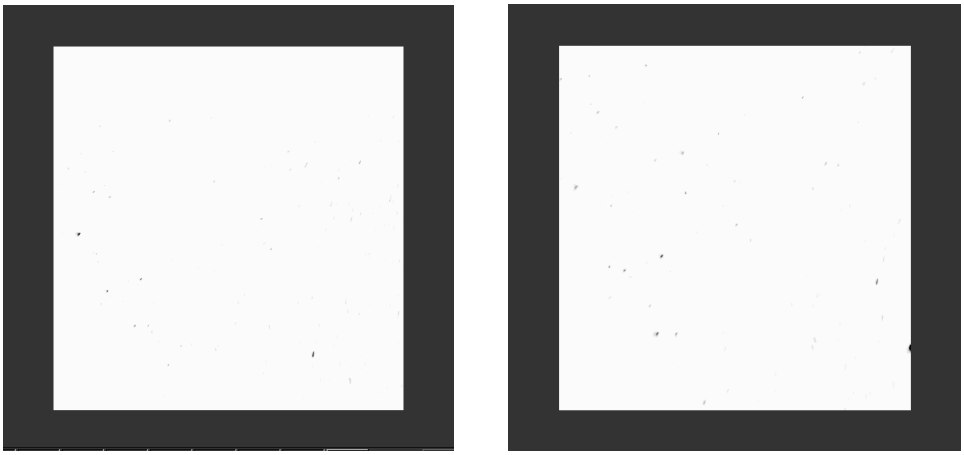

(a) (b)

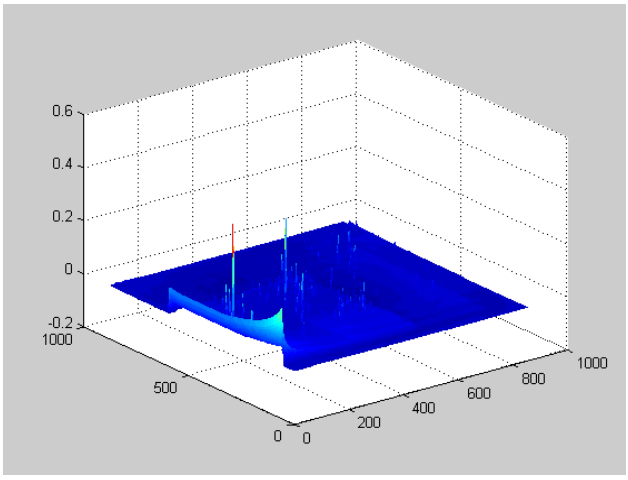


(c)

Figure 4.16 - Frames of seeded condensate flow yielding no useful correlation

The plot above shows that it was nearly impossible to excite the seed within the condensate. This was purely due to the fact that the seeds where quickly covered making it impossible to obtain a view. Note that the GVF used here was about 50%.

## 4.4 Sources of Uncertainty

The first step in minimising sources of error in an experiment is in recognising and understanding them, as many sources of error can be minimised. Those that cannot be minimised can be characterised and can be accounted for, resulting in a quantifiable uncertainty. A few assumptions were made whilst executing this work:

- Seed particles follow the fluid motion
- Seed and tracer particles are distributed homogeneously
- There is uniform displacement within the interrogation region
- The time delay between the laser pulses are long enough to capture the displacement of the tracer particles and short enough so that the particles with an out-of-plane velocity component leave the light sheet
- The size of the interrogation area is small such that there is no significant velocity gradient within the interrogation area

### 4.4.1 Loss of Pairs

Loss of pairs occurs when the signal from a particle is recorded in only one of the two frames. Loss of pairs is primarily caused by two factors:

(1) The finite nature of interrogation regions

(2) Out of plane velocity

Because an interrogation region is bounded, there will be particles that cross the region's boundary from frame one to frame two (the pulse delay), and this crossing is most pronounced near the borders and is exacerbated by longer pulse delays. With an estimate

of the bulk velocity, this error can be mitigated by setting the pulse delay to a value corresponding to a small expected displacement.

As a rule of thumb, it is recommended that the average displacements should correspond to less than one fourth of the interrogation region size. There are also filters and other processing techniques that aid in the reduction of this error.

The three main techniques are:

(1) Use of overlapping interrogation regions

(2) Interrogation region centre-biasing

(3) Data validation

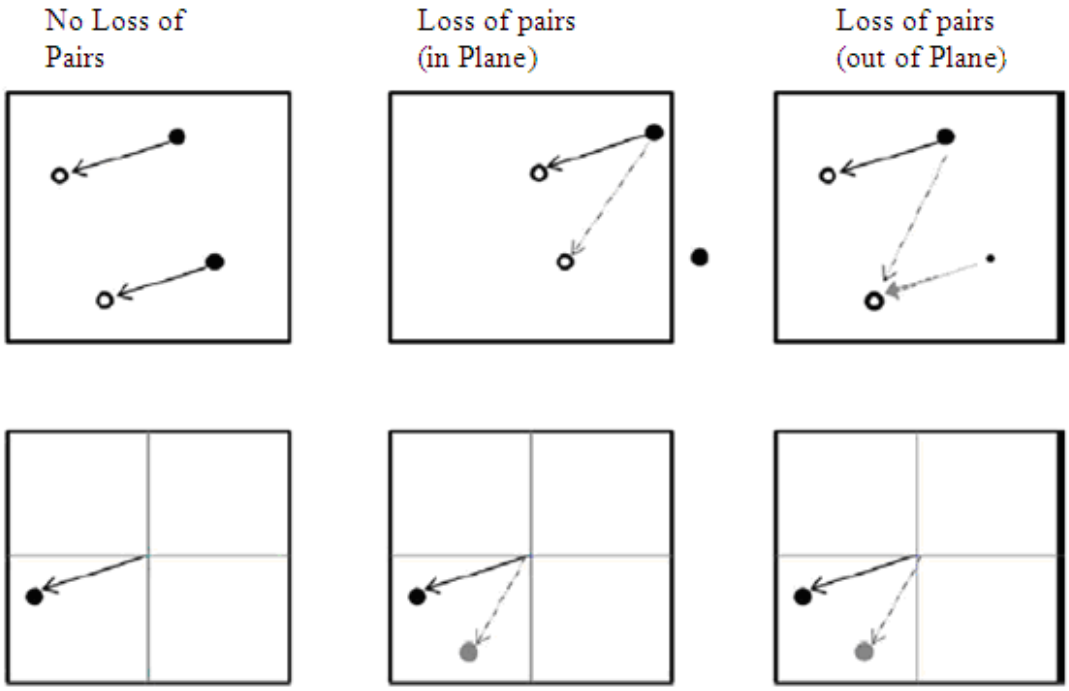


Figure 4.17 - Error due to lost of pair

In Figure 4.17 the top row shows three examples of interrogation regions with their image pairs overlapped. The solid dots represent signals from image one and the hollow

dots represent signals from image two. The solid arrows show true displacements and the dashed arrows show false displacements over the pulse delay. The bottom row shows the displacement vectors calculated from the cross-correlation. Similarly, the solid arrows are the correct displacements and the dashed arrows are false. In the leftmost column there is no loss of pairs and this is the control group. In the middle column, loss of pairs occurs with one of the particles as its initial position is outside the interrogation region. This results in a 1:1 ambiguity, in that the particles in image two are both equally likely to be the final position corresponding to the particle in image one. In this case, the cross-correlation would result in two equal peaks and the true displacement would be unknown. The second main cause of loss of pairs is out of plane velocity, as shown in the rightmost column of Figure 4.17. This loss occurs when the particle velocity is not parallel to the focal plane. The particle at the top of the interrogation region shows in-plane motion. That is, it is travelling in the experimental plane over which the camera is focused. The bottom particle in the figure is travelling with the same top right to bottom left motion, but also has an "out-of-the-page" component in its velocity vector. Because of this out-of plane component, the particle is behind the experimental plane in image one but moves into the experimental plane in image two. The image map from frame one shows only one particle, but the second shows two particles, and this loss of pairs result in the same error as in the first example – an ambiguity the cross-correlation cannot resolve.

### 4.4.2 Parallax Effects

Any out of plane velocity small enough relative to the experimental plane's thickness such that both images are still captured, will introduce an error due to the effect of parallax. The parallax effect results from the projection of 3-D motion onto a 2-D image,

but is different from the inability for a 2-D measurement to capture 3-D effects. Error from the parallax effect is a function of the image scale factor, in that two images at different depths within the experimental plane are multiplied by the same scale factor even though they are at different distances from the camera's CCD. The maximum error caused by the parallax effect is directly proportional to the thickness of the experimental plane and inversely proportional to the camera's scale factor. Therefore, a thinner laser sheet and camera placed farther away from the experimental plane will allow for less error due to the parallax effect.

### 4.4.3 Zero-Velocity Biasing

There appeared to be a natural bias towards zero particle displacement. In the experimental setup, the pulse delay setting the camera and laser timing was chosen so that the average particle displacement between frames will be less than one quarter of the interrogation region size. In a steady one-or two-dimensional flow parallel to the illumination area, this experimental design should have provided accurate flow measurements.

However, the problem was that the flow-field was not already known and it was rarely a steady 2-D flow. The experimental setup and timing of equipment was based on estimates. Even in a fairly steady and well developed flow there will be irregularities. The seed particles moving at the bulk velocity or lower will be measured with a high degree of accuracy; however, seed particles entrained by quickly moving eddies or other turbulent flows are far more likely to have their initial or final position outside the interrogation area, and are therefore less likely to be accurately recorded. This propensity

toward measuring the slower velocities with more accuracy is known as "zero velocity biasing". Quick pulse delays, sufficient particle seeding, and certain post processing techniques mitigate this problem.

### 4.4.4 Uncertainty due to Correlation

Although the cross-correlation technique is straightforward and relatively simple, there is a major pitfall: correlation is drawn between disturbances and not fluid velocities. In a fully developed turbulent flow, the larger eddies live longer, and thus contribute preferentially to the cross-correlation function. The peak in the cross-correlation function between the two measurements represents the "time of flight" of a flow feature between the two measurement positions. The cross-correlation method, although not as dependant on calibration, suffers from several problems; it can find non-valid correlation peaks due to camera senor noise, lighting variation, out-of-plane particle movement and particle rotation, too long a time delay between the pictures. These non-valid correlation peaks result in erroneous velocity vectors that have to be filtered from the result. The most important to note is that to measure the velocity, a distinct flow feature is required. The problem here is that of relating this velocity to the fluid velocity with sufficient accuracy.

### 4.4.5 Uncertainty due to Varying Liquid Flow Rate

Flow rates for liquids are not constant within turbulent multiphase flows but vary over time, which can range from minor changes to severe fluctuations, like those in the slug flow regime.

In the case of wet gas well flows, this effect is enhanced by the variability of the liquid hold-up in the tubing; however, this has consequences for the tracer dilution technique and causes concerns regarding fluctuations at time scales larger than the time scale of the axial dispersion of the tracer mixing between injections and imaging areas. Axial dispersion of the mixing can best be understood by the following thought experiment.

Imagine that in a very short time a pulse of tracer solution is injected into the flow line. The transportation velocity of this pulse of tracer solution will not be the same for every molecule, so if the tracer concentration at the sampling point can be determined, then a gradual increase to a maximum value and a gradual decrease until it vanishes would be observed. The time scale of this rise-and-fall is a measure of the axial dispersion. Compare this with the widening of peaks in chromatography, which is a similar phenomenon. The longer the distance between injection and imaging points, the larger the time scale of the axial dispersion will be. It should also be noted that a larger pipe diameter has the opposite effect.

The presence of fluctuations with large time scales means that the instantaneous tracer concentration also fluctuates. However, the tracer concentration is inversely proportional to the liquid flow rate and the relation is therefore non-linear. However, the sampling requires a time, which is significantly longer than the time scale of the axial dispersion, which means that the average tracer concentration is not equal to the inverse of the average liquid flow rate. As a result, the liquid flow rate will show a systematic error (a too low value), which rapidly increases with the amplitude of the large-scale liquid flow rate variations. A simulation result is shown below, in which a sinusoidal change in liquid flow rate is assumed and the maximum amplitude is 50% of the average value. As can be seen, the

error rapidly increases with increasing amplitude. Therefore the tracer technique can only be applied in "steady" flow regimes like stratified and annular flows and not in unsteady flow regimes like slug flow. This is a fundamental limitation of the tracer dilution technique and therefore, one has to estimate the stability of the liquid flow rate before the tracer testing is undertaken.

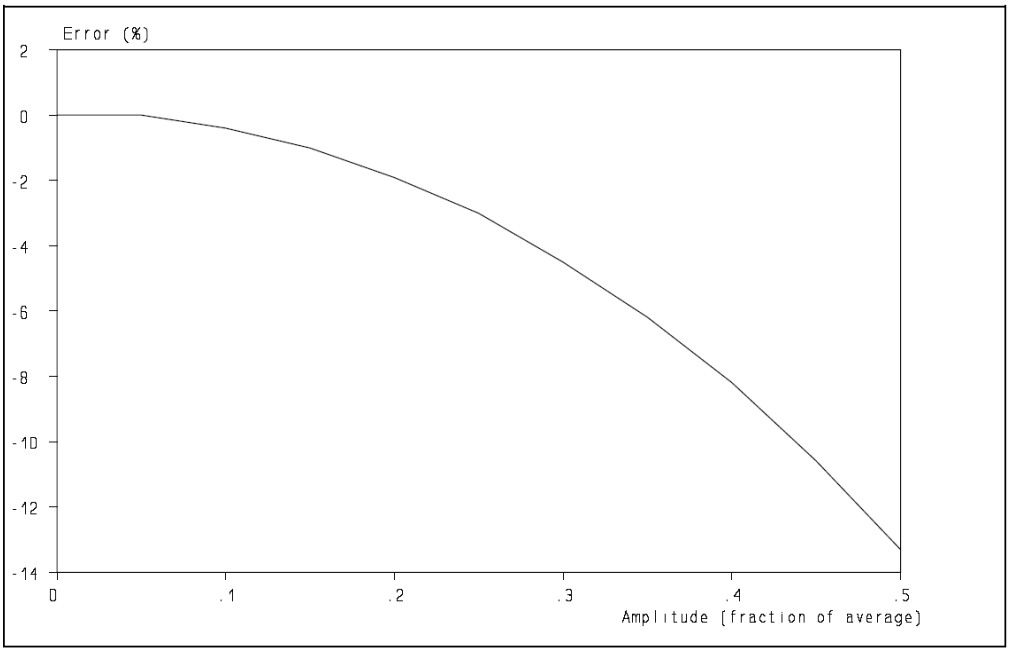


Figure 4.18 - Error of the tracer dilution technique due to varying liquid flow rate

## 4.5 Liquid Flow Measurement

The basis of the tracer dilution technique is relatively simple: a fluorescent tracer is injected upstream of the PIV spool piece into the pipeline, which is diluted by the condensate flowing through the pipeline as shown in Figure 4.19. After sufficient mixing

with the condensate, the liquid is sampled and the ratio of the concentrations of the injected liquid and the sampled liquid determines the liquid flow rate. Silicon Carbide (SiC) was the fluorescent tracer used for the condensate. It was diluted 10.2 and injected in the process at a known flow rate using a calibrated syringe pump. After mixing of the solution with the condensate phase, a sample was taken and from the dilution ratio between the injected tracer solution and the sample, the liquid flow rates was determined using equation 4.1.

$$Q_p \approx \frac{c_i}{c_p} Q_i \qquad 3.1$$

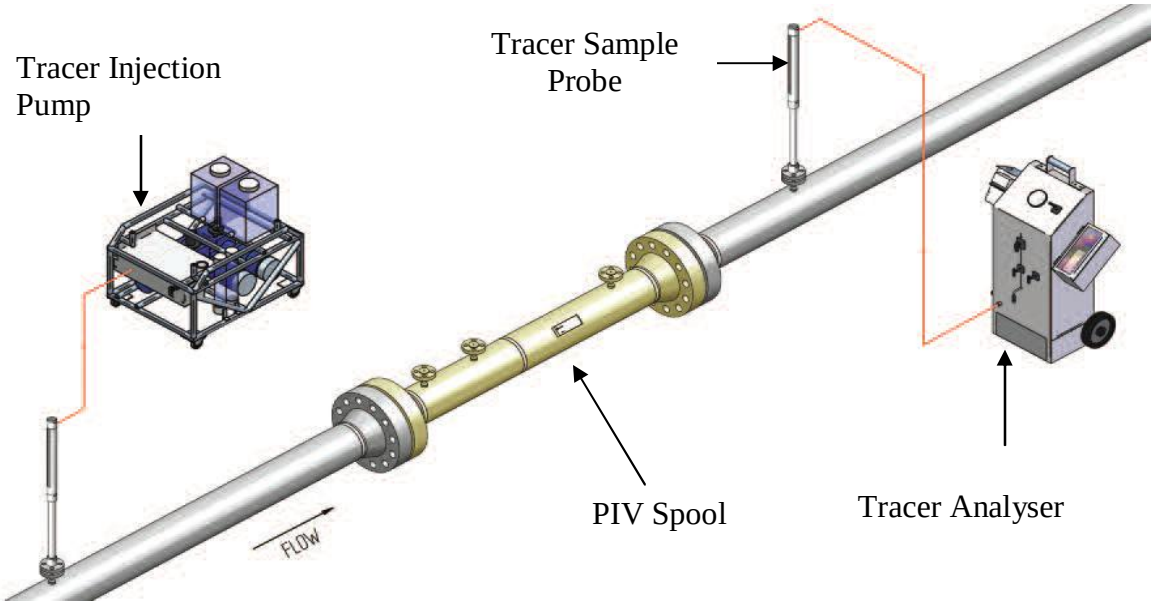


Figure 4.19 - Schematic of tracer dilution technique

### 4.5.1 Operation Principles of Rig

The experimental setup for the tracer dilution technique included the following:

- Calibrated measuring flasks or pipette.

- Tracer injection pump
- SiC tracer duly mixed in solution
- Filter for the samples to eliminate turbidity.
- Fluorometer was used for fluorescence measurements
- An auto sampler

The control samples consisted of the "blank" condensate, and the fluorescence was measured and recorded.

The tracer injection pump was started in a continuous injection mode, and the start time was noted. Five different samples were taken and analysed, and the tracer concentration was measured by means of the fluorescence of the sample. The fluorometer used was a Turner 10-AU-005 field fluorometer which uses cylindrical test tubes.

The following procedure was applied:

1. From the injected tracer fluid a diluted sample was prepared with a tracer concentration close to the concentration in the retrieved samples downstream of the PIV spool. This requires some iterative steps and practical values for the dilution rate.
2. From this sample a small amount (1 ml.) was mixed with a small amount of pure condensate, as the liquid retrieved at the sampling point is also mixed with this liquid.
3. This mixture was diluted with heptane until a precisely known volume (25 ml.) is obtained.

4. A small amount of the retrieved sample was diluted in the same way with heptane until again a known volume was obtained (identical to the volume at step 3). In this way the samples to be analysed by the fluorometer were similar.

5. A small amount (e.g. 1 ml.) of the pure condensate was diluted with heptane until again a known volume (identical to that used in steps 3 and 4) was obtained. This acts as a measure for the background fluorescence.

### 4.5.2 Results:

Table 4.3: Condensate tracer data for Sample A

| Sample Num | Injection flowrate ($m^3/h$) | | Fluorescence | Flow rate ($m^3/h$) |
|---|---|---|---|---|
| **Background** | | | 13.8 | |
| **Control** | | | 230 | |
| **Dilution ratio** | | 10.2 | | |
| **1** | 0.9 | | 149 | 5.74 |
| **2** | 0.9 | | 142 | 5.44 |
| **3** | 0.9 | | 148 | 5.70 |
| **4** | 0.9 | | 144 | 5.53 |
| **5** | 0.9 | | 139 | 5.32 |
| **Average Flow rate** | | | | **5.55** |

Table 4.4 Condensate tracer data for Sample B:

| Sample Num | Injection flowrate ($m^3/h$) | | Fluorescence | Flow rate ($m^3/h$) |
|---|---|---|---|---|
| **Background** | | | 13.8 | |
| **Control** | | | 230 | |
| **Dilution ratio** | | 10.2 | | |
| **1** | 0.9 | | 210 | 8.33 |
| **2** | 0.9 | | 214 | 8.50 |

| | | | | |
|---|---|---|---|---|
| **3** | 0.9 | | 212 | 8.42 |
| **4** | 0.9 | | 188 | 7.40 |
| **5** | 0.9 | | 198 | 7.82 |
| **Average Flow rate** | | | | **8.09** |

Table 4.5: Condensate tracer result for Sample C

| **Sample Num** | **Injection flowrate ($m^3/h$)** | | **Fluorescence** | **Flow rate ($m^3/h$)** |
|---|---|---|---|---|
| **Background** | | | 14.8 | |
| **Control** | | | 283 | |
| **Dilution ratio** | | 10.2 | | |
| **1** | 1.2 | | 271 | 11.69 |
| **2** | 1.2 | | 257 | 11.05 |
| **3** | 1.2 | | 261 | 11.24 |
| **4** | 1.2 | | 263 | 11.33 |
| **5** | 1.2 | | 260 | 11.19 |
| **Average Flow rate** | | | | **11.30** |

### 4.5.3 Discussion of Results

In section 4.3 there were three sample bottles labelled A, B and C which were used and the sample was set to flow at a rate of $125m^3/h$ on the rotameter.

1. Sample A has a GVF of 96% (0.96).
2. Sample B has a GVF of 92% (0.92).
3. Sample C has a GVF of 88% (0.88).

From Table 4.3 it can be seen that the average volumetric flow for the condensate was recorded at $5.55m^3/h$, for Sample A. This result closely resembles that anticipated flow of $5m^3/h$. From Table 4.4, the average volumetric flow for the condensate was recorded at $8.09m^3/h$. With a GVF for Sample B of 0.92 and a set volumetric flow rate of $125m^3/h$ for the gas, it was anticipated that the volumetric flow rate for the liquid in the same flow

would be $10m^3/h$. Finally, in Table 4.5, the average volumetric flow for condensate was recorded as $11.03m^3/h$. Given the GVF for Sample C is 0.88, with a set volumetric flow rate of $125m^3/h$ for the gas, it was anticipated that the volumetric flow rate for the liquid in the same flow would $15m^3/h$. Therefore there appears to be a systematic decline in the liquid flow rate recorded as GVF reduces, demonstrating more hold up at the wall.

## 4.6 Measurement Error of Liquid (HC) Phase Measurement

The errors from the tracer technique come from the following sources

- The injected tracer solution and the target liquid must be mixed completely. Although no detailed study has been undertaken in the exact requirements, a distance of 150 Diameters (in accordance with the ISO standard on gas tracers) between the injection and sampling points is found to be sufficient in practice. Additional bends, valves and Ventures, which all increase the turbulence and thus enhance the mixing, are attractive.
- The implicit assumption of the tracer dilution technique is that the flow is steady. Unsteady flow (e.g. slugging) leads to systematic errors due to the inverse relationship between the concentration and the liquid flow rate which affects the averaging during sampling.
- The tracer dilution technique is still in the developmental stage and rather labour intensive. Automation could reduce the amount of work involved significantly,
- The tracer dilution technique cannot be applied continuously, so the liquid flow rate determination remains a "spot" measurement.

Despite these limitations, the tracer dilution technique offers an option for the determination of the liquid flow rates without the use of a test-separator. However, as the

tracer solution injection flow rate and the tracer concentration can easily be adapted to the conditions in the flow line, the tracer dilution technique has a very high turn-down ratio: a factor of 1000 is easily achieved, thus outperforming any test separator, even when different instruments or transmitters are used.

## 4.7 Conclusions

The tracer measurements did not go smoothly. The first problem encountered was the blockage of the sampling point and solving this required de-pressurisation of the pipeline. More serious problems occurred with the injection pump, and as can be inferred from the tracer equation, the injection volume is linearly related to the value obtained for the condensate flow rate. This injection flow rate, however, proved to be unstable. However, the tracer technique gives values for the water flow rates which are in good agreement with the test-separator readings.

The stability of the tracer injection volume flow rate is essential to obtain accurate results, but the injection pump used in these measurements was not suited for its task. A skid with either a feedback control or an independent injection volume flow measurement (or possibly both) would have been preferred but was not available. The tracer procedure is rather laborious and manual, which can also lead to error.

# CHAPTER 5: CONCLUSION AND FUTURE WORK

Multiphase Flow Measurement is not a new technology, but still relatively nascent in the oil and gas industries. The general consensus is that there is no single multiphase flow meter design capable of providing the required accurate measurements of oil and gas fractions, as well as the phase velocities under all flow conditions. However, this research work has demonstrated that low cost and simple non-intrusive imaging system, in combination with a complex digital processing technique can be used to infer the superficial gas and liquid phase velocities of very high GVF. It enables the individual component mass flow rates of the wet-gas flow to be determined to a degree of accuracy that may surpass some commercially available multiphase flow meters.

In this thesis, a PIV image visualisation and tracer technique combined approach has been proposed. The concept has been implemented using CCD camera, MATLAB platform based algorithm in a rig in Shell. The experiments have been conducted using this rig under a range of different phase fractions and at various flow rates. The gaseous phase and liquid phase measurement have been validated by comparison of the measured flow rate and the controlled flow rate. The measurement errors have been analysed. Based on the literature review, theoretical analysis and experimental verification, the following conclusions can be drawn:

1) The proposed technique can be used to measure wet gas for HC fraction below 10%, it is non-intrusive. Compared to other systems, it is low cost.

2) This method can provide the velocities of both liquid HC and gaseous phase, with liquid gas chromatography to provide phase fraction information, the flow rate of each phase can be obtained.

3) This system does not need preconditioning of the flow. It however needs prior knowledge of either phase (the HC liquid fraction needs to be lower than 10%)

4) PIV is not suitable for HC liquid measurement, because as the liquid flows on the pipe wall it blocks the camera view giving no reasonable data for analysis. That is the reason why the liquid phase has to be measured using tracer technique in this method.

5) For multi-phase flow with HC fraction above 10%, this method will not be reliable because of the reflection from liquid film formed on the pipe wall can "blind" the camera.

6) For selected three different gas and liquid fraction samples, the measurement accuracy for different velocities and phase fractions is acceptable and comparable to that of those systems commercially available at present.

7) MATLAB has provided a very useful platform for building the test software and algorithm implementation. However for industrial application, more reliable software is required.

8) The focus of this research was on volume flow rate of gas and liquid phase measurement of wet gas under prevailing (i.e. actual) pressure and pressure conditions. However for mass flow measurement, or standard volume flow rate (under 1 atmosphere pressure and $20^{o}$C) the pressure and temperature compensation will be vital, because the density of gaseous and HC liquid phases will depends on these two parameters. In the software, the entry point for such compensation has been reserved.

9) The reference readings were based on the readings from the Rotameter. Due to the error of this reference meter (it actually read the flow rate of wet-gas, not the separate readings of gas and HC condensate), the error analysis in Chapter 4 is not satisfactory. At the current stage, the main purpose is to show the viability of the proposed method, however for future calibration purpose, a rig which allow to add pure gas, pure HC liquid before they are mixed, needs to be developed, so that the gas phase flow rate and liquid flow rate can be measured using reliable single phase flow meters to provide accurate references for the proposed system.

## 5.1 Key Learning and Findings

Science they say travels on a gravel road. The approach to provide a novel multiphase flow meter based on combining *Particle Image Velocimetry* and tracer dilution would at this point only be useful in the laboratory, which of cause is important to gain understanding of the fluid mechanics governing the flow. For use in the "field", especially for control purposes, a few technological hurdles have to be solved before accurate flow rates can result.

Employing pattern recognition for multiphase flow analysis has been documented by researchers to resolve the multiphase parameter measurements or to identify the prevalent flow regime. However, the flow in this meter involves non-intrusive measurement components.

No information has been published in the public domain on the use of non-intrusive image visualization technique that detect shifts in flow conditions (flow structure,

pressure etc.), to provide phase composition and velocity information simultaneously without the need for pre-conditioning or prior knowledge of either phase.

This research work has demonstrated that relatively low cost cameras can be exploited, in combination with digital signal processing, to infer the superficial gas and liquid phase velocities for very high gas volume fraction of (95 – 100%), thus enabling the individual component mass flow rates of the multiphase flow to be determined to a degree of accuracy comparable with several commercially available multiphase flow meters. The measurement system used for this research consists of a CCD cameras, laser, synchronization system, MATLAB program all integrated as a single horizontal spool piece. Seeds and tracer particles were used as the key ingredients to follow the flow and infer the velocities of the different phases.

## 5.2 Project Challenges

Though sampling of the process was never the subject of investigation in this thesis, it must be stated that getting a representative sampling in a multiphase flow is difficult, and requires that rigorous procedures are followed. However, if a well-designed procedure is followed, sampling and offline analysis of the water/liquid ratio can be a very efficient method for tracking the performance of a MPFM. Obtaining a representative liquid sample is by no means straightforward, and the complexity may vary between applications. Issues to consider during sampling include but not limited to:

- The sampling point should be in a vertical leg of the flow line, best position is immediately downstream a flow line component providing a mixing effect.

- A number of subsequent samples (minimum 5) should be taken. Each sample must be allowed to completely separate before the GVF is measured.
- All samples must be taken within a time frame where the GVF is stable, i.e. with variations less than the uncertainty required for the verification.
- The sampling point should be close to the MPFM, and the time frame for the samples must be selected such that the samples are representative for the liquid passing through the MPFM during the same time frame.
- If the difference between the highest and the lowest WLR of the samples obtained is greater than the uncertainty required for the evaluation, the verification test should be terminated, and a complete new set of samples must be obtained.
- The average GVF of the samples should be used for the comparison with the MPFM. The uncertainty of the average GVF will be no better than 2 times the standard deviation of the samples.

## 5.3 Future Work

At this stage, the primary objectives of this research work have been achieved. However further development work is vital for industrial application. Preliminary discussions have been opened with Yokogawa to explore this approach. Some recommendations for further enhancements are stated below.

1. In its current form, the "*Uletech*" measurement model developed will only be useful in the laboratory, but in the "field", it would be impossible due to fouling of windows. Application of the technique developed to other installations will require further developmental work.

2. The present study utilised one type of HC oil (Forties Beryl). No attempt was made to establish the relationship between features' responses and fluid physical properties. This type of study is necessary to generalise the proposed technique. Key parameters that should be considered are oil density, oil viscosity, increased levels of water salinity, from a variety of salts, especially sodium chloride, which is the predominantly occurring natural salt encountered in oil and gas exploration.

3. The operating pressure, pipe line diameter, and pipe orientation, as well as temperature should also be considered.

4. The tracer injection method is still very laborious and further work will be necessary to automate the process.

5. There are at the moment no florescent tracers for gas, which would not need to be separated from the flow. For "*Uletech"* to become applicable for control purposes, florescent gas tracer needs to be developed.

6. The repeatability of the setup needed to be further evaluated. There was not enough time to drill into this aspect.

7. The limitation from the rig is that simultaneous measurement of the gaseous and condensate flow rate could not be done. The liquid had to be analysed separately using tracer dilution method. Although, this was not a lot of concern as the experiment was to

validate the suitability of the method for wet gas measurement, for the further development, the rig needs to be further modified to accommodate such experiments.

8. The water content can be measured, but the experiments have not been conducted. To measure wet gas, water content cannot be avoided. The future work will also include this aspect.

# REFERENCES


1. Accuflow *AMMS Product Technology Information* [online]. Available at: <http://www.accuflow.com/default2.asp?active_page_id=197>.

2. Adrian, R.J. and Westerweel, J. (2011) *Particle Imaging Velocimetry*. Cambridge University Press: New York, pp.261–304.

3. Agar, J. (2010) New Coriolis based multiphase flow meter for heavy oil mature fields. *SPE Russian Oil and Gas Technical Conference and Exhibition, Moscow, October 2010*,Vol.1, pp.453-464.

4. Agar, J., Fachy, D. and Agar Corporation. (2002) Wet Gas Metering Using Dissimilar Flow Sensors: Theory and Field Trial Results. *SPE Annual Technical Conference and Exhibition, San Antonio, Texas.*

5. Al-Bourni, H.A., Samizo, N., Bakhteyar, Z, and Alvi, A. (2005) Application of New Multiphase Flow Measurement Systems with Satellite-Based Monitoring in Offshore Khafji Field. *International Petroleum Technology Conference, Doha, Qata*r, *November 2005*.

6. Al-Taweel, A.B. and Barlow, S.G. (1999) Field Testing of Multiphase Meters. *SPE paper 56583, Annual Technical Conference and Exhibition, Houston, Texas.*

7. Anisimov, L. (2012) Productivity index change as a result of reservoir compressibility. *SPE Production and Operations Symposium, May 2012, Doha, Qatar*, Vol.1, pp.200-206.

8. Atmaca, S., Sarica, C., Zhang, H.-Q. and Al-Sarkhi, A.S. (2008) Characterization of oil water flows in inclined pipes. *Proceedings of SPE Annual Technical Conference and Exhibition 2*, pp.1273-1286.

9. Babelli, I.M.M. (2002) In search of an ideal multiphase flow meter for the oil industry. *Arabian Journal for Science and Engineering*, Vol.27, No.2, pp.113-126.

10. Baker, O. (1954) Simultaneous Flow of Oil and Gas. *Oil and Gas Journal*, Vol.53, pp.85- 195.

11. Beck, M.S. and Plaskowski, A. (1987) *Cross Correlation Flow Meters: Their Design and Application.* Adam Hilgar: Bristol.

12. Bendiksen, K. and Espedal M. (1992) Onset of slugging in horizontal gas-liquid pipe flow. *International Journal of Multiphase Flow*, Vol.18, pp.237-247.

13. Blaney, S. and Yeung, H. (2007) Gamma Radiation Methods for Cost-Effective Multiphase Flow Metering. 13th *International Conference on Multiphase Production Technology, Edinburgh, Scotland.*

14. Blaney, S. (2008) *Gamma Radiation Methods for Clamp-On Multiphase Flow Metering*, PhD Thesis, Cranfield University.

15. .Brill J.P, Schmidt, Z., Coberly, W.A., Herring, J.D. and Moore, D.W., (1981) Analysis of twophase tests in large diameter flowlines', SPE Journal, Vol.6, pp. 363-378.

16. Brill, J.P. and Arirachakan, S.J. (1981) State of the Art in Multiphase Flow. *Journal of Petroleum Technology*, Vol.44, No.5, pp.538-541.

17. Brown, R.D. (1985) Seeding Materials-Health and Safety Concerns. *Proceedings of a workshop held at NASA Langley Research Center, March 19-20*. NASA Conference Publication 2393.

18. Busaidi, K. and Bhaskaran, H. (2003) Multiphase Flow Meters: Experience and Assessment in PDO. *SPE Annual Technical Conference and Exhibition, Denver*, pp. 4013-4020.

19. Cavalcanti Nunes, G. (2005) Design for compact three-phase separation unit. *Boletim Tecnico da Petrobras*, Vol.48, No.1-2, pp.18-24.

20. Ceccio, S.L. and George, D.L. (1996) A Review of Electrical Impedance Techniques for the Measurement of Multiphase Flows. *ASME Journal of Fluids Engineering*, Vol.118, pp.391-399.

21. Chisholm, D. (1967) Flow of Incompressible Two-Phase Mixtures through Sharp-Edged Orifices. *Journal of Mechanical Engineering Science*, Vol.9, No.1, pp.72- 78.

22. Christien, G.J, van Spronsen, G. and Hudson J.D. (2008) Key multiphase and hydrate learning points from the main gas condensate systems in the Shell Group. *Shell Report* SIE- 99-5508.

23. Clemens, N.T., Petullo, S.P. and Dolling, D.S. (1996) Wide-field PIV study of shock induced turbulent boundary layer separation. *AIAA Journal*, Vol.34, pp.62–70.

24. Costa, D., Couput, J.-P., Hollaender, F. Pinguet, B. and Koshy, T. (2008) Extending the range of multiphase metering to challenging high water-cut gas-lifted wells: TOTAL ABK field application. *13th Abu Dhabi International Petroleum Exhibition and Conference*, Vol.3, pp.1434-1447.

25. Dantec Dynamics (2006) *2D PIV Reference Manual* (2nd ed.) DK-2740 Skovlunde, Denmark.

26. Darwich, T., Toral, H. and Archer, J.S. (1989) An Expert System for Multiphase Flow Measurement and Flow Regime Identification. *SPG Paper presented at SPG Petroleum Computer Conference, Lake Conroe, Texas.*

27. de Leeuw, H. (1997) Liquid Correction of Venturi Meter Readings in Wet Gas Flow. *Proceedings of North Sea Flow Measurement Workshop, Kristansand, Norway*.

*28.* de Leeuw, H. (1994) Wet gas flow measurement using combination of venturi meter and tracer technique. *Proceedings of North Sea Flow Measurement Workshop, Peebles, Scotland.*

29. Dickin, F.J., Williams, R.A. and Beck, M.S. (1993) Determination of Composition and Motion of Multicomponent Mixtures in Process Vessels using Electrical Impedance Tomography – I. Principles and Process Engineering Applications. *Chemical Engineering Science*, Vol.48, pp.1883-1897.

30. Dutton, R. (2004) Determination of Net Oil for Well Performance Measurement. *Class LM2100,* Daniel, Emerson Process Management.

31. Dykesteen, E., et al, (2005) *Handbook of Multiphase Metering,* Revision 2. Norwegian Society of Oil and Gas Measurement, NFOGM.

32. Falcone, G., Hewitt, G.F., Alimonte C. (2002) Multiphase Flow Metering: Current Trends and Future Developments. *SPE Annual Technical Conference and Exhibition, New Orleans, SPE – 74689*.

33. Fang, L., Cao, S., Li, J. and Cheng, H. (2010) Venturi wet gas measurement based on homogenous and chisholm model. *2nd International Conference on Computer and Automation Engineering, ICCAE, Singapore*, Vol.4, pp.87-191.

34. Franca, F., Acikgoz, M., Lahey, R.T. and Clausse, A. (1991) The Use of Fractal Techniques for Flow Regime Identification. *International Journal of Multiphase Flow*, Vol.17, pp.545- 552.

35. Fries, D.M., Waelchli, S.,and Rudolf von Rohr, P. (2007) Gas-liquid two-phase flow in meandering microchannels. *Chemical Engineering Journal*, Vol.135, Suppl.1, pp. S37-S45.

36. *Pattern Recognition Techniques for Multiphase Flow Measurement, Flow Measurement Guidance Note No. 15* (1998) National Engineering Laboratory, Glasgow, United Kingdom, and CALTEC, Cranfield, UK.

37. George, D.L., Ceccio, S.L., O'Hern, T.J., Shollenberger, K.A. and Torczynski, J.R. (1998) Advanced Material Distribution Measurement in Multiphase Flows: a Case Study. *Proceedings of the 1998 ASME International Mechanical Engineering Conference and Exposition*, American Society of Mechanical Engineers: New York, FED-Vol.247, pp. 31-42.

38. *Haimo MFM Product Brochure* [online]. Available at: <http://www.haimotech.com/downloads/MFM%20Brochure.pdf>

39. Haimo Technology Inc. (2005) *Haimo Newswire*, Issue 3.

40. Hajek, G. (1993) *Basic data and phase behaviour method*. DEP 20.00.10.10-Gen.

41. Hall, A., Griffin, D., Steven, R. (2007) A Discussion on Wet Gas Flow Parameter definition. *Proceedings of 25th North Sea Flow Measurement Workshop*.

42. Hall, A.R.W. (2000) *Evaluation of the FlowSys TopFlow Multiphase Flowmeter*. NEL, Project No FSY001, Report No 200/2000.

43. Hammer, E.A. and Nordvedt, J.E. (1991) The Application of a Venturi Meter to Multiphase Flow Meters for Oil Well Production. *Proceedings of the 5th Conference of Sensors and Applications.*

44. Henry, M., Tombs, M., Duta, M., Zhou, F., Mercado, R., Kenyery, F., Shen, J., Morles, M., Garcia, C. and Langansan, R. (2006) Two-phase flow metering of heavy oil using a Coriolis mass flow meter: A case study. *Flow Measurement and Instrumentation*, Vol.17, No.6, pp.399-413.

45. Hewitt, G.F. (1989) Multiphase Flow Metering. *Proceedings of the 2nd International Symposium on Multiphase Flow and Heat Transfer, Xi'an, China*.

46. Hewitt, G.F., Shires, G.L., Harrison, P.S. and Parry, S.J. (1997) The Mixmeter Flowmeter - Another step towards Routine Multiphase Flow Measurement? *8th International Conference on Multiphase Production Technology, Cannes, France.*

47. Hill, T.J and Wood, D.G. (1994) *Slug Flow: Occurrence, consequences and Prediction*. SPE 2790.

48. Hua, C., Geng, Y. (2012) Wet gas meter based on the vortex precession frequency and differential pressure combination of swirlmeter. *Journal of the International Measurement Confederation*, Vol.45, No.4, pp.763-768.

49. Huerta, V.A., Lanchimba, A., Porlles, J.W. (2012) Modeling condensate banking in lean gas condensate reservoirs. *SPE Latin American and*

*Caribbean Petroleum Engineering Conference Proceedings, Mexico City*, Vol.2, pp.1132-1146.

50. Jamieson, A.W., Smeenk, R.G. and Vriezen, P.B. (1985) Multiphase Flow Measurement at Production Platforms. *Petroleum Review*, pp. 23, 25-26, 28.

51. Jamieson, A.W. (1998) Multiphase Metering – The Challenge of Implementation. *16th North Sea Flow Measurement Workshop, Gleneagles, Scotland*.

52. Jamieson, A.W. (1999) *High Performance Multiphase Metering – A Personal Perspective*, Norflow Seminar. Available at: < http://www.iceweb.com.au>.

53. Kirby B.J. and Hanson R. K. (1999) Linear Excitation Schemes for IR PLIF Imaging of CO and $CO_2$. *Applied Physics B*, Vol.69, pp.505–507.

54. Klepsvik, I., Dahl, E.O. and Baker, A.C. (2000) Multiphase Flow Test Report –TopFlow. *Christian Michelsen Research*, Report CMR-00-F10021.

55. Lacy, R., Proot, M. and Zabaras, G. (2006) Testing of the Shell Flow Correlations. *Shell Global Solutions Report*.

56. Leggett, R.B., Borling, D.C., Powers, B.S. and Shehata, K. (1996) Multiphase Meter Successfully Measures Three-Phase Flow at Extremely High Gas Volume Fraction. *SPE Paper 36837, European Petroleum Conference, Milan, Italy*.

57. Letton, W., Svaeren, J.A. and Conort, G. (1997) Topside and Subsea Experience with the Multiphase Flow Meter. *SPE Paper 38783*, pp. 345-355.

58. Lin, J.C. and Rockwell, J.C. (1994) Cinematographic System of High-Image-Density Particle Image Velocimetry. *Experiments in Fluids*, Vol.17, pp.110–118.

59. Lindken, R. and Merzkirch, W. (2002) A novel PIV technique for measurements in multiphase flows and its application to two-phase bubbly flows. *Experiments in Fluids*, Vol. 33, pp.814-825.

60. Ling, K. and Shen, Z. (2012) Including the effect of capillary pressure to estimate critical rate in water coning well. *North Africa Technical Conference and Exhibition 2012:Managing Hydrocarbon Resources in a Changing Environment*, Vol.2, pp.1273-1283.

61. Lockhart, R.W. and Martinelli, R.C. (1949) Proposed correlation of data for isothermal two-phase, two-component flow in pipes. *Chemical Engineering Progress*, Vol. 45, 1949, pp. 39-45.

62. MacKay, D.J.C. (1992) Bayesian Interpolation. *Neural Computation*, Vol.4, No.3, pp.415-447.

63. Mandhane, J. M., Gregory, G.A. and Aziz, K. (1974) A Flow Pattern Map for Gas-Liquid Flow in Horizontal Pipes. *International Journal of Multiphase Flow*, Vol.1, pp.537-553.

64. Mazzoni, A., Halvorsen, M. and Aspelund, A. (2001) *Field Qualification – FlowSys TopFlow Meter*. Agip Test Facility, Trecrate, Italy.

65. McNulty, J.G. and Beg, N.A. (1997) Survey of Multi-Phase Flow Metering Systems. *Caltec Report CR 6660*, BHR Group, UK.

66. Meinhart, C.D., Wereley, S.T. and Santiago, J.G. (2000) A PIV algorithm for estimating time-averaged velocity fields. *Journal of Fluids Engineering, Transactions of the ASME*, Vol.122, No.2, pp.285-289.

67. Mulleners, K., Henning, A., Mai, H., Raffel, M., Le Pape, A. and Costes, M. (2009) Investigation of the unsteady flow development over a pitching airfoil by means of TR-PIV. *27th AIAA Applied Aerodynamics Conference, San Antonio, Texas*, Code79128.

68. Murdoch, J.W. (1962) Two-Phase Flow Measurements with Orifices. *Journal of Basic Engineering*, Vol.84, pp.419-433.

69. Murugesan, K. (2002) Multiphase flow meter: Trends in well performance testing. *Chemical Engineering World*, Vol.37, No.12, pp.151-153.

70. National Engineering Laboratory (2001) Notes from *Multiphase Flow Measurement Training Course*, 17 January.

71. Nicklin, D.J., Wikes, J.C. and Davidson, J.F. (1962) Two Phase Flow in Vertical Tubes. *Transactions of the Institution of Chemical Engineering*, Vol.40, pp.61-68.

72. Nyfors, E. and Vainikainen, P. (1989) *Industrial Microwave Sensors*. Artech House.

73. Olsen, A.B. (1993) Framo Subsea Multiphase Flow Meter System. *Proc. Sem. Multiphase Meters and their Subsea Applications*, London.

74. Packman, C. and Braaten, N. (2011) Developing a retrieval system for subsea sensors and transmitters. *Proceedings of the Annual Offshore Technology Conference, Brazil*, Vol.1, pp.265-273.

75. Perry R.H. (1997) *Perry's Chemical Engineers Handbook*. McGraw-Hill.

76. Raffel, M., Willert, C.E. and Kompenhans, J. (1998) *Particle Image Velocimetry: A Practical Guide*. Springer: Berlin.

77. Reeder, M.F., Crafton, J.W., Estevadeordal, J., Delapp, J., McNiel, C., Peltier, D. and Reynolds, T. (2010) Clean seeding for flow visualization and velocimetry measurements. *Experiments in Fluids*, Vol.48, No.5, pp.889-900.

78. Sanderson, M.L. (1998) Lecture Notes for *Probes, Integration Methods and Tracers. Introduction to Flow Measurement*, Deptartment of Process & Systems Engineering, School of Engineering, Cranfield University.

79. Scheers, L. and Wee, A. (2007) Challenges at High Accuracy Multi-Phase and Wet-Gas Measurements. *Multiphase Measurement Roundtable.*

80. Scheers, L., Busaidi, K., Parper, M., Halvorsen, and Wideroe, T. (2002) Multiphase Flow Metering Per Well – Can it be Justified? *20th North Sea Flow Measurement Workshop, St. Andrews, Scotland*.

81. Scott, S.L., Shoham, O. and Brill, J.P. (1987) Modelling slug growth in large

diameter pipes. *Proceedings of the 1st International Conference on Multiphase Flow*, Vol.1, pp.55-64.

82. Shen, J.J.S. and Riley, R.C. (1998) Field Evaluation of a Multiphase Meter in Well-Testing Operation. *SPE Production & Facilities*, pp.109-117.

83. Sivaiah, M., Parmar, R. and Majumder, S.K. (2012) Gas entrainment and holdup characteristics in a modified gas-liquid-solid down flow three-phase contactor. *Powder Technology*, Vol.217, pp. 451-461.

84. Spedding, P. L. and Nguyen, V.T. (1980) Regime Maps for Air-Water Two-Phase Flow. *Chemical Engineering Science*, Vol.35, pp.779-793.

85. Spedding, P. L. and Spence, D.R. (1994) A Novel Approach to Flow Regime Prediction in Gas-Liquid Flows. *Developments in Chemical Engineering SST*, Vol.14, No.2, pp.407-431.

86. Spitzer, D.W. (2006) Nasty flows need novel flowmeters (Short Survey ). *Control*, Vol.19, No.4, p.96.

87. Stapelberg, H.H. and Mewes, D. (1990) The Flow of Two Immiscible Liquids and Gas in Horizontal Pipes – Pressure Drop and Flow Regime. *European Two-Phase Flow Group Meeting, Varese, 21st-24th May*.

88. Stewart, D.G. (2002) *The Evaluation of Dry Gas Meters in Wet Gas Conditions*. A Report for the National Measurement System Directorate, Department of Trade and Industry, UK.

89. Taitel, Y., Barnea, D. and Dukler A.E. (1980) Modelling Flow Pattern Transitions for Steady Upward Gas-Liquid Flow in Vertical Tubes. *AIChE Journal*, Vol.26, No.6, pp.345-336.

90. Ting, V.C. (2001) Utilization of an Inline Rotary Separator as a Wet Gas Meter. *Proceedings of the 19th North Sea Flow Measurement Workshop, October 22–25, Kristiansand, Norway*, NEL, Glasgow.

91. Tosic, S. and Mehdizadeh, P. (2010) Multiphase well-rate measurements applied to reservoir analysis. *SPE Production and Operations*, Vol.25, No.2, pp.155-160.

92. TSI, Inc., *Laser Diagnostics: Seed Particle Specifications product information sheet* [online]. Available at: <http://www.mie.uth.gr/ekp_yliko/ SeedParticles_2980461.pdf> [Accessed March 2011].

93. Tuss, B., Perry, D. and Shoup, G. (1996) Field Tests of the High Gas Volume Fraction Multiphase Flow Meter. *Proceedings of SPE Annual Technical Conference, Denver, USA*.

94. van Maanen, H.R.E. (1999) Cost Reduction for Wet-Gas Measurement using Tracer-Venturi Combination. *Proceeding of the workshop Practical Development in Gas Flow Metering, East Kilbride, Scotland*, paper 2.

95. Vogel, A. and Lauterborn, W. (1998) Time-resolved Analysis of Cavitation Induced by CW Lasers in Absorbing Liquids. *Optical Lasers Engineering.* Vol. 21, pp.274-294.

96. Waelchli, S. and Rudolf von Rohr, P. (2006) Two-phase flow characteristics in gas-liquid microreactors. *International Journal of Multiphase Flow,* Vol.23, pp.791-806.

97. Wang, M., Ma Y., Holliday, NT., Dai, YF., Williams, RA., Lucas, G. (2005) A High Performance EIT System', *IEEE Sensor Journal*, Vol. 5, pp. 289-299

98. Wieneke, B. (2005) Stereo-PIV using self-calibration on particle images. *Experiments in Fluids*, Vol.39, No.2, pp.267-280.

99. Willert, C., Stasicki, B., Klinner, J. and Moessner, S. (2010) Pulsed operation of high-power light emitting diodes for imaging flow velocimetry. *Measurement Science and Technology*, Vol.21, No.7, Art. no.075402.

100. Wu, H.L. (2006) Guidelines for hydraulic design of two-phase flow pipelines and risers. *Shell Report*, EP 93-2270.

101. Xie, D., Liang, G. and Wang, F. (2007) Analysis on dynamic differential

pressures of multi-loop flowmeter for the measurement of gas-liquid two-phase flow. *5th International Symposium on Measurement Techniques for Multiphase Flows*, Vol.914, pp. 683-688.

102. Xu, Y., Zhang, Q., Yu, L., Du, S., Zhang, T., Li, Z. and Wu, Q. (2011) Non separation two phase flow measurement of natural gas condensate. *Natural Gas Industry*, Vol.31, No.4, pp.103-108.

# APPENDIX A: PROGRAM EXCERPTS

The following is the MATLAB code for analysing the PIV data processed by PIVPROC. This code utilises a function called "piv_vec2mtx" The file takes the .VEC file output by PIVPROC and converts it into an m x n x 2 matrix, where m and n are the x and y interrogation regions, respectively, m x n x 1 is the u-component of velocity and m x n x 2 is the v-component of velocity.

```
% vector averaging file
clear all
        clc
         ppi = 480; %pixels per inch
                dt = 0.000015; %delta t (seconds)
                AR = 1; %aspect ratio used in PIVPROC iterations
        freestream = 100;  %maximum velocity shown in the PIV measurements

n=165; %total number of vector files

dirfile='F:\uleh\Research\PIV data\sampleA';
dirsave='F:\uleh\Research\PIV data\sampleA';

% vectors_avg=zeros(128,84,2,165*4);
        for folder=1:4
        for sequence=1:n
if sequence<10
filename = fullfile(dirfile,[num2str(folder)],[num2str(folder) '_000' num2str(sequence)
'.VEC']);

%original file directory
        savefile = fullfile(dirsave,[num2str(folder) '_000' num2str(sequence)]);
        savefile2 = fullfile(dirsave,[num2str(folder) '_000' num2str(sequence)
'momentum']);
```

```
        elseif sequence<100filename = fullfile(dirfile,[num2str(folder)],[num2str(folder)
        '_00' num2str(sequence) '.VEC']);%original file directory
        savefile = fullfile(dirsave,[num2str(folder) '_00' num2str(sequence)]);
        savefile2 = fullfile(dirsave,[num2str(folder) '_00' num2str(sequence)
'momentum']);

elseif sequence<1000
        filename = fullfile(dirfile,[num2str(folder)],[num2str(folder) '_0'
num2str(sequence) '.VEC']);
%original file directory
        savefile = fullfile(dirsave,[num2str(folder) '_0' num2str(sequence)]);
        savefile2 = fullfile(dirsave,[num2str(folder) '_0' num2str(sequence)
'momentum']);
end

% vectors_avg(:,:,:,sequence+(n*(folder-1)))=piv_vec2mtx(filename,ppi,dt);
        vectors=piv_vec2mtx(filename,ppi,dt);
%save(savefile,'vectors')
                individual(vectors,filename,savefile,savefile2,ppi,dt,AR,freestream);
                %for individual files
        end
end

save('vectors_avg')

        % average(vectors_avg,filename,ppi,dt,AR,freestream,n);
        function individual(vectors,filename,savefile,savefile2,ppi,dt,AR,freestream)
        %This function takes the individual runs and produces spanwise vorticity,
        %quiver, and momentum contour plots that are saved in a folder specified by
        %the user in the "savefile", "savefile2", and "savefile3" variables. It
        %also saves an Excel spreadsheet compatible with Tecplot in the folder
        %specified by the "savefile" variable.
% [omega,angularvelocity] = curl(vectors(:,:,1),vectors(:,:,2));
        %
```

```
        % range=[-1 5];%% I3=figure(3);
        % contour(flipdim(angularvelocity,1),range)
        % colorbar % axis([0 84 0 125])
        % set(gca,'XTick',0:(84/2):84)
        % set(gca, 'XTickLabel',[0:1.3:2.6]);
        % set(gca,'YTick',0:(125/2):125)% set(gca,'YTickLabel',[0:1:1.8]);
        % xlabel('x (in)')
        % ylabel('y (in)')

% saveas(I3,savefile,'bmp')
                % saveas(I3,savefile,'fig')
                % close(3)vectors(:,:,1)=vectors(:,:,1)+0.8*freestream;
                %Figure 1 is the quiver plot. Figure 2 is the momentum layer
                plot.I=figure(1);
                quiver(flipdim(vectors(:,:,1),1),flipdim(vectors(:,:,2),1),3,'.k')
                axis([0 82 0 61])
                set(gca,'XTick',0:(82/2):82)
                set(gca,'XTickLabel',[0:1.3:2.6]);
                set(gca,'YTick',0:(61/2):61)
                set(gca,'YTickLabel',[0:1:2]);
                xlabel('x (in)')
                ylabel('y(in)')
                saveas(I,savefile,'bmp')
                saveas(I,savefile,'fig')
        close(1)
I2=figure(2);
contourf(flipdim(vectors(:,:,1),1),5)
                colormap(gray)
                axis([0 82 0 61])
                set(gca,'XTick',0:(82/2):82)
                set(gca, 'XTickLabel',[0:1.3:2.6]);
                set(gca,'YTick',0:(61/2):61)

                (gca,'YTickLabel',[0:1:2]);
```

```
                xlabel('x (in)')
                ylabel('y (in)')
                saveas(I2,savefile2,'bmp')
                saveas(I2,savefile2,'fig')
close(2)

vectordim = size(vectors);
        b=1;
                for n=1:(vectordim(1))  %n corresponds to x position
                for m=1:(vectordim(2))  %m corresponds to y position
                u(b)=1.5*vectors(n,m,1);
                v(b)=vectors(n,m,2);
                x(b)=2.6/84*m;
                %FOV was 2.6 inches in x-directiony(b)=2/62*(62-n);
                 %FOC was 2 inches in y-direction
                b=b+1;
        End
End
vectordim2 = size(u);
                xyuv = zeros(vectordim2(2),7);
                xyuv(:,1) = x';
                xyuv(:,2) = y';
                xyuv(:,3) = u';
                xyuv(:,4) = v';
                uprime = xyuv(:,3)+0.8*freestream; %adding because vectors are negative
                xyuv(:,5) = uprime;
                xlswrite(savefile,xyuv)
        end

function average(vectors_avg,filename,ppi,dt,AR,freestream,n)
        %This portion of the code takes information from every vector file and
        %averages the values. They are then placed into an Excel spreadsheet
        %
        vectorsum=zeros(61,82,2);
```

```
        n=4*165;
        for sequence=1:nvectorsum=vectorsum+vectors_avg(:,:,:,sequence);
end

vector_avg=vectorsum/sequence;
save vector_avg
                vectordim = size(vector_avg);
                b=1;
                for n=1:(vectordim(1)) %n corresponds to x position
                for m=1:(vectordim(2)) %m corresponds to y position

                %u(b)=vectors_avg(n,m,1)*1/ppi*(1/12)*(1/dt);
                % v(b)=vectors_avg(n,m,2)*1/ppi*(1/12)*(1/dt);
                u(b)=vector_avg(n,m,1);
                v(b)=vector_avg(n,m,2);
                x(b)=2.6/82*m; %FOV was 2.6 inches in x-direction
                y(b)=2/61*(61-n); %FOC was 2 inches in y-direction
                 b=b+1;
                end
        end

vectordim2 = size(u);
        xyuv = zeros(vectordim2(2),4);
        xyuv(:,1) = x';
        xyuv(:,2) = y';
        xyuv(:,3) = u';
        xyuv(:,4) = v';
        % filename='100_5ft_smallparticles';
        % xlswrite(filename,xyuv)
figure(1)
                contourf(flipdim(vector_avg(:,:,1),1),20)
                axis([0 82 0 61])
                set(gca,'XTick',0:(82/2):82)
                set(gca, 'XTickLabel',[0:1.3:2.6]);
```

```
            set(gca,'YTick',0:(61/2):61)
        set(gca,'YTickLabel',[0:1:2]);

        xlabel('x (in)')
        ylabel('y (in)')
end
```

%import Wizard created variables in the current workspace.

%Import Wizard created variables in the current workspace.

```
>> obj= imshow(charsflow)

obj =

  101.0017

>> imshow(charsflow1)

>> c=normxcorr2(charsflow(:,:,1),charsflow1(:,:,1));

>> figure,surf(c),shading flat
```

Import Wizard created variables in the current workspace.

```
>> c=normxcorr2(charsflow(:,:,1),charsflow2(:,:,1));

>> figure,surf(c),shading flat
```

# APPENDIX B: FLUID PROPERTIES

## B.1 Relevant Physical Properties for Multiphase Flow

Important physical properties for multiphase flow transport are the split into liquid and gas, the gas and liquid densities, and the gas and liquid viscosities. To a lesser extent the gas-liquid surface tension is also of importance. These physical properties depend on pressure and temperature, which will vary along the pipeline.

Different parameters can be used to describe the split between liquid and gas, such as the gas-volume fraction (GVF), liquid-volume fraction (LVF), gas-oil ratio (GOR), and condensate-gas ratio (CGR). If water is part of the composition then the water-gas ratio (WGR) and the water-cut can also be introduced.

For gas systems, usually the CGR is specified, with units of either bbl/MMscf or $m^3/MMsm^3$. The CGR can be deduced as follows:

$$\text{CGR} = \frac{\varphi_o MW_o / \rho_o}{23.64\varphi_G} 10^6 \text{ in units } m^3/MMsm^3 \qquad \text{B.1}$$

Dividing this by (0.1589/0.0283168) give 5.61 which is the CGR in bbl/MMscf. Where:

$\varphi_G$ is the mole fraction gas in the total fluid (i.e. gas + oil + water) (in units mole/mole)

$\varphi_o$ is the mole fraction oil (condensate) in the total fluid (i.e. gas + oil +water) (in units mole/mole)

$MW_G$ is the molecular weight of the gas (in units kg/kmole)

$MW_o$, is the molecular weight of the condensate (in units kg/kmole)

$\rho_G$ is the gas density (in units $kg/m^3$)

$\rho_o$ is the condensate density (in units $kg / m^3$)

The factor 0.1589 converts $m^3$ condensate into *bbl* condensate

The factor 0.0283168 converts $m^3$ gas into $ft^3$ gas

The factor 23.64 converts *kmol* gas at actual pressure and temperature conditions to $m^3$ gas at standard conditions.

If a specified CGR is used as the input to a multiphase flow study, it is very important to double-check how the CGR is defined. In some cases the CGR can be the result of multistage flashing; for example, first the fluid is flashed at the first stage separator arrival conditions, second the resulting liquid is flashed at the second stage separator conditions. The gas contributing to the CGR consists of gas from the first stage separator (converted to standard conditions), plus associated gas flashed off from the liquid in the second stage separator. Therefore, the liquid in the CGR consists of liquid leaving the second stage separator.

It is straightforward to convert the CGR into alternative parameters to describe the gas-liquid split (such as GOR, LVF, and GVF). The CGR is usually applied for gas (dominated) systems, and the GOR for oil (dominated) systems.

The water-cut is usually defined as $\varphi$, the percentage volume of free water in the water/oil liquid phase. For gas systems the WGR is usually defined as the water volume (in $m^3$ or in bbl) per volume dry gas (in million $Sm^3$, in million $Nm^3$, or in MMscf). For the determination of the WGR, an expression similar to the one for the CGR as given above can be applied, replacing the oil properties ($\varphi_o$, $MW_o$, and $\rho_o$) by the water properties ($\Delta_W$,$MW_W$, and $\rho_W$):

$$\text{WGR} = \frac{\varphi_W MW_W / \rho_W}{23.64\,\varphi_G} 10^6 \text{ in units } m^3/MMsm^3 \qquad \text{B.2}$$

Dividing this by (0.1589/0.0283168) gives 5.61 which is the WGR in bbl/MMscf. Obviously the water-cut (fraction) is equal to the ratio of the WGR and the CGR.

## B.2 Phase Envelope

Figure B.1 gives the LVF for a specified composition of a gas system, which depends on the local pressure and temperature. The red line with 0% LVF (i.e. the curve on the right) is the dew-point line, and the dark blue line with 100% LVF (i.e. the curve on the left) is the bubble point line. Any location in the production pipeline with a pressure and temperature inside the region bounded by the dew-point line and the bubble point line will operate in the multiphase flow regime. All lines with a constant LVF end at the point with critical pressure and critical temperature. Points in the multiphase flow region with a pressure marginally higher than the critical pressure and a temperature higher than the critical temperature operate under retrograde condensation, i.e. a pressure decrease at constant temperature will result in more liquid.

The cricondentherm/cricondenbar is the maximum temperature/pressure at which two phases can still exist. A gas system at a pressure above the cricondenbar gives a dense phase operation, and the gas has now been compressed so far that it seems to behave as a liquid. Shell has a few pipelines (e.g. Offshore Gas Gathering System (OGGS) at low flow in Nigeria) that are operated with the dense phase regime. The hydrate curve in the

figure gives the hydrate equilibrium temperature (HET) for increasing temperature, and all point on the left-hand side of the curve operate in the hydrates regime.

Figure B.1 also shows the pressure and temperature along the pipeline at various production rates (2, 4 and 6 $mmNm^3/d$), with N refering to normal conditions, which is 0°C and 1 Atm). Pressure and temperature decreases from the inlet to the outlet of the pipeline; the inlet temperature is about 45 °C for all three production rates, and the arrival pressure is fixed at about 20 bara. The pipeline operational envelope falls within the multiphase flow regime at each location along the pipeline. Part of the pipeline operates in the hydrates formation regime. This shows that some measure of hydrates inhibition (e.g. methanol injection) is required to prevent hydrates blocking the pipeline.

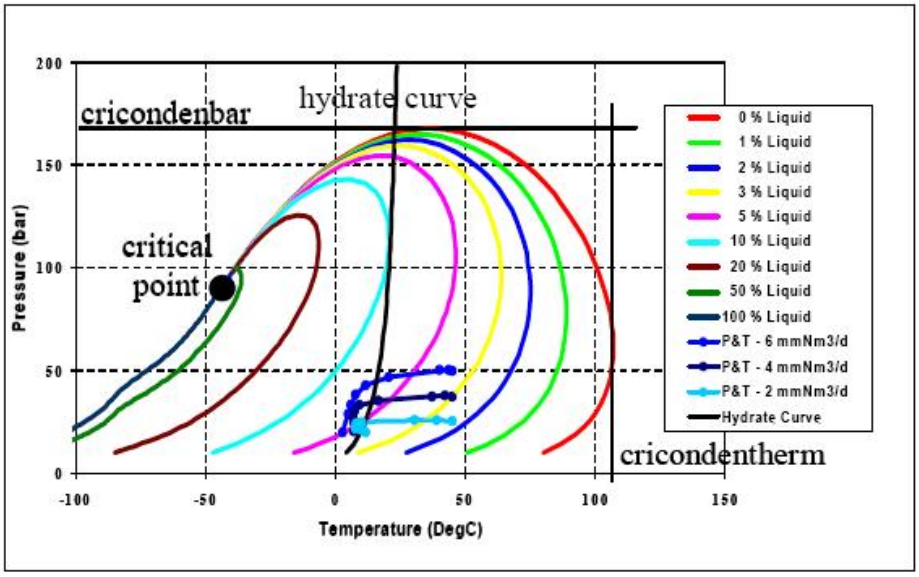


Figure B.1 - LVF for a specified composition of a gas system

## B.3 Single Phase Flow

The pressure drop in a single-phase flow pipeline follows from applying Newton's second law to the flow through a pipe section. Newton's law dictates how the pressure drop balances forces by an unsteady contribution, acceleration, gravity, and wall friction:

$$-A\frac{\partial P}{\partial x}=\frac{\partial}{\partial t}\rho AU+\frac{\partial}{\partial x}\rho AU^2+\rho Ag\sin\varphi+\tau S \qquad \text{B.3}$$

Here $t$ denotes time, $x$ is the stream wise coordinate, $\rho$ is the density, $A$ is the pipe cross sectional area, $U$ is the fluid velocity averaged over the pipe cross sectional areas, $P$ is the pressure, $g$ is the gravitational acceleration, $\varphi$ is the pipe inclination with respect to the horizontal, $S$ is the internal pipe diameter, and $\tau$ is the wall shear stress.

Mass conservation gives:

$$\frac{\partial}{\partial t}\rho A+\frac{\partial}{\partial x}\rho AU=0 \qquad \text{B.4}$$

However, by using the mass conservation equation, the momentum equation can also be written as:

$$\rho\frac{\partial U}{\partial t}+\rho U\frac{\partial U}{\partial x}=-\frac{\partial P}{\partial x}-\rho g\sin\varphi-\frac{\tau S}{A} \qquad \text{B.5}$$

In the absence of friction ($\tau$ =0), equation B.5 is actually the Bernoulli equation for unsteady flow of a compressible fluid, and this equation in it's well known form is:

$$P+\rho gH+\frac{1}{2}\rho U^2 \qquad \text{B.6}$$

Where H is the local vertical height (i.e. H = $x\sin(\varphi)$).

A well-known expression is the $D^5$ law. For the steady state flow in a horizontal pipeline, the pressure drop balances the wall shear stress, i.e.:

$$A\Delta p = \tau\pi D \qquad \text{B.7}$$

Here $\Delta p$ is the pressure drop per meter pipe length. Using the definition of the Fanning friction factor, this force balance can also be written as:

$$\Delta p = 2f\rho V^2/D \qquad \text{B.8}$$

Using the expression for the volumetric flow rate, i.e. $Q = VA$, the pressure drop turns out to be:

$$\Delta p = \frac{32\ f\rho Q^2}{\pi^2\ D^5} \qquad \text{B.9}$$

This is the $D^5$ -law for the pressure drop. The law says that for a fixed production $Q$, the pressure drop decreases with the 5th power of the chosen pipe diameter (note that a fixed value for the Fanning friction factor f is assumed, which is a good approximation for turbulent flow where the Fanning friction factor only weakly depends on the Reynolds number). An alterative expression is that of Christien (Christien, 2008):

$$Q = D^{5/2}\ \sqrt{\Delta p}\ \sqrt{\pi^2/32f\rho} \qquad \text{B.10}$$

Although the $D^5$-law has been derived for single-phase flow, it also serves as a good approximation for the pressure drop (depending on the pipe diameter and on the flow rate) for gas-condensate multiphase flow.

## B.4 Multiphase Flow

The pressure drop along a multiphase flow pipeline follows from applying Newton's second law to each of the phases. Newton's law dictates the force balance with contributions from pressure, acceleration, wall friction, and gravity. Applying Newton's law to the gas layer and to the oil layer in a multiphase flow through a pipeline section, as sketched in Figure B.2 from Hajek (1993) gives the following two force (or: momentum) balances (Wu, 1993):

$$\frac{\partial}{\partial t}\rho_G A_G U_G + \frac{\partial}{\partial x}\rho_G A_G U_G^2 =$$
$$-A_G\frac{\partial P}{\partial x} - \rho_G g\cos\varphi A_G\frac{\partial h_L}{\partial x} - \rho_G A_G g\sin\varphi - \tau_G S_G - \tau_{OG}S_{OG}$$
$$\frac{\partial}{\partial t}\rho_O A_O U_O + \frac{\partial}{\partial x}\rho_O A_O U_O^2 =$$
$$-A_O\frac{\partial P}{\partial x} - \rho_O g\cos\varphi A_O\frac{\partial h_L}{\partial x} - \rho_O A_O g\sin\varphi - \tau_O S_O - \tau_{WO}S_{WO} + \tau_{OG}S_{OG}$$

B.11

These equations hold for stratified flow, i.e. the multiphase flow regime where gas flows as a separate layer on top of the liquid layer. The subscript "*G*" denotes the gas phase, "*O*" denotes the oil phase, and "*W*" denotes the water phase. In the presence of free water, a momentum equation for the water layer applies that is quite similar to the one for the oil phase.

In the equations t denotes time, $x$ is the stream wise coordinate, $\rho$ is the density, $A$ is the cross sectional area covered by a certain phase, $U$ is the phase velocity, $P$ is the pressure, $g$ is the gravitational acceleration, φ is the pipe inclination with respect to the horizontal, $h_L$ is the height of the liquid layer (with respect to the pipe wall), $S$ is the wall perimeter wetted by a certain phase, and $\tau$ is the wall friction of a certain phase or the interfacial friction between the phases.

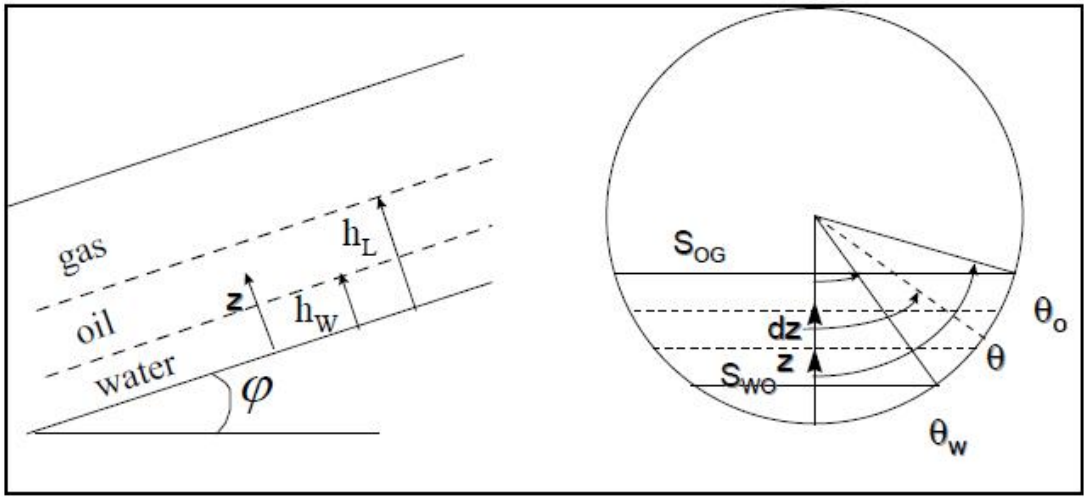


Figure B.2 - View and cross section of the pipe with three separate layer of gas, oil and water (i.e. stratified flow)

Mass conservation of the gas and oil phases respectively gives:

$$\frac{\partial}{\partial t}\rho_G A_G + \frac{\partial}{\partial x}\rho_G A_G U_G = 0 \qquad \text{B.12}$$

$$\frac{\partial}{\partial t}\rho_O A_O + \frac{\partial}{\partial x}\rho_O A_O U_O = 0 \qquad \text{B.13}$$

## B.5 Liquid Holdup

The fluid composition and the thermodynamics determine the split between gas and liquid for a given total throughput. The gas/liquid split depends on the local pressure and temperature in the pipeline. The resulting volumetric gas flow $Q_G$ and volumetric liquid flow $Q_L$ are often scaled by the pipe cross section $A$. This gives the superficial velocities:

$$V_{SG} = Q_G/A \text{ and } V_{SL} = Q_L/A \qquad \text{B.14}$$

The mixture velocity is the sum of the superficial gas velocity and the superficial liquid velocity:

$$V_M = V_{SG} + V_{SL} \qquad \text{B.15}$$

The LVF, being a thermodynamic property, can also be written as the ratio of the superficial liquid velocity and the mixture velocity:

$$LVF = V_{SL}/V_M \qquad \text{B.16}$$

## B.6 Flow Regimes

### B.6.1 Flow Pattern Map

In general, flow patterns for multiphase flow can be quite complex. The flow can be laminar or turbulent, steady or unsteady, gas and liquid can be segregated, liquid can flow as droplets within the gas, or gas can flow as bubbles within the liquid. To simplify the description, a limited number of typical multiphase flow structures, or so-called flow patterns are distinguished. Typical flow patterns for horizontal and vertical upward inclined pipeline sections are depicted in Figures B.3 and B.4, respectively (Scott, 1987).

***Horizontal pipe sections***

At high gas production, the gas will form the continuous phase, liquid is transported as droplets with the gas and this is called annular mist flow. A liquid film may be formed along the wall and if this is the case the flow regime is called annular dispersed (or core annular flow). If the configuration is horizontal or mildly inclined, the liquid layer along the bottom side of the pipeline will be significantly thicker than the liquid layer along the topside.

If the gas production is reduced, then the liquid entrainment with the gas will become less, and liquid droplets will no longer reach the top of the pipe. This will result in the transition from annular flow to stratified flow, where liquid and gas flow as segregated (separated) layers, with the heavier liquid below the lighter gas. There may be some entrainment of liquid droplets into the gas layer.

If at moderate gas flow rates the liquid flow rate is increased, the gas/liquid interface can become unstable, transiting from stratified flow to hydrodynamic slug flow (also referred to as intermittent flow). In this flow regime unstable liquid waves will reach the top pipe wall and form a liquid slug. Some gas will be captured as bubbles in the liquid slug body and a gas bubble is found behind the liquid slug.

If the liquid flow rate is further increased, at moderate to low gas flow rates the gas bubble behind the liquid slug body will become unstable and it will break up into smaller gas bubbles. Now liquid will form the continuous phase, with a dispersion of small gas bubbles and this flow regime is called bubble flow (or dispersed bubble flow).

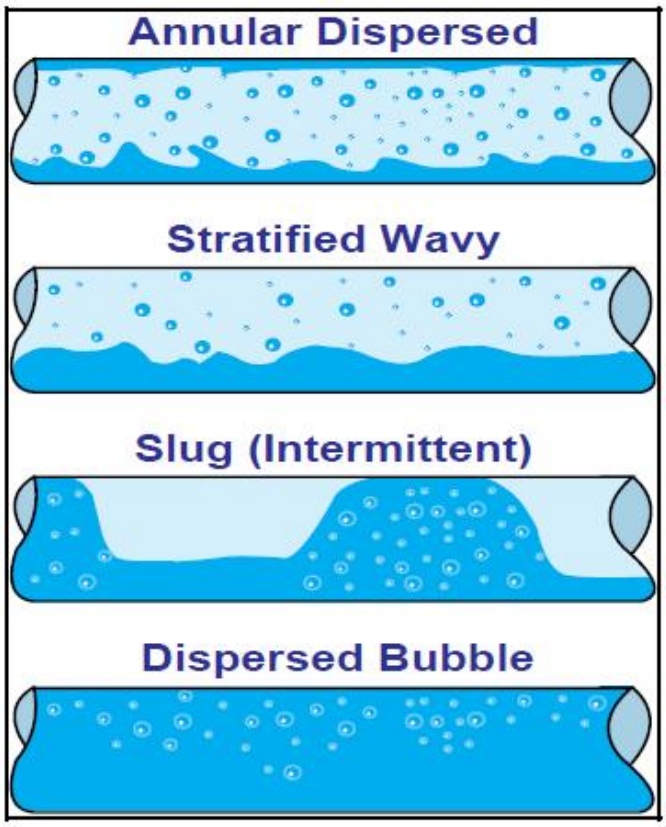


Figure B.3 - Flow patterns in a horizontal pipeline

***Vertical pipe sections (upward flow)***

If the liquid flow rate is high, and the gas flow rate is low, liquid will form the continuous phase. Gas travels as small bubbles within the liquid and this is the bubble flow regime. If the liquid flow rate is decreased, while the gas flow rate is still relatively low, small gas bubbles may collapse to form large gas bubbles. Now the liquid forms a slug body with entrained small gas bubbles, followed by a single large gas bubble; this is the hydrodynamic slug flow regime (or intermittent flow) **(**Scott, 1987).

If the low gas flow rate is increased while the liquid production remains low, the large gas bubbles can become unstable, giving a chaotic transport of gas bubbles of various shapes

and sizes. This is the chum-flow regime. Most models do not distinguish between slug and chum flow, and treat chum flow the same as slug flow.

Increasing the gas flow rate, while keeping the liquid production low, will result in the transition to annular dispersed flow (or core annular flow). Gas will form the continuous phase in the core of the pipe, with liquid being entrained as small droplets. A liquid film is formed along the pipe wall, which at very high gas flow rates will disappear, and all liquid will be transported as droplets; this is annular mist flow (annular flow).

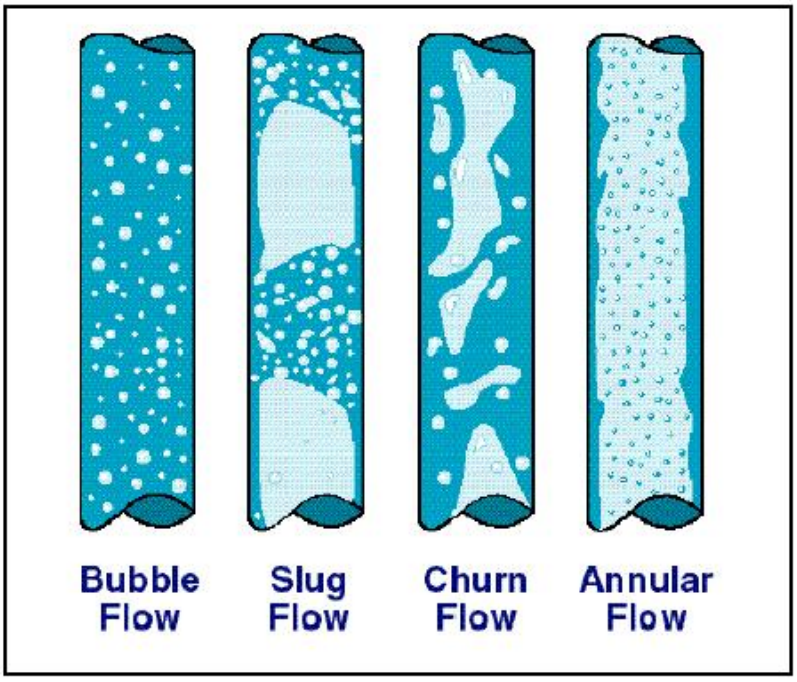


Figure B.4 - Flow patterns in vertical upward pipeline

The flow pattern is determined by the following parameters: pipe diameter, pipe inclination, gas and liquid superficial velocities, gas and liquid densities, gas and liquid viscosities, and gas/liquid surface tension. As all these parameters may change along the pipeline, the flow pattern can also change along the pipeline. The dependence of the flow regime on the mentioned parameters defines the flow pattern map. Very often, the flow

pattern map is determined as a function of the gas and liquid flow rates (having fixed all other parameters). Figure B.5, shows the flow pattern as a function of the superficial gas velocity $V_{SG}$ (on the horizontal axis) and the superficial liquid velocity $V_{SL}$ (on the vertical axis). The results in the figure are predictions for a certain configuration using the Shell flow correlations. Sometimes, instead of using superficial velocities along the axes, the velocity is non-dimensionalised by using, $\sqrt{gD}$ as the reference velocity (here $g$ is the gravitational acceleration, and $D$ is the pipe diameter). This gives the Froude number which is estimated using the expression of Perry et al. (1997):

$$Fr_G = V_{SG}/\sqrt{gD} \text{ and } Fr_L = V_{SL}/\sqrt{gD}. \qquad \text{B.17}$$

Alternatively, the densimetric Froude number may be used and this is calculated using the expression (Perry et al., 1997):

$$Fr_G^* = \sqrt{\frac{\rho_G}{\Delta\rho}\frac{V_{SG}^2}{gD}} \text{ and } Fr_L^* = \sqrt{\frac{\rho_L}{\Delta\rho}\frac{V_{SL}^2}{gD}} \qquad \text{B.18}$$

Where $\rho_G$ the gas density, $\rho_L$ is the liquid density and $\Delta\rho = \rho_L - \rho_G$

Using these dimensionless numbers in the flow pattern map may suggest that the resulting flow pattern map is universal and no longer depends on the pipe diameter: this is not true. For each choice of parameter (pipe diameter, pipe inclination, etc.) a new flow pattern map needs to be generated.

The multiphase flow correlations in the pipeline simulation tools contain sub-models to determine the transition from one flow regime to the other. These transition models are often based on stability theory containing parameters that have been determined from (laboratory) experiments. Scale-up of laboratory data is not straightforward, and as a result, the transition prediction is not always very accurate.

Multiphase flow correlations have been developed and validated for gas-condensate systems and conventional oil systems. Now and in the near future, unconventional transport, and/or transport of unconventional hydrocarbons through multiphase pipelines will take place. An example of unconventional transport is the flow of gas, oil, and water, with slurry of hydrates or water particles. An example of the flow of unconventional hydrocarbon is heavy oils. Slurries and heavy oils require the extension of the set of multiphase flow correlations. This has partly already been done (e.g. to account for the non-Newtonian behaviour of slurries) but needs to be continued in the coming years (e.g. high-viscosity models). Design of these non-conventional multiphase flow systems should be undertaken with great care and requires expert's advice.

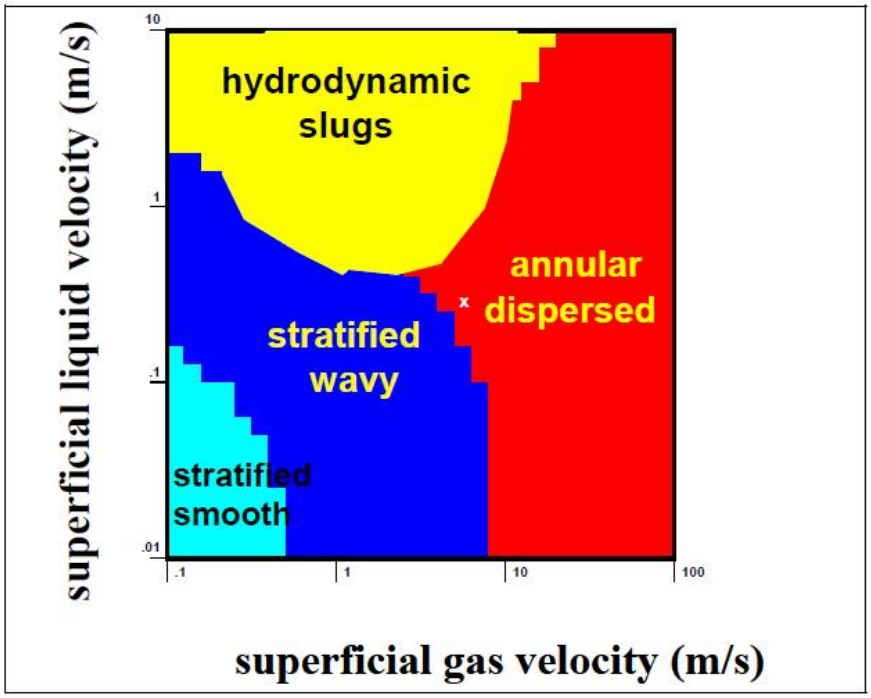


Figure B.5 - Typical flow pattern map for a horizontal pipeline

Taken from Brill et al. (1981)

### B.6.2 Description of Flow Regimes

***Stratified flow***

This flow pattern is often the most common and preferred condition for stable operation and minimum pressure drop. As stratification persists in the lower velocity range of operation, it should be recognised that water may settle out on the pipe bottom and/or that corrosion inhibitors will not be able to protect the upper pipe walls because of poor wetting conditions. Water accumulation at low production rates can become very large. Therefore, in the presence of water it is very important to run the simulation tools in the three-phase mode, which means that water is handled as a separate phase (in addition to the gas and oil phases), and this is particularly true at low production rates. At higher production rates the two-phase mode may be used, which assumes that water and oil are fully mixed and can be handled as a single liquid phase (Nicklin et al., 1962).

For the stratified flow to exist, the gas/liquid interface needs to be stable against small flow disturbances. This means that small variations (e.g. in inlet temperature or in flow rate) will not cause a transition to hydrodynamic slug flow. However, under low-pressure conditions, the stratified flow may be meta-stable, which means that a sufficiently large disturbance can cause a so-called growing slug, which can contain a large amount of liquid (Baker, 1954).

The interface (over the pipe cross section) between the gas and liquid in stratified flow is essentially flat at very low velocities but tends to curve upwards over the pipe wall as flow is increased. The upward distribution of the liquid is caused by two phenomena: firstly, it is due to secondary circulation of the gas with upward motion near the walls; and secondly it is due to the occurrence of entrainment, i.e. liquid drops being taken up by the gas because of shear action, and subsequent deposition on the pipe wall. If the upward

moving liquid film reaches the upper part of the pipeline, there is transition to annular flow (Brill, 1981).

An example of stratified flow is given in Figure B.6, which illustrates flow visualisation over the cross section of the 8" Bacton test loop. Gas/condensate is flowing at about 70 bara through the horizontal pipe section (no water), the superficial gas velocity is 0.5 m/s, and the superficial liquid velocity is 0.15 m/s. The LVF is 0.23, and the liquid holdup fraction is about 0.5. The superficial flow velocities correspond to a gas production of about 3.5 MMscfd, and a liquid production of about 2600 bpd. Note that the condensate gas ratio is about 750 bbl/MMscf, much larger than what is normally found in gas-condensate fields (typically up to 20 for lean gas, and up to 50 to 100 for rich gas). For such real-life CGRs the liquid holdup fraction for all except for very small flow rates will be up to a few percent only. This means that the liquid layer in stratified flow will be much thinner than that shown in the figure. However at a low flow rate, liquid will accumulate in upward inclined pipe sections and the liquid holdup can become as large as shown in the figure.

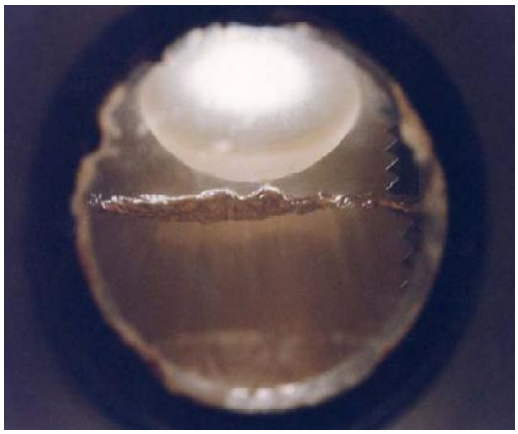

Figure B.6 - Flow visualization through the cross section of an eight inch Bacton flow loop with large CGR (750 bbl/MMscf).

Stratified flow with gas layer flowing on top of the condensate layer.

It should be noted that most gas condensate systems have a much lower CGR giving only a very small liquid film at the bottom (Lacy et al., 2006).

***Annular flow***

At higher gas and liquid velocities the liquid layer for stratified flow will be spread upwards over the pipe walls to form an annular flow pattern. This is caused by entrained droplets depositing on the upper wall and by an internal secondary circulating flow in the pipe causing the interface to curve upwards. Better wall wetting and less chance of water settling can be assured in this flow pattern because of all round liquid distribution, faster velocities and greater turbulence in the liquid layer.

For typical gas and condensate systems entrainment occurs for higher gas velocities, usually in excess of 5 m/s, which cause liquid to shear away from the stratified liquid surface. The onset of a line sweep can be observed when the gas velocity in a pipeline exceeds this value and liquid will be displaced by entrainment. The phenomenon occurs in the stratified as well as the annular flow pattern conditions, and is one of the factors causing the transition from stratified to annular flow.

Wall wetting occurs with liquid entrainment as the droplets eventually deposit. This is favourable for corrosion prevention and improves the distribution of corrosion inhibitors at the same time. The entrainment process is dependent on the densities of the gas and liquid and on surface tension. Measurements in the 8 inch diameter pipeline at Bacton for gas condensate showed that the concentration of entrained droplets is highest near the stratified liquid surface and decays sharply with height. The question of whether the top of the pipe is also wetted depends on the gas velocity and on the pipe diameter. Complete wall wetting was observed when the gas velocities were in excess of 7 m/s.

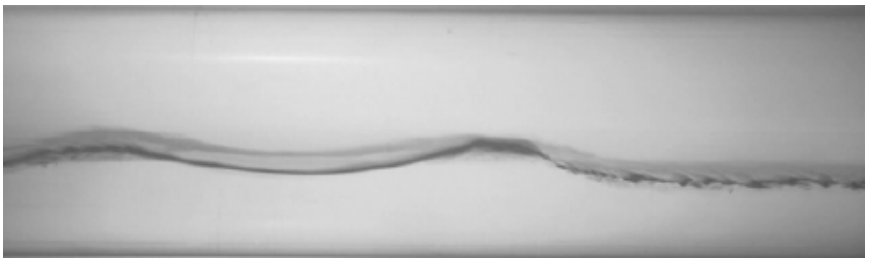

(a) $V_{SG}$=*1 m/s,* $V_{SL}$ = *O.1m/s*

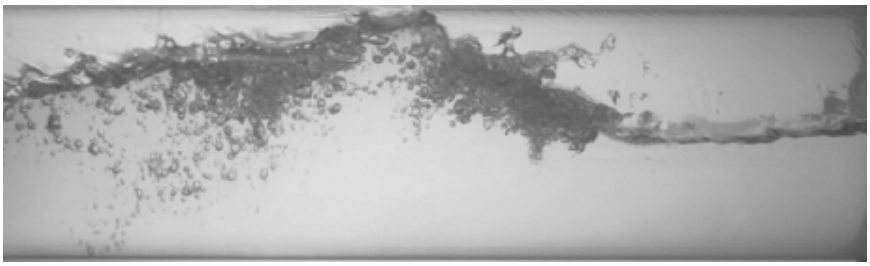

(b) $V_{SG}$=*1 m/s,* $V_{SL}$ = *O.4 m/s*

Figure B.7 - Transition from stratified flow to slug flow in the 4” inch test rig of IFE in Norway

SF6 gas and water at 7 bara. Flow from left to right. Taken from Bendiksen (1992).

***Intermittent flow***

Hydrodynamic slug flow is an important characteristic of the intermittent flow pattern. The occurrence of slug flow is due to the instability of the interface (so-called Kelvin Helmholtz instability) causing liquid waves to reach the top of the pipe. Figure B.8 shows how Kelvin Helmholtz waves grow and initiate a slug.

The typical slug structure is shown in Figure B.8 (Hill et al., 1994). The slug unit comprises of a liquid slug body, in which the liquid covers the full cross section of the pipe, with some entrained gas bubbles. A typical void fraction (local gas hold-up) in the liquid slug body is 50%. The liquid slug is transported with about the same velocity as the mixture through the pipeline, and behind the slug body, there is a gas bubble and a liquid

film. The liquid slug body can be represented by a homogeneous mixture of liquid and gas and the slug bubble can be represented by a stratified flow in horizontal pipe sections, and by annular flow in vertical pipe sections.

The size of a slug depends on the complicated balance of gas and liquid mass and momentum transfer to its head and tail sections. Laboratory experiments show that the average stable length of liquid slugs is 10 to 50 pipe diameters and the maximum slug length is 2 to 3 times the average value. The slug lengths produced over time form a statistical distribution around the mentioned average sizes. Scale up of the lab experiments to real-life conditions shows that pipe undulations have a significant effect on the resulting slug sizes. If the superficial liquid velocity is increased, then the gas bubble behind the liquid slug body will shrink until it disappears and all that is left behind is the liquid slug body with the entrained small gas bubbles. This is called the bubble flow regime.

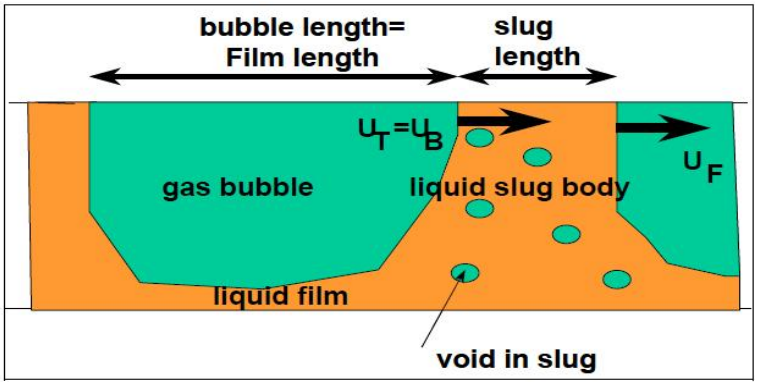


Figure B.8 - Typical structure of a liquid slug flow from left to right

### B.6.3 Encountered Flow Regimes

***Gas-condensate systems***

Gas-condensate pipelines usually operate in the annular flow regime at high and maximum production rates (both in the flow line and in the riser). Following turndown,

the flow regime in the pipeline will be stratified flow, whereas it is still annular flow in the riser. At minimum production rate, the flow in the pipeline will be stratified, except for some upward inclined sections where the flow will be in the hydrodynamic slugging regime and the riser will be in the hydrodynamic slugging regime. Figure B.9 and Figure B.10 give an overview of the typical flow regimes in gas-condensate systems.

For pipeline operations with minimum pressure drop and maximum stability, the stratified or annular flow patterns may be preferred. When corrosive gases are involved it is desirable to have flow patterns that cause complete pipe wall wetting and improve the distribution of corrosion inhibitors. These are the annular, slug, bubble or the stratified entrained flow patterns. The latter flow pattern is found in the higher velocity range of stratified flow when liquid is entrained as droplets into the gas stream.

Often pipeline and process engineers are overly worried when part of the pipeline operates in the hydrodynamic slugging regime. Usually these relatively small hydrodynamic slugs (with a length of up to about 50 pipe diameter) are harmless and can be handled by the production separator. For the design of liquid handling facilities the large transient and operational slugs produced with stratified flow are the base flow regime, and occur at low flow rates.

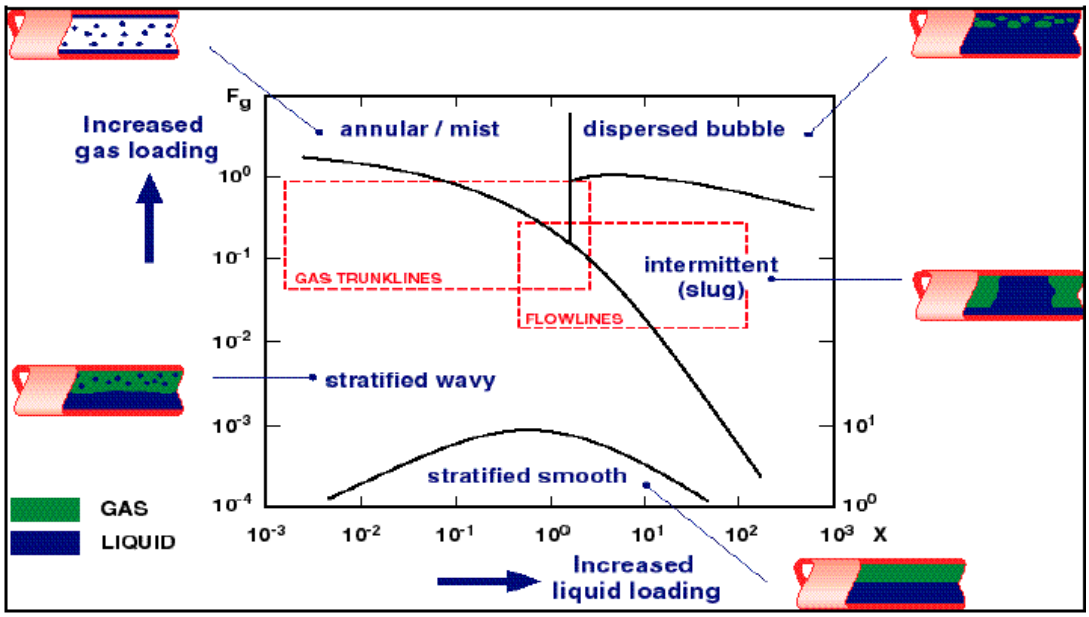


Figure B.9 - Typical flow pattern map with operational envelope for gas-condensate systems

The parameter X along the horizontal axis is the Lockhart-Martinelli parameter (which is a scaled liquid throughput), and the parameter Fg along the vertical axis is the gas-Froude number (which is a scaled gas throughput) (Lockhart et al, 1949).

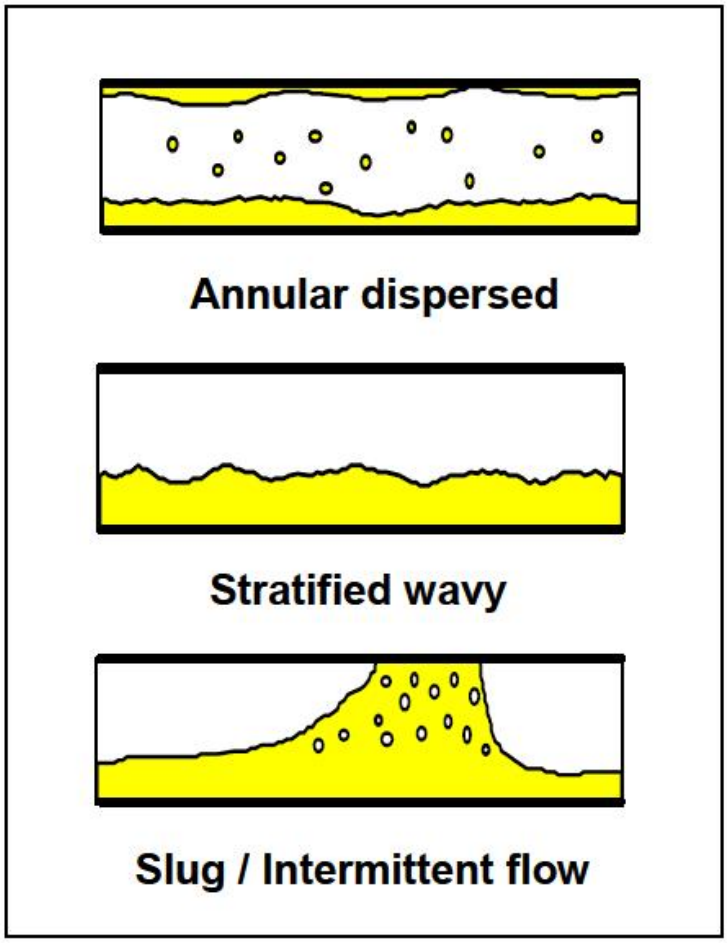


Figure B.10 - Flow regimes in gas-condensate flowlines and trunklines

***Oil systems***

Oil systems (i.e. oil/water with associated gas) are designed to operate in the stratified flow regime for all production rates. Risers will show either the hydrodynamic slugging regime or the bubble flow regime. For the prediction of the pressure drop at increasing flow rates, it is important to know the dispersion and emulsion behaviour in the stratified flow regime (which depends on both the physical and flow properties). At a low production rate (typically below an actual liquid velocity of about 1 to 1.5 m/s), the water

will settle from the water/oil dispersion, and form a separate layer. At low flow in inclined sections, large amounts of water may accumulate.

At very large liquid production rates, or for a production with increased water-cut, the gas (liquid interface in the nearly horizontal pipeline) will become unstable and will lead to operation in the hydrodynamic slugging regime. Due to the large liquid holdup in oil systems, the pipeline design can often not prevent parts of the pipeline (particularly the upward inclined sections) from operating in the hydrodynamic slugging regime. At increased liquid production rate, the hydrodynamic slugging regime in the riser will be replaced by bubble flow, which guarantees a smooth liquid/gas production into the separator. For both oil and gas systems, hydrodynamic slugging in the pipeline or riser is usually not a problem.

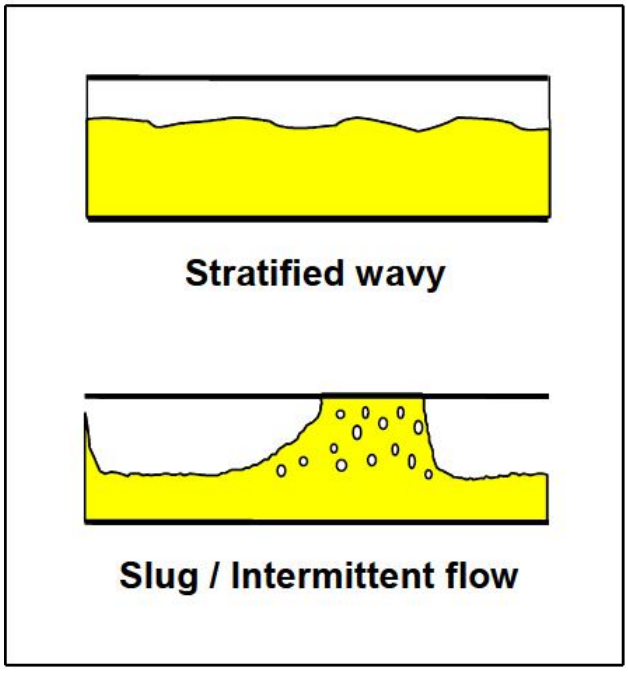


Figure B.11 - Flow regimes in oil systems

The need for reliable and yet cost-effective multiphase meters has become increasingly important. Multiphase meters are especially needed in cases where several operators share the use of production and transportation facilities in the exploitation of marginal oil and gas reserves from different locations.

The simultaneous flow of oil, water and gas in a pipeline is a complex phenomenon, making it difficult to understand, predict and model. Well established single-phase flow characteristics, including boundary layer, velocity profile and turbulence, are rendered ineffective in describing their nature (Sanderson, 1998). A multiphase flow regime, observed under a specific set of flow conditions, depends on a number of factors, including flow line geometry (size and shape), orientation (horizontal, inclined or vertical), and flow direction in vertical or inclined flows (up or down). Further complicating the matter is the physical distribution of the phases in the pipe and component transport properties (density, viscosity and surface tension). In a gas-liquid mixture, if there is no heat transfer between the phases, the flow rates (velocities) will increase progressively as the lower density and viscosity of the gas phase causes it to flow at a higher velocity relative to the liquid phase – a physical characteristic known as slippage. When multiphases (oil, water and gas) flow simultaneously in pipes, the flow regime, pressure and velocity fields are strongly connected. Perhaps the most distinguishing aspect of multiphase flow is the variation in the physical distribution of the phases in the pipe, a characteristic already described as the flow regime. During multiphase flow in pipes, the flow regime that exists depends on the relative magnitude of the forces that act on the fluid: gravity, buoyancy, turbulence, inertia, shear and surface tension forces, vary significantly with flow rates, pipe diameter, inclination angle, and fluid properties of the phase. Multiphase phase flow regimes may therefore be viewed as a consequence of the interaction between these forces.

Figure B.12 shows the operating envelopes for multiphase meters. This is an approach commonly used in other disciplines for displaying properties of three component mixtures.

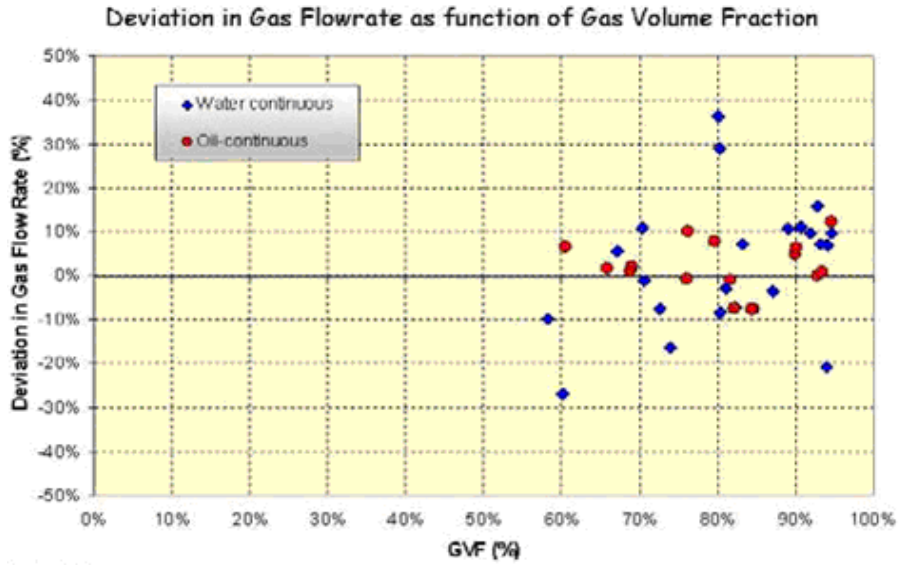


(a)

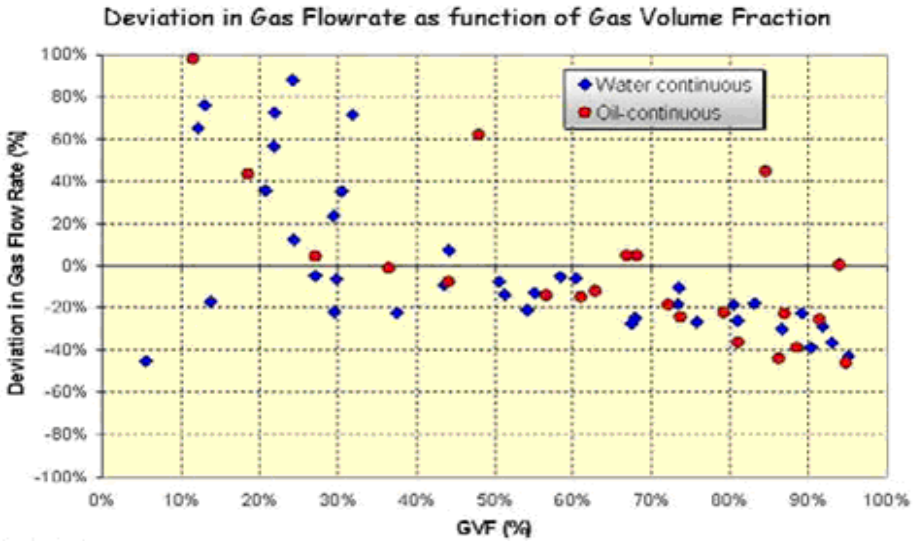


(b)

Figure B.12 - Operating envelopes for multiphase meters

A 4" FlowSys prototype meter was tested at a gathering station in series with a two-phase test separator and a test tank. Extensive work was carried out to prepare and calibrate the test separator and its associated measurement equipment, to ensure proper reference measurements. The GVF on some of the Rabi wells are not only very high but fluctuate a lot due to long horizontal pipelines between the well heads and the gathering station. These long horizontal pipelines also generate severe slugging and fluctuating water-cut, which is a challenge for any multiphase meter. The operating pressure for the multiphase meter at the gathering station was about 10-12 bar. The potential in the meter can be illustrated when studying the liquid flow rates for the tests carried out in water-continuous flow. Here, 92% of the tests were within an uncertainty limit of 7.5%.

Prior to the start of the Shell test campaign, FlowSys discovered that the meter requires a minimum liquid flow rate to operate accurately, this is because with upward flow through the MPFM liquid might fall back at the low velocities. This discovery resulted in a reduction in the operating envelope of the meter and unfortunately it was found that more of the Rabi wells fell below this limit. Consequently, not all the wells could be tested; however, for the wells whose rates were within the operating envelope and with sufficiently low GVFs (<90%), the FlowSys meter could measure the liquid within plus or minus 10%. For the higher GVFs the deviation between the references and the FlowSys meter were higher. For the water-cut in particular it was seen that also by comparing the two available references (well head samples and tank dipping) a ±10% difference were observed between the references (figure B.13)

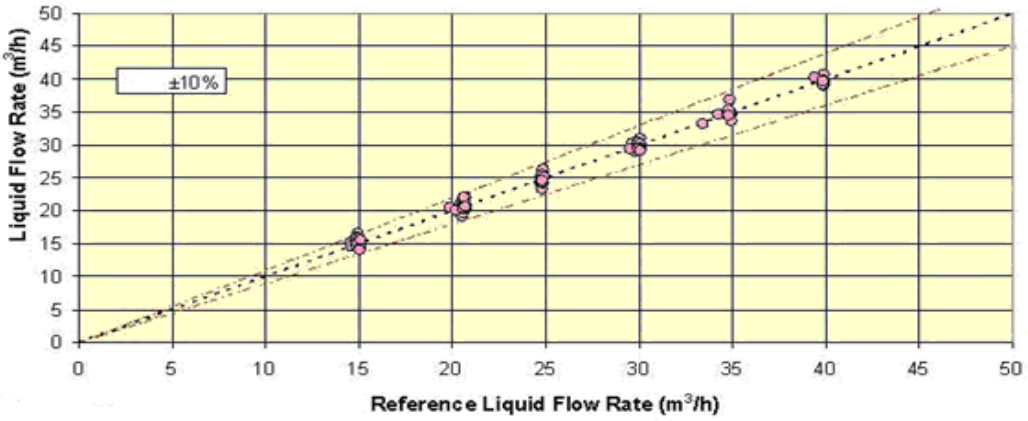


Figure B.13 - Difference observed between the two references

# APPENDIX C: MORE INFORMATION ON CAMERAS

Charge coupled device (CCD) and complementary metal oxide semiconductor (CMOS) image sensors are two different technologies for capturing images digitally that were considered for this work. Each has unique strengths and weaknesses giving advantages in different applications. Neither is categorically superior to the other, although vendors selling only one technology have usually claimed otherwise. In the last five years much has changed with regards to both technologies, and many projections regarding the demise or ascendance of either have been proved false. The current situation and outlook for both technologies is vibrant, but a new framework exists for considering the relative strengths and opportunities of CCD and CMOS imagers.

Both types of imagers convert light into electric charge and process it into electronic signals. In a CCD sensor, every pixel's charge is transferred through a very limited number of output nodes (often just one) to be converted to voltage, buffered, and sent off-chip as an analogue signal. All of the pixel can be devoted to light capture, and the output's uniformity (a key factor in image quality) is high. In a CMOS sensor, each pixel has its own charge-to-voltage conversion, and the sensor often also includes amplifiers, noise-correction, and digitisation circuits, so that the chip outputs digital bits. These other functions increase the design complexity and reduce the area available for light capture. With each pixel doing its own conversion, uniformity is lower, but the chip can be built to require less off-chip circuitry for basic operation.

CCDs and CMOS imagers were both invented in the late 1960s and 1970s, respectively. CCDs became dominant, primarily because they gave far superior images with the

fabrication technology available. CMOS image sensors required more uniformity and smaller features than silicon wafer foundries could deliver at the time, and it wasn't until the 1990s that lithography developed to the point that designers could begin making a case for CMOS imagers again. Renewed interest in CMOS was based on expectations of lowered power consumption, camera-on-a-chip integration, and lowered fabrication costs from the reuse of mainstream logic and memory device fabrication. While all of these benefits are possible in theory, achieving them in practice while simultaneously delivering a high image quality has taken far more time, money, and process adaptation than original projections suggested.

Both CCDs and CMOS imagers can offer excellent imaging performance when designed properly. CCDs have traditionally provided the performance benchmarks in the photographic, scientific, and industrial applications that demand the highest image quality (as measured in quantum efficiency and noise) at the expense of system size. CMOS imagers offer more integration (more functions on the chip), lower power dissipation (at the chip level), and the possibility of smaller system size, but they have often required tradeoffs between image quality and device cost. Today there is no clear line dividing the types of applications each can serve. CMOS designers have devoted intense efforts to achieving high image quality, while CCD designers have lowered their power requirements and pixel sizes. As a result, one can find CCDs in low-cost, low-power cell phone cameras and CMOS sensors in high-performance professional and industrial cameras, directly contradicting the early stereotypes. It is worth noting that the producers succeeding with "crossovers" have almost always been established players with years of in depth experience in both technologies.

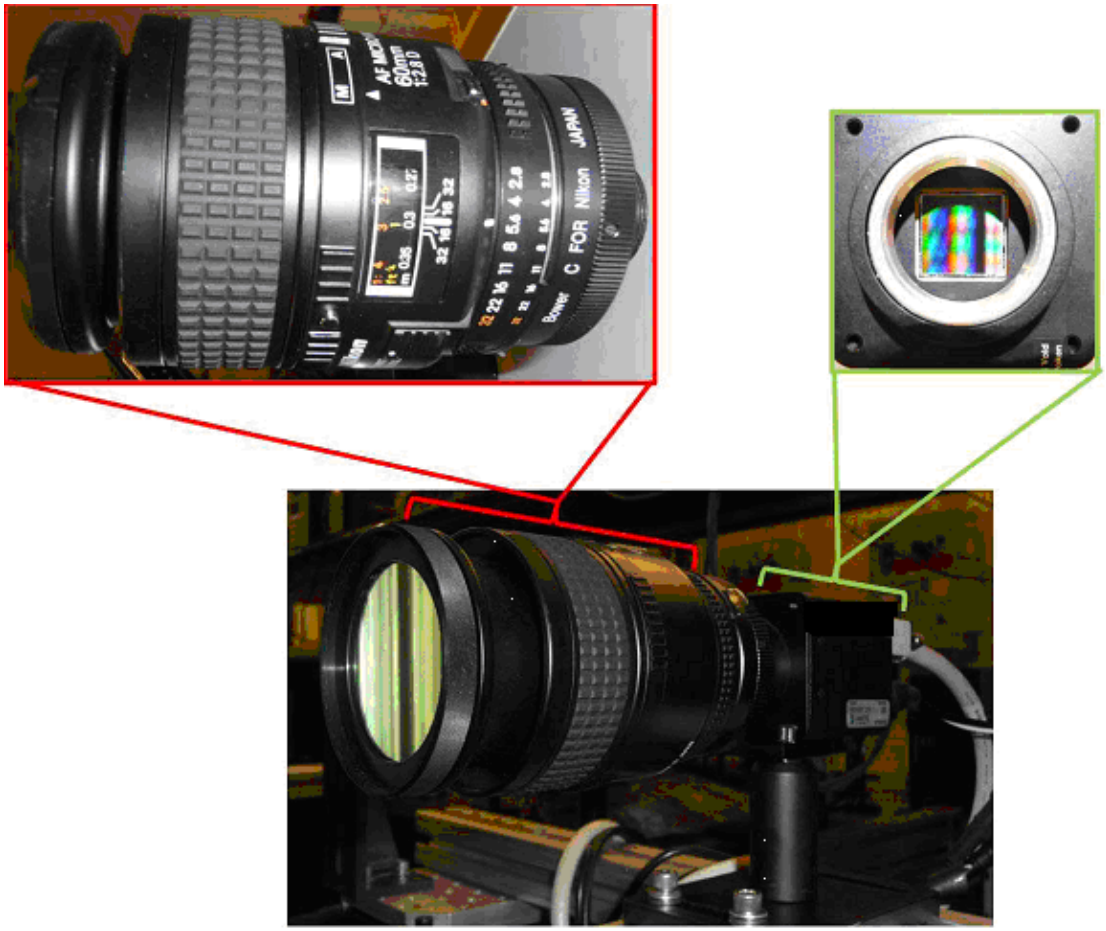


Figure C 1 - HiSpec 4 camera showing filter, lens, and CCD

Costs are similar at the chip level. Early CMOS proponents claimed CMOS imagers would be much cheaper because they could be produced on the same high-volume wafer processing lines as mainstream logic or memory chips; however this has not been the case. The accommodations required for good imaging performance have required CMOS designers to iteratively develop specialised, optimised, lower-volume mixed-signal fabrication processes very much like those used for CCDs. Adapting these processes for successively smaller lithography nodes (0.35µm, 0.25µm, 0.18µm, etc.) has been slow

and expensive, and those with a captive foundry have an advantage because they can better maintain the attention of the process engineers.

CMOS cameras may require fewer components and less power, but they still generally require companion chips to optimise image quality, thereby increasing cost and reducing the advantage they gain from lower power consumption. CCD devices are less complex than CMOS, so they cost less to design. CCD fabrication processes also tend to be more mature and optimised; in general, it will cost less (in both design and fabrication) to construct a CCD than a CMOS imager for a specific high-performance application. However, wafer size can be a dominating influence on device cost. The larger the wafer, the more devices it can yield, and the lower the cost per device. The value of 200mm is fairly common for third-party CMOS foundries while third-party CCD foundries tend to offer 150mm. Captive foundries use 150mm, 200mm, and 300mm production for both CCD and CMOS.

While cost advantages have been difficult to achieve and on-chip integration has been slow to arrive, speed is one area where CMOS imagers can demonstrate considerable strength because of the relative ease of parallel output structures. This gives them great potential in industrial applications. CCDs and CMOS will remain complementary and the choice continues to depend on the application and the vendor more than the technology.

Table C.1 - Feature and Performance Comparison of CCD Vs CMOS Technique

| Feature | CCD | CMOS |
|---|---|---|
| Signal out of pixel | Electron packet | Voltage |
| Signal out of chip | Voltage (analog) | Bits (digital) |
| Signal out of camera | Bits (digital) | Bits (digital) |
| Fill factor | High | Moderate |
| Amplifier mismatch | N/A | Moderate |
| System Noise | Low | Moderate |
| System Complexity | High | Low |
| Sensor Complexity | Low | High |
| Camera components | Sensor + multiple support chips + lens | Sensor + lens possible, but additional support chips common |
| Relative R&D cost | Lower | Higher |
| Relative system cost | Depends on Application | Depends on Application |
| Performance | CCD | CMOS |
| Responsivity | Moderate | Slightly better |
| Dynamic Range | High | Moderate |
| Uniformity | High | Low to Moderate |
| Uniform Shuttering | Fast, common | Poor |
| Uniformity | High | Low to Moderate |
| Speed | Moderate to High | Higher |
| Windowing | Limited | Extensive |
| Antiblooming | High to none | High |
| Biasing and Clocking | Multiple, higher voltage | Single, low-voltage |